UNIVERSITY OF CAPE TOWN

FACULTY OF ENGINEERING & THE BUILT ENVIRONMENT

Msc(Eng) Structural Mechanics Research

Buckling Behaviour of Thin Concrete Arch Dams

Student:

Malefetsane David Letsika (LTSMAL008)

Supervisor:

Professor Alphose Zingoni

This research is submitted in fulfilment of the requirement for the degree of
Master of Science in Engineering in Structural Engineering & Materials

Plagiarism Declaration

1. I know that plagiarism is wrong. Plagiarism is to use another's work and pretend that it is one's own.
2. I have used the Harvard-UCT convention for citation and referencing. Each contribution to, and quotation in, this body of work, from the work(s) of other people has been attributed and has been cited and referenced.
3. This report is my own work.
4. I have not allowed, and will not allow, anyone to copy my work with the intention of passing it off as his or her own work.
5. I acknowledge that copying someone else's work, or part of it, is wrong, and declare that this is my own work.
6. This thesis/dissertation has been submitted to the Turnitin module (or equivalent similarity and originality checking software) and I confirm that my supervisor has seen my report and any concerns revealed by such have been resolved with my supervisor.

Name and Surname: Malefetsane David Letsika

Student Number: LTSMAL008

Date: 09th January 2023

Signature: Signed by candidate

Acknowledgements

The completion of this research could not have been possible without the input, guidance and counsel from various individuals. I would like to acknowledge and thank each one of them for their invaluable contributions:

- My wife and daughter Penelope Letsika and Oyena Lindi who have been supportive during the course of this thesis.
- Professor Alphose Zingoni: For his guidance, counsel and endless patience during the course of this thesis.
- My two sisters who have been supportive during the course of this thesis.

Abstract

The buckling strength of concrete arch dams in the form of thin-walled shells having single and double curvature has been studied. When subjected to the hydrostatic pressure applied by the retained water, the shell undergoes mostly compressive internal reactions, which can lead in the thin shell buckling. The buckling strength of the arch dam is influenced by a variety of factors. These include the valley shape, thickness variation of the shell, the arch's geometry, and the degree of arch bulging. In this research, finite element modelling is used to assess the buckling behaviour of concrete arch dams (single and double curvature) having constant, linear, and quadratic thickness variation. The results are presented in the form of design plots that allow a safe set of design parameters to be selected while simultaneously indicating the safety factor linked with the implemented design.

Several noteworthy observations have been made. It is seen that the buckling pressures drop drastically with increasing the arch dam depth (aspect ratio), with the rate of decrease diminishing as the depth increases. The bulging of the shell (rise ratio) has a notably large impact on the buckling strength of the arch dam and can thus be utilized to enhance the buckling strength of an arch. The geometric aspect of the valley shape does have a significant effect on the buckling strength with a decrease in the dam base width increasing the buckling strength significantly. the mathematical form of the arch (parabolic/circular) has no appreciable impact on its buckling strength.

Table of Contents

List of Figures

List of Tables

Symbols and Abbreviations

P_{cr} – Critical Buckling Pressure (kN/m^2).

FEM – Finite Element Modelling.

ξ **-** The ratio of the elliptic paraboloid's critical buckling pressure to those of the comparable parabolic cylinder.

b/a – Aspect Ratio Depth.

h/a – Rise Ratio.

c/a – Arch Dam's Base width Ratio.

ν - Poisson's Ratio.

E – Young's Modulus.

1. Introduction

1.1 Background Knowledge

The safety of an arch dam is defined as its ability to withstand an uncontrolled discharge of reservoir water. Because overstressing, sliding, and other conceivable modes of collapse are unlikely to occur, the structural integrity of the dam remains intact and it is regarded safe. As a result, a safety study should identify all important failure mechanisms and undertake necessary studies in order to ensure that the structural stability of the dam is sustained.

Arch dams are the only type of dams that withstand water loading solely due to the compressive strength of the concrete used to construct them. If the arch dam is designed properly, it is theoretically feasible for the entire concrete structure to operate under the same stress for a given loading. This implies that no bending moments induced in the shell, as the tension would normally vary with its thickness. Although this is the case, it can only occur if the arch dam is designed in the shape of a funicular of the hydrostatic load as well as dead weight, and the thickness changes with the normal forces acting on the shell. On the other hand, it should be noted that, in contrast to the distribution of weight along a line, for a distribution of load along an arbitrary surface - such as the water pressure in the upstream face of a dam - there is an infinite of funicular forms to choose from (V.D da Silva 1995).

1.2 Problem Statement

Analysis and design of thin concrete arch dam is essential in the context of economizing the excess use of concrete material incorporated in concrete walls. When considering the history of arch dam construction, a larger factor of safety has been integrated into the design of arch dams, resulting in the usage of thicker concrete dam walls to resist hydrostatic pressure. Recent studies by (Zingoni et al., 2013) have revealed that there are more advanced measures or possible solutions for making concrete arch dam walls more durable while remaining thin.
However, the proposed solution on the use of shell analysis (thin walls) has its implications due to the stability effect of dam walls being compromised. One key mode of failure incorporated with thin-walled structures is buckling failure. When subjected to the hydrostatic pressure exerted by the retained water, the shell undergoes mostly compressive internal reactions, which can result in the thin shell buckling.

The buckling strength of the arch dam is influenced by a variety of factors. These factors include the valley's shape, the geometry of the arch surface, the degree of arch bulging, shell-thickness variation, and boundary conditions.

An examination into the buckling strength of concrete arch dams in the form of thin shells with single and double curvature having constant thickness and built in rectangular valleys was conducted in 2013. However, the 2013 paper did not cover the arch dams having linear and quadratic varying thickness built in triangular and trapezoidal valleys.

In this research, FEM modelling is used to assess the effect of key parameters on the critical buckling pressure of cylindrical and elliptic-paraboloidal arch dams having linear and quadratic varying thickness and built in triangular and trapezoidal valleys. Design curves for cylindrical arch dams are shown, together with information on determinants of safety against buckling. The benefits of double curvature are evaluated by comparing the findings for the elliptic paraboloid with those for the parabolic cylindrical arch.

A number of observations to be expected is that the shape of the arch does not have a significant effect on the buckling strength. The geometry of the arch dams and valley shape seem to have a greater effect on the buckling strength of arch dams. The thickness variation is utilized in a way that the pressure at the surface level of the retained water is zero and therefore the shell is expected to have the least thickness at that level. The pressure at the bottom surface of the retained water is maximum and therefore the shell is expected to be thicker at that level.

This research will examine the buckling behaviour of thin concrete arch dams when subjected to hydrostatic pressure. Additionally, FEM will be utilized to deduce the effect of shell curvature, shell shape, and thickness change on buckling behaviour.

1.3 Objectives of the Research

The eigenvalue solutions for various modes of the perfect shell under hydrostatic pressure will be computed using Finite Element Modelling (FEM). The modes of forms to be examined encompass cylindrical and elliptic-paraboloidal arch dams with thickness that varies linearly and quadratically, constructed within valleys of triangular and trapezoidal shape.

The primary objective of calculating the critical eigenvalue solutions, specifically the lowest eigenvalue, is to determine critical buckling loads and investigate the buckling behaviour of thin concrete arch dams and how does the geometric aspect of the valley shape and the mathematical form of the arch (parabola/circular) affect the arch's buckling strength when the thickness varies linearly and quadratically. The findings of this study will enable the acquisition of a safe set of design parameters for thin concrete arch dam design.

1.4 Research Scope and Limitations

Linear perturbation analysis (LBA) was the main analysis procedure used in this research. This analysis is used to determine the perfect structure's critical buckling load (lowest eigenvalue) and related critical buckling mode (eigenmode), assuming minimal pre-buckling bending deformations to obtain the eigenvalue solutions. However, this research had limitations and did not consider the following:

- Nonlinear analysis which incorporates nonlinear effects originating from geometrical nonlinearities (large deformations) and material nonlinearities (elasto-plastic material).
- Modal response analysis which incorporates the linear response of the arch dam subject to a continuous stream of harmonic excitations.
- Geometric and material nonlinear analysis with imperfections analysis which incorporates the arch dam geometric imperfections. Imperfections may include variations in the midsurface of the shell, inconsistencies in the boundary conditions, residual stresses, or combinations of these.

1.5 Plan of Development

The comprehensive literature review on thin concrete arch dams will cover shapes and geometry of arch dams, numerical modelling of arch dams, structural analysis of the arch, optimization of shape and geometry of the arch, structural design and construction of the arch.

The methodology of the research will be to compute the eigenvalue solutions for various modes of form of the perfect shell under hydrostatic pressure using Finite Element Modelling (FEM). The FEM software to be used is ABAQUS, a widely known shell analysis program. Furthermore, FEM will be utilized to investigate the effect of shell curvature, geometry, and thickness change on buckling behavior.

1.6 Conceptual Framework

The most important ‘concepts’ that will govern the literature of this research are listed below.

1. Shapes and Geometry of Arch Dams.
2. Numerical Modelling of Arch Dams.
3. Structural Analysis of the Arch.
4. Optimization of Shape and Geometry of the Arch.
5. Structural Design and Construction of the Arch.

The correlational and interconnections between these concepts are also illustrated below.

- The history of Arch Dams is linked to all of these concepts through establishing the developments methods in the analysis and design of arch dams.
- Concept (1) and (4) are linked to one another. Arch dams are classified according to their shape and geometry, which are determined by the nature of the valleys in which they are built. Additionally, the angle, radius, and curvature are all taken into consideration when classifying a shape. Upon Establishing the shape/Geometry then optimizing that shape/geometry is one necessary critical step. The purpose of optimization design is to determine the optimal shape of an arch dam given boundary conditions and constraints.
- Concept (2) and (3) are linked to one another. Structural deformations have proved to represent the dam’s operating regime intuitively and consistently. As a result, building a predictive numerical model that is accurate is critical for a risk-based assessment.

- All of the concepts (1-4) are linked to the concept (5). Structural Design entails the numerical modelling and analysis of concrete arch dams in which hydrostatic pressure and the accompanying structural deformations are computed prior to the design stage taking place.

2. Literature Review.

2.1 Introduction

The literature review for this research will involve further investigation of the buckling behaviour of thin concrete arch dams. The comprehensive literature review will cover:

1. **Shapes and Geometry of Arch Dams:** The current state of research pertaining to this specific subtopic will contribute to a more comprehensive interaction between the geometric properties of an arch and its susceptibility to buckling.
2. **Numerical Modelling of Arch Dams:** Numerical modelling serves as the fundamental technique for undertaking this research. This is because buckling theory is described by a partial differential equation (PDE). Therefore, an approach of obtaining a closed-form solution analytically can be tedious, particularly when studying structures with complex geometric shapes. The utilisation of numerical modelling, particularly in conjunction with finite element methods for discretizing complex geometries, proves to be highly advantageous in this regard.
3. **Structural Analysis of the Arch:** The investigation of this subtopic has significance in enhancing comprehension of the structural response exhibited by an arch when subjected to diverse loading conditions. Additionally, the investigation of various boundary conditions applied to a structure is essential to comprehending the influence of valley shapes on arch dams, as the fixity of the arch dams is contingent upon the characteristics of the valley shape.
4. **Optimization of Shape and Geometry of the Arch:** Arch dams are categorised based on their shape and geometry, which are influenced by the characteristics of the surrounding valleys in which they are constructed. Hence, the optimisation of arch shapes holds significant importance as the structural integrity of an arch is greatly influenced by its specific shape. This subtopic will also contribute to the understanding of the extent to which the thickness of an arch affects its buckling strength in comparison to its shape.

5. **Structural Design and Construction of the Arch:** Structural Design involves the application of numerical modelling and analysis methods to concrete arch dams. This step is important because it includes the calculation of hydrostatic pressure and the resulting structural deformations, which are essential considerations prior to the commencement of the design phase.

The geometry and shape of arch dams are categorized based on the types of valleys in which they are constructed. The next required and crucial step after establishing the shape or geometry is to optimize it. Finding the ideal shape for an arch dam given boundary conditions and limitations is the goal of optimization design. The operating regime of the dam has been demonstrated to be intuitively and consistently represented by structural deformations, particularly for this research, is the eigenmodes obtained for each eigenvalue solution in linear buckling analysis. Building an accurate predictive numerical model is therefore essential for a risk-based evaluation.

2.2 Shapes and Geometry of Arch Dams.

The membrane approach has shown to be the most effective method for obtaining the shape of an arch dam. However, prior to the advent of the computer, this approach had to be tested experimentally. The test consists of an initially flat rubber membrane mounted in a frame resembling the dam's abutments on the valley's slopes, which is loaded by water pressure (simulating hydrostatic load) and forces acting vertically upward, which correspond to the dam's own weight. Due to its lack of bending rigidity, the distorted membrane takes the shape of a funicular. When all forces are reversed, the equilibrium is maintained and the tensile stresses convert to compressive stresses. On the surface, this implies that a dam shell with that shape can have only compressive stresses that are constant in thickness. Although this is not entirely accurate, because the shell is bending rigid, its deformation results in bending moments, particularly in the abutments. However, knowledge gained via this approach and testing the produced forms demonstrates that forms free tensile stresses may be created (Dias et al., 1997). Due to the disadvantages of the experimental membrane technique in terms of time and expense, empirical rules were established based on the findings acquired using this method in order to eliminate the experimental shape determination.

Arch dams are classified according to their shape and geometry, which are determined by the nature of the valleys in which they are built. Additionally, the angle, radius, and curvature are all taken into consideration when classifying a shape. Depending on the natural form of the valleys, arch dams are categorized into four types: variable radius arch dams, constant radius arch dams, double curvature arch dams, and constant angle arch dams.

2.2.1 Constant Radius Arch Dam

A dam in which the outer side curve (also known as extrados) of the arch has a constant radius over its full elevation. Concurrently At the same time, the inner curve (also known as intrados) of the arch is formed, with the radius of the curve decreasing from the top to the bottom of the dam. In response to the variable hydrostatic pressure distribution, the thickness of the dam is larger at the base, where the hydrostatic pressure is at its greatest, and thinner at the top, where the hydrostatic pressure is the least. The cross section of a constant radius arch dam resembles a right angled triangle, with the vertical line representing extrados and the hypotenuse indicating intrados on each side of the dam. These are the most commonly seen kind of arch dams, and they are generally used in valleys with a U-shape (The Constructor, 2008).

2.2.2 Variable Radius Arch Dam

Extrados (outer side - upstream) and intrados curves (inner side - downstream) have different radii depending on the elevation, as suggested by their names. The radius of the dam is largest at the top of the structure and smallest at the bottom. In this case, the central angles of the arch rings are also adjusted at various heights of the arch dam. Variable radius arch dams are more cost effective than constant radius arch dams. In comparison, it only consumes 58% of the concrete necessary for a constant radius arch dam. Valleys having a V-shaped shape are more suitable for this kind of arch dam.

2.2.3 Constant Angle Arch Dam

A constant angle arch dam is one whose central arch ring maintains a constant angle throughout its height. This is accomplished by adjusting the radius of the variable radius arch dam. This type of arch dam is more economical than the other two, using just 43% of the concrete necessary for a constant radius arch dam (The Constructor, 2008). A constant angle arch dam is better suited to valleys that take on the shape of a V.

2.2.4 Double Curvature Arch Dams

The double curvature arch dam is curved both horizontally and vertically. Due to the dam's overall shape resembling a shell, it is sometimes referred to as the shell arch dam. Due to the twofold curvature, the thickness of the arch wall is minimized. These non-vertical dams, on the other hand, are more difficult to construct than the other three types. Additionally, they need more robust foundations. Shell arch dams are more suited to narrow valleys (The Constructor, 2008).

2.3 Numerical Modelling of Arch Dams.

Arch dams regarded as shell structures, are lightweight and flexible, with a high capacity for overloading owing to the material's full use. China now owns 40% of the world's arch dams (Zhao & Wu, 2021). These arch dams include Jinping-I Dam (see Fig. 2.1) having double curvature which is 305m tall, 568m long and 3600MW generation capacity, the Xiaowan Dam (see Fig. 2.2) having double curvature which is 292m tall, 902m long and 4200MW generation capacity, the Xiluodu Dam (see Fig. 2.3) having double curvature which is 286m tall, 700m long and 13 860MW generation capacity. However, for a long period of time, just the safety factor has been used as an assessment index in actual engineering structures, neglecting numerous uncertainties such as material characteristics, load variations, and so on (Baecher, 2016).

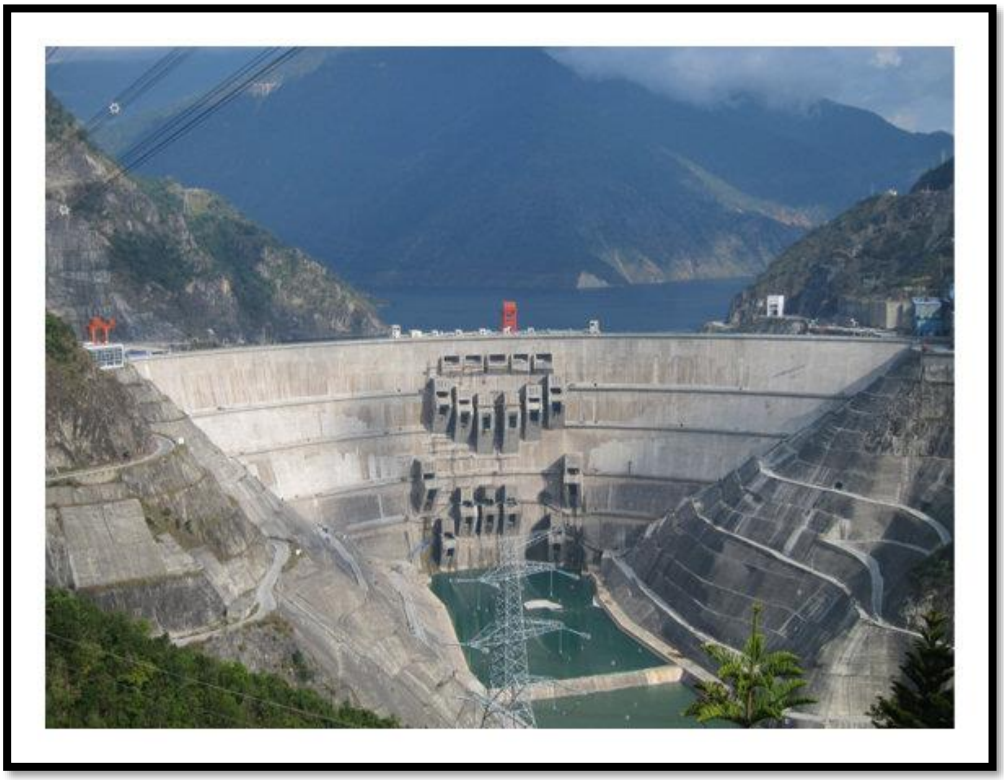

Figure 2.1: Jinping-I Dam. (Z. Meng 2020).

Figure 2.2: Xiaowan Dam (reduper.com/xiaowan-dam).

Figure 2.3: Xiluodu Dam ("Xiluodu Dam, Jinsha River, China". Water Technology, 2014).

Hydropower, flood control, shipping, irrigation, and water supply all rely on the engineering and supervision of high arch dams. Failure of these huge arch dams might have catastrophic implications to the public residing nearby. Structural deformations have proved to intuitively and consistently represent the dam's operating regime. As a result, building a prediction model that is accurate is critical for risk-based assessment.

The existing and future arch dams' safety state may be determined by comparing the estimated structural reactions to the given load combination to the measured values. Since the 1960s, research on the stability of structures with uncertain characteristics has provided an effective technique for assessing structural safety using probability theory (Zhao & Wu, 2021). According to (Zhao & Wu, 2021), numerous safety monitoring models have been developed to date, and they fall into three categories: statistical models, hybrid models, and deterministic models. The statistical model is based on data collection, and the hybrid and deterministic models are based on numerical modelling which involves use of finite element modelling.

These probabilistic (statistical model) and non-probabilistic (hybrid and deterministic models) reliability models have been extensively utilized in conjunction with interval theory (Wen-gui, Yong-jie & Ming-hua, 2007), design optimization (Meng et al., 2016), convex models, and experimental data (Lu et al., 2011). However, the probabilistic reliability (statistical model)

model has gradually demonstrated its limitations when uncertain variables are assumed to be arbitrary (Dutta, 2020), because sufficient sample data will be required to determine the validity and numerical characteristics of the influence factors.

On the other hand, with non-probabilistic reliability method which involves finite element modelling, the model has proved to be useful with accurate results as well. However, some critical aspects, such as the material variability, constitutive model (M.A. Hariri-Ardebili 2018), boundary conditions, mesh discretization, and the solution method (R. Malm 2016), should be carefully chosen to prevent bias in the findings and to build a realistic and reliable model. Non-probabilistic reliability model is useful when evaluated the buckling capacity of the arch dam where finite element modelling is used to solve for eigenvalue solutions.

2.4 Structural Analysis of the Arch.

2.4.1 Stress Analysis of the Arch

In structural analysis of an arch, it is first important to understand the basic function of an arch which was first introduced by ancient Romans. The fundamental feature of an arch is that it can support its own weight and external loads compressively, that is, without transferring tensile forces onto the structure (Yau & Yang, 2008). This form of structural shape is particularly well-suited to elements or materials that can withstand compressive stresses rather than tensile ones, such material that is strong in compression is concrete. With comparable mechanical features to that of arch structures, a vertical curved dam wall may transfer compressive hydrostatic loads more efficiently than a straight dam wall due to the bending-tension coupling effect (Yau & Yang, 2008). However, this coupling effect has shown to have complicated deformation behaviors of curved wall structures significantly more than straight wall structures.

By so noting, to compute the stresses of curved dam walls, they will be idealized into a series of curved beam elements (representing a ring strip of a dam wall) in order to make the analysis much simpler. Finite element modelling has been widely used in computation of deformations for curved beam elements, but according to (Prathap, 1985) , the analysis makes use of low-order independent polynomial interpolations for both tangential and normal displacements which have introduced some substantial inaccuracies in the computational results. Prathap (Prathap, 1985) has reviewed this phenomena, often referred to as membrane locking.

To address this issue, researchers have employed techniques such as the strain element method (Choi & Lim, 1993), the reduced integration method, and isoparametric elements method (D.G.Ashwell & A.B.Sabir, 1971).

Numerous curved-beam elements have been developed in the literature for analysis of free vibration (A.B.Sabir & D.G.Ashwell, 1971), buckling analysis (Veletsos et al., 1972), and post-buckling analysis of curved beams (Sabir & Lock, 1973). Pi et al. (Pi, Bradford & Uy, 2005) demonstrated that many general-purpose finite element programs, such as ABAQUS and ANSYS, were incapable of properly predicting the elasto-plastic behavior of curved components in space.

Though some improvement has been achieved in the study of curved beam problems in the past, the coupling behavior which encompasses bending-tension of curved beams (Yau & Yang, 2008), continues to be a mathematical impediment in deriving a consistent displacement field for the curved beam element in order to avoid the membrane locking problem.

Yang (Yang, Kuo & Yau, 1991) proved that a curved beam element may be approximated by a series of straight-beam components by taking into account the equilibrium for structural connections linking non-collinear parts in the deformed configuration.

Yau (Yau & Yang, 2008) enhanced Yang's technique (Yang, Kuo & Yau, 1991) by developing a suitable structural strategy for generating a planar curved beam element. He introduced the elastic stiffness matrix of the curved beam as the sum of the chord-wise stiffness matrix of the two straight-beam components used to describe the curved beam (see Fig 2.1 below).

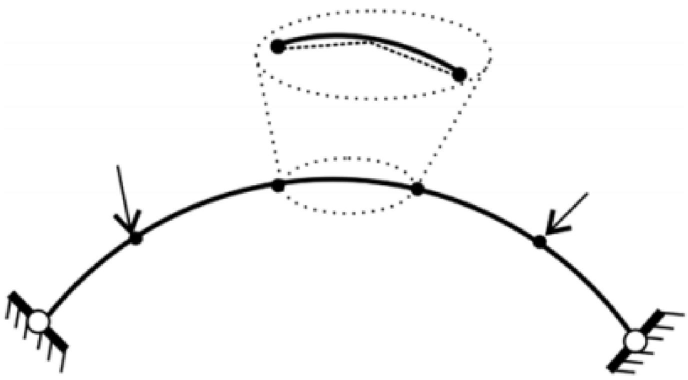

Figure 2.4: Finite Element Modelling for Curved Beam Element (Yau & Yang, 2008).

In Fig. 2.2, the curved beam element of interest is shown with a radius *R* and subtended angle *2φ*. This geometric stiffness matrix of the curved beam will be obtained using the notion of rigid displacements (Yang, Lin & Chen, 2007), by converting the geometric stiffness matrix of the straight beam with equal nodal degrees from rectangular to curvilinear dimensions. In Yau's article (Yau & Yang, 2008), four examples of linear static, buckling, and geometrically nonlinear assessments of curved-beam members were investigated to demonstrate the usefulness and correctness of the curved-beam element described above.

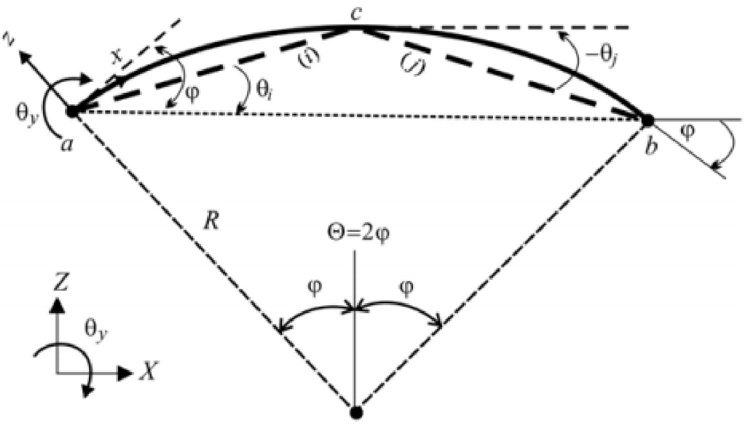

Figure 2.5: Two chord-wise straight-beam elements (Yau & Yang, 2008).

With regards to the Yau's formulation of the elastic stiffness matrix for the linear behavior, two straight beam elements *ac* and *cb* in Fig.2.2, also referred to as beam elements *i* and *j* which share the intermediate node *c*, at the mid-point of the curved beam element, shall be approximated to the curvy-beam element in Fig. 2.2. Additionally, θ_i and θ_j denote the included angles of segments *ac* and *cb* with respect to the curved element's chord *ab* in the coordinate system depicted in Figure 2 (Yau & Yang, 2008).

In Yau's article (Yau & Yang, 2008), the following assumptions were made for the analysis of curved beam elements.

- The material is elastic and uniform in composition (homogenous).
- The curved beam's cross-section is uniform and doubly symmetrical.
- During deformation, each cross-section stays undistorted.
- The length and radius of the curved beam are greater than the beam's cross-sectional dimensions.
- The curved beam's shearing deformation is neglected in this analysis.

- Only concentrated loadings are permitted at the curved-beam element's two ends.

With Yau's (Yau & Yang, 2008) analysis, consideration for uniform or non-uniform stresses was not taken into account. Modeling the effect of hydrostatic pressure is critical in determining the stability of concrete dams (Mazighi & Mihoubi, 2018). Hydrostatic pressure results in extra material degradation and decreases fracture resistance. It is also a key parameter in determining the buckling resistance of thin concrete arch dam walls (Zingoni et al., 2013).

H. Mazighi (Mazighi & Mihoubi, 2018) introduced a numerical modeling technique for calculating the distribution of water pressure in concrete dams. The technique is based on the Drucker Prager model and entails an isotropic elastic-plastic mechanics at the upstream face under hydrostatic pressure (Mazighi & Mihoubi, 2018). Numerous authors, notably A. Zingoni et al. (Zingoni et al., 2013), have used the Finite Analysis program ABAQUS to predict hydrostatic pressure and its implications on concrete arch dams. However, the majority of the study was conducted in the elastic range and not much done in the post-buckling area utilizing ABAQUS software.

Apart from Yau's 2008 (method) for curved beam analysis, several standard techniques are used for all types of arch dam analysis. These approaches, which comprise cylinder theory, the method of independent arches, trial load, and model analysis, were shown to have limits for multiple radius arch dams above 100 m in height. Later, accurate methods were required to ensure safety and economy, which resulted in numerical approaches such as finite difference, finite element, and boundary element for arch dams. Among these approaches, finite element is the most effective for dealing with continuous structures such as arch dams because it produces a more realistic stress distribution and offers greater flexibility in terms of geometry and boundary conditions than the methods mentioned above. As a result, this research presents a critical investigation of how the finite element approach using ABAQUS resolves complexity in the instance of an arch dam with changing geometry.

2.4.2 Stability Analysis of Arch Dams

Fumagalli (Fumagalli, 1973) created a geomechanical model test in the 1960s for analyzing the stability of arch dams at the Institute of Structure Model Experiment and Simulation (ISMES). Even though numerical approaches, particularly the finite element method (FEM), have been widely used to simulate geological structures in recent decades due to the rapid development of computer science, geomechanical model testing remains an indispensable method for dam stability and reinforcement analysis (Liu et al., 2013). The benefits of geomechanical model testing include the ability to replicate intricate real-world structures and the ability to directly detect the failure mechanism throughout the loading process (Liu et al., 2013).

Other methods involved in the stability analysis of arch dams is particularly on abutment stability. The failure of concrete arch dams demonstrated that the primary cause of concrete arch dam failure is the instability of the rock abutment.

Different techniques such as block theory, limit equilibrium analysis, the Distinct-Element Method, and the Finite Element Method can be used to analyze the stability of an abutment (Chen, 2015).

2.4.3 Buckling Analysis of Arch Dams

Buckling of high arch dams is a complicated problem due to the huge series of aspects involved, including the shape of the valley through which the dam is built, the geometry of the arch, the bottom and side foundation conditions (Zingoni et al., 2013). W. Zhou (Zhou & Chang, 2004) conducted an eigenvalue linear buckling analysis of a high arch dam, concluding that the dam was safe from buckling if the estimated buckling load exceeded the strength-limit load. The buckling of arch dams is a subset of the more fundamental issue of shell buckling. G. Papadakis (Papadakis, 2008) offered an analytical solution for the buckling of thick cylindrical shells subjected to external pressure, a solution that is applicable to the situation involving some arch dams. A. Zingoni et al. (Zingoni et al., 2013) used FEM modeling to investigate the effect of critical buckling pressure on cylindrical and elliptic-paraboloidal arch dams. According to some of the findings in his study, the buckling pressure decreases significantly as the relative depth aspect ratio b/a (see Fig. 2.3) of the arch dam increases, with the rate of decrease slowing as b/a increases (Zingoni et al., 2013).

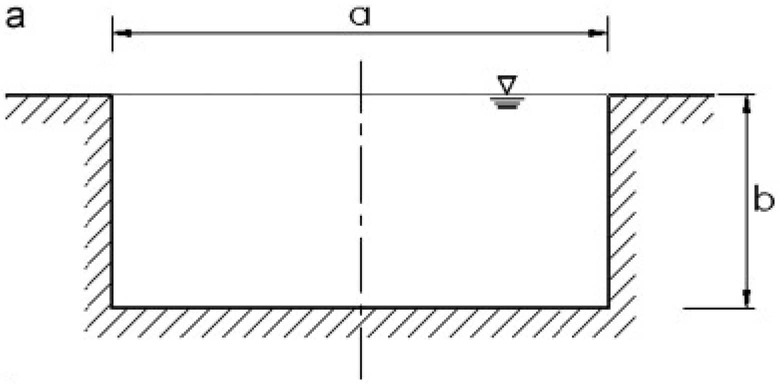

Figure 2.6: Front view of a horizontally-curved arch dam in a rectangular valley (Zingoni et al., 2013).

A. Zingoni et al. (Zingoni et al., 2013) also concluded that the shell rise ratio h/a (see Fig. 2.4) has a significant effect on the buckling strength of an arch dam, and therefore may be utilized to improve the buckling strength of an arch with specified dimensions *a* and *b* without increasing the shell thickness, thereby conserving concrete material.

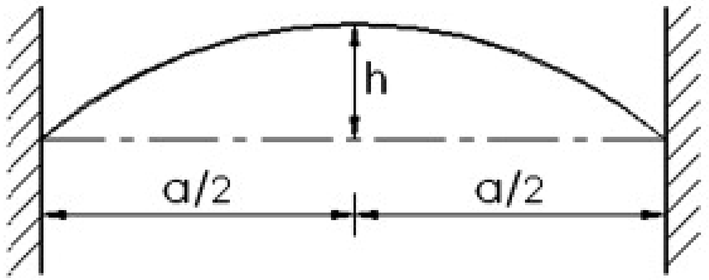

Figure 2.7: Circular arch plan view (Zingoni et al., 2013).

With this being said, the shape of the arch has no influence on the buckling strength. Other geometric variables, such as the rise ratio h/a, the aspect ratio b/a, and the thickness all have a far huge impact on the buckling strength arch dams (Zingoni et al., 2013).

2.4.4 Dynamic Analysis of Arch Dams

Water retained by concrete arch dams can shift under the influence of earthquakes due to vibrations in the dams. This results in hydrodynamic pressure being produced on the dam's lateral surface, which can increase the burden on the dam body and negatively impact dam safety. As a result, seismic design of dams must take into account the hydrodynamic pressure on the lateral surface of the dam (Ye, Zhou & Zhou, 2023). The analytical framework for determining the maximum hydrodynamic pressure on concrete arch dams subjected to harmonic vibration load (seismic load) was first proposed by (H.M Westergaard, 1933).

$$p_{max} = \frac{4\rho \mathrm{a}_m}{\pi} cos\ \omega t \sum_{n=1}^{\infty} \frac{1}{(2n-1)c_n} e^{-c_n x}\ sin\ \lambda_n z \tag{1}$$

Where:

p_{max} = maximum hydrodynamic pressure.

a_m = peak ground acceleration.

ω = circular frequency

ρ = water density

c_n = wave velocity

λ_n = wave length

The five presumptions below form the basis of the aforementioned equation, which considers the interaction between a dam body and the water in its reservoir. Five assumptions are made here: (1) the dam is rigid and its surface is vertical; (2) the reservoir water is incompressible and inviscid; (3) the reservoir section is rectangular and the water depth is limited; (4) the gravity surface wave caused by the vibration of the dam is disregarded; and (5) the dam body performs a harmonic motion with very small amplitude in the horizontal direction (Ye, Zhou & Zhou, 2023).

Since equation (1) comprises infinite series in the form of which is too complex to be employed in real engineering problems further simplification of the equation (1) is presented as

$$p_{max} = \frac{7}{8} \mathrm{a}_m \rho \sqrt{Dz} \tag{2}$$

Where:

a_m = peak ground acceleration.

ρ = water density.

D = water depth

z = distance from the point to the dam bottom.

Westergaard's simplified equation is a common technique of calculation utilized in several national design current standards.

However, the simplified equation has the following drawbacks: (1) it cannot be applied to dams with inclined lateral sides; (2) it is only applicable in cases when the vibration amplitude of dam is minimal; (3) it does not account for the gravity wave in front of dams that is caused by the dam's vibration; (4) the predicted maximum hydrodynamic pressure is broadly not acceptable with measured values (Ye, Zhou & Zhou, 2023).

A quicker and more accurate approach in dynamic analysis of arch dams is the use of Finite Element Method. It can be applied to the resolution of a wide variety of engineering issues, including those that are stable, transient, linear, or nonlinear (Bathe, 1996). When it comes to software that uses the finite element approach, ABAQUS has a reputation for being one of the most accurate and useful pieces of software in both commercial settings and academic research when performing dynamic analysis such as water wave loading and seismic loading on structures (M.A. Lotfollahi Yaghin and M.A. Hesari, 2008). Creating a mathematical model that is formed of separated parts that mimic the real continuous structures is the most significant phase in the process of conducting structural analysis using the finite element method (FEM). In order to develop dynamic equilibrium equations of structural elements, the virtual work principle is utilized (M.A. Lotfollahi Yaghin and M.A. Hesari, 2008).

There are other variety of dynamic analysis alternatives for concrete dams. Nonetheless, the Finite Element-(Finite Element–Hyper Element)) is used for the thorough analysis of concrete arch dam–reservoir systems. This signifies that the dam is partitioned by solid finite elements, whilst the reservoir is divided into two parts mainly a near field region often having an irregular shape in the area of the dam and a far field region (assuming a uniform channel) that spreads infinitly. The first region is discretized using fluid finite elements, whereas the far field region is represented using a three-dimensional fluid hyper-element (Aftabi Sani & Lotfi, 2007).

Another form of arch dam vibration analysis is the use of structural health monitoring systems which have been connected with static data. This is the situation with dams, which are traditionally outfitted with devices for detecting displacements, stresses, relative movement between joints, and temperatures in order to analyze the structural static behavior (Gomes, 2021).

However, vibration-based health monitoring systems are becoming more prevalent and have been successfully deployed in a variety of big civil engineering projects, including stadiums (Martins et al., 2014) and bridges (Martins et al., 2014). The performance of forced vibration tests on dams, which provide accurate and trustworthy results (Gomes et al., 2018), has been common and very useful in the past (Pereira et al., 2021), but the installation of vibration-based health monitoring systems on dams is still a rather rare occurrence in the industry (Pereira et al., 2021).

Two dams were investigated, Hitotsuse dam in Japan (Okuma et al., 2008) and the Cabril dam in Portugal. The primary goal of both applications was to track the development of natural frequencies over time, and in order to accomplish this, the first three vibration modes of these structures were tracked for approximately one year in the Japanese and Portuguese cases (Pereira et al., 2021), respectively, over a period of approximately one year. S. Oliveira et al. (Pereira et al., 2020) recently gave an update on the monitoring of the Cabril dam.

S. Pereira has published a study (Pereira et al., 2021) on the vibration-based structural health monitoring of Portugal's Baixo Sabor arch dam, outlining the findings of the several processing stages required to obtain the capacity to identify deterioration of arch dams.

He implemented Automated Operational Modal Analysis (AOMA) to the data collected within the first three years of surveillance, and then studied and minimized the effects of environmental and operational conditions affecting modal properties using a combination of principal components analysis and weighted regression models (Pereira et al., 2021). Lastly, damages are recreated in a numerical model of the dam, and the results are utilized to determine if damage detection techniques are capable of detecting these abnormalities (Pereira et al., 2021).

2.5 Optimisation of Shape and Geometry of the arch

The shape design is one of the key elements in the design of arch dams. The study on optimizing arch dam design began in the late 1960s overseas and in the late 1970s in China, but China has taken the lead in the world at the moment. The purpose of optimization design is to determine the optimal shape of an arch dam given boundary conditions and constraints. This is accomplished through the use of mathematical programming, which overcomes the shortcomings of conventional repetition design methods, such as high work capacity, trivial process, and low efficiency. There are several optimization approaches that have been often utilized in recent years, including the penalty function method, multiplier method, complex method and genetic algorithm, immune evolutionary programming, and annealing algorithm. According to Jalal Akbari (Akbari, Ahmadi & Moharrami, 2011), shape and geometry has a significant impact on the safety and efficiency of arch dams.

Typically, the shape of an arch dam is determined by the designer's experience, model tests, and trial and error techniques. To create a more desirable shape, the designer should choose numerous alternative schemes with varying patterns and adjust them in order to obtain a variety of possible shapes. The final shape is chosen based on design economy, structural concerns, and safety. The dam shape obtained in this manner is practical, but not necessarily optimal or even desirable. Additionally, the design period is somewhat lengthy due to the involvement of trial and error method.

To overcome this problem of trial and error, Fialho (Fialho, 1955) and Serafim (Serafim, 1966) investigated membrane-type solutions that neglected the elasticity and bending stresses of the foundation and addressed just a single, basic loading condition. Rajan (Rajan, 1968), Mohr (Mohr, 1979) and Sharma (Sharma, 1983) substantially developed membrane shell theory solutions that were based on membrane shell theory. Sharpe (Sharpe, 1969) introduced the concept of optimization as a mathematical programming problem.

Additionally, Rickeets and Zienkiewicz (Ricketts & Zienkiewicz, 1975) utilized the finite element approach to conduct stress analysis on arch dam structures and utilized the Sequential Linear Programming method to optimize their design.

Sequential Linear Programming method (SLP) was used to address the optimization problem. Other studies in this subject include those by Rahim (Rahim, 1983), Yao (Yao & Choi, 1989), Guohua (Guohua & Shuyu, 1990). Fanelli (Fanelli, Fanelli & Salvaneschi, 1993) defined a near optimum arch dam form using a neural network method. Maheri (Maheri & Bidokhti, 2001) conducted research on the optimal form using a basic genetic algorithm. Salajegheh et al. (Salajegheh et al., 2008) determined the optimal design using the simultaneous perturbation stochastic approximation (SPSA) approach.

2.6 Structural Design and Construction of the Arch.

2.6.1 Structural Design of the Arch

Structural design of concrete arch dams is a serious challenge, particularly when structural failure can lead to a significant loss of lives and material. The correct design of arch dams in dam engineering is of paramount importance. With optimization approaches being involved, the design may be idealized reliably. In recent years, several researches have been reported on optimizing the design of arch dams (Hamidian & Seyedpoor, 2010).

2.6.1.1 Shape Optimization Design of Arch Dams

The shape of an arch dam is strongly connected to the valley's topography, the condition of the dam's foundation rock mass, and the embedment depth of the dam base. Considerations should be given to the sliding stability and seismic resistance for any given shape of the arch damn. These outcomes are dependent on the optimization method used and the maximum permitted stress level (Wang, 2016). With the advancement of computer technology, mathematical optimization has been primarily used in the design of arch dam shapes. This optimization involves use of mathematical programming which uses the volume of the dam as the objective function to investigate all probable arch types, including the linear parabolic arch and the elliptical arc (Wang, 2016).

2.6.1.2 Dam Base Design

Due to the large water loads carried by arch dams, the foundation and abutments must have an adequate bearing capacity, deformation stiffness, and sliding stability. Thus, one of the critical challenges in designing and constructing of arch dams is determining the geology of the foundations and the topography of the dam base. R. Wang (Wang, 2016) developed a digital model that provides an intuitive visual representation of the spatial relationship between the dam base, the foundation treatment pattern, various rock classes, fault lines, and the major joint sets. With this model applied, the topographical characteristics which set as aid in the design of arch dam foundations, can be determined.

2.6.1.3 Arch Dam Concrete Strength, Sliding Stability, and Overall Dam Safety Design

For a long period of time, the safety requirements for dam design were centred on the safety factor of the dam's concrete strength and the safety factor for the dam abutment's sliding stability. With the advancement of numerical modelling, an examination of the dam's total stability has been widely conducted, taking into account the dam's interaction with the foundation. Along with the strength safety factor of the dam concrete and the sliding safety factor of the dam abutment, the overall safety factor of the dam and abutment is an important component of the safety criterion for arch dam designs (Wang, 1991).

The safety factor for dam’s concrete strength is the ratio of the design standard strength to the allowable stress (Wang, 2016). According to the design standard (DL/T 5346—2006), it should be more than 4.4 for a high arch dams, and the design compressive strength of concrete is established in the design standard (Design Specification for Concrete Arch Dams, DL/T 5346—2006) as the 90-day strength of 15 cm3 concrete specimens with at least 80% passing rate. The recommended concrete's compressive strength design values for arch dams are 40 MPa, 45 MPa, and 40 MPa (Wang, 2016).

The dam abutment's sliding safety factor is computed using the rigid limit equilibrium method (Wang, 2016). The Design standard for concrete arch dams (DL/T 5346—2006) defined the sliding safety factor's calculation and parameters, as well as its design safety control index.
The overall stability safety factor of an arch dam, which refers to the dam's and foundation's capacity to withstand overload as an integrated structure against water pressure, may be calculated using the nonlinear finite element method (FEM) in three dimensional space (Wang, 2016).

2.6.2 Construction of Arch Dams

As stated by the United States Army Corporation of Engineers Division in 1994, some of the considerations taken into account during the construction of an arch dam include but not limited to excavation of foundation, monolith joints, concrete etc.

2.6.2.1 Monolith Joints

Proper construction of arch dams is of paramount importance when considering the effect of thermal stresses which tend to cause cracking in early stages of construction (Lange, 2002). Volumetric deformations occur during construction as a result of the internal temperature rise caused by the heat generated by the cement hydration process. When these deformations are restricted either internally or externally, they can result in the development of significant tensile stresses and, as a result, the cracking of concrete (Conceição et al., 2020). In order to avoid thermal cracking during the construction of arch dams using ordinary concrete, blocks with restricted volumes are required (Concrete dams: control and treatment of cracks. International Commission on Large Dams; 1997, 1997). Arch dams are separated into individual monoliths during construction by means of vertical contraction joints, which are typically spaced by 15–20 m (Conceição et al., 2020).

J. Conceição (Conceição et al., 2020) also investigated the implementation of temperature control measures. One of the most important operations is the circulation of water through embedded coils, which is also utilized to cool the concrete to the proper temperature prior to grouting the contraction joints. He proposed a new approach for simulating the post-cooling effect, in which the heat removal by the cooling coils is replicated by the use of synthetic convective boundaries.

2.6.2.2 Excavation of Foundation

Excavation will necessitate the removal of any weak subsoils until adequate ground conditions can be established that are capable of bearing the pressures applied. When foundations are made of hard rock and blasting is required, extra attention must be paid to the procedure to ensure that the rock foundations are not damaged during the blasting operation.

2.6.2.3 Concrete

The majority of the dam wall is constructed of concrete. It is recommended that special attention be paid to the selection of the kind of formwork and the techniques of moving them. A very significant component of construction is the usage of formwork, because the shape of the concrete will be determined by the shape of the formwork.

If the formwork is not done properly, it has the potential to disintegrate during the concrete pouring process, resulting in the dam wall taking on a shape other than that planned. There are many different forms of formwork available, but the self-lifting cantilever formwork is the most encountered.

2.7 Comprehensive Literature Review Summary

The extensive study of the literature on thin concrete arch dams included topics such as the structural analysis of the arch, optimization of the shape and geometry of the arch, and structural design and construction of the arch. It also addressed the shapes and geometries of the arch dams as well as numerical modelling of arch dams.

Research by Dias et al. (1997) has shown the significance of arch dam geometry and how single and double curvature arch dams respond differently to hydrostatic pressure. Zhao and Wu (2021) research have shown the importance of numerical modelling on evaluating structural deformations that consistently and intuitively represent the dam's operating regime. Further literature was conducted on buckling behaviour of arch dams which is the focus of this current study and has shown that buckling of arch dams is a subset of the more fundamental issue of shell buckling. G. Papadakis (2008) offered an analytical solution for the buckling of thick cylindrical shells subjected to external pressure, whilst A. Zingoni et al. (2013) used FEM modelling to investigate the effect of critical buckling pressure on cylindrical and elliptic-paraboloidal arch dams. However, research paper by A. Zingoni et al. (2013) did not investigate arch dams having linear and quadratic varying thickness built in triangular and trapezoidal valleys. The current study will assess the effect of key parameters on the critical buckling pressure of cylindrical and elliptic-paraboloidal arch dams having linear and quadratic varying thickness and built in triangular and trapezoidal valleys.

3. Modelling

3.1 Introduction

A finite element model of the concrete arch dam was built using the ABAQUS finite element program. In this research, three idealized dam valley shapes (see Fig. 3.1) were explored. For each dam valley, buckling analysis was performed on arch dams having linear and quadratic varying thickness built in triangular and trapezoidal-valleys in order to determine the effect of shell curvature, shell geometry, and thickness variation on the dam's buckling behaviour.

Arch dams with single and double curvature were modelled for each valley shape in an attempt to better understand the buckling behaviour of a concrete dam with shell curvature as one of the influencing elements. Also, the thickness variation of the arch, which is crucial, was taken into account by considering dams with constant, linear and quadratic thickness variation.

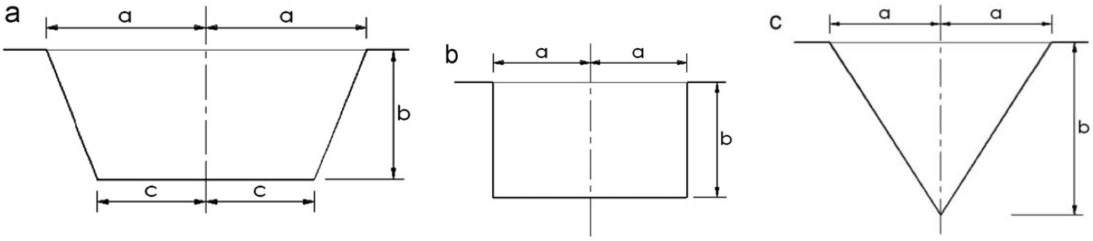

Figure 3.1. Idealised dam valley shapes: a. Trapezoidal shape, b. Rectangular shape, c. Triangular shape (Zingoni et al., 2013).

For concrete arch dam, the following material properties were assumed

- $E = 28 \times 10^9$ N/m^2 – Young's modulus.
- $\nu = 0.15$ – Poisson's ratio.

The arch was modelled using thick, double-curved, quadrilateral shell elements with 8 nodes and reduced integration. The edges were completely restrained (see Fig 3.2), with the exception of the top edge (free). Then, an analysis of linear eigenvalue buckling was performed. The hydrostatic loading was simulated using a triangular variation of loading with a value of zero at the top and 1 kN at the base of the wall. Multiples of this applied loading were then used to calculate the necessary eigenvalues (buckling loads).

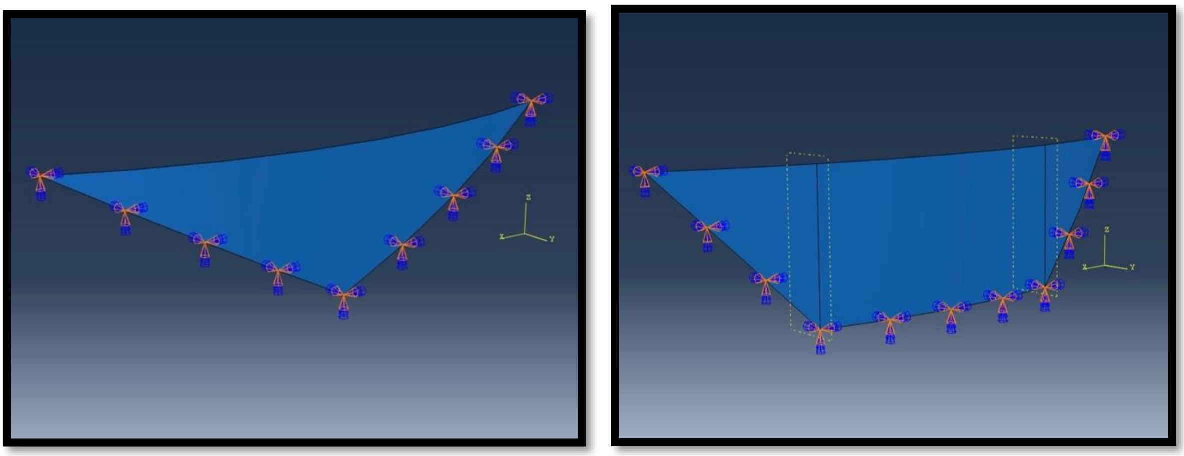

Figure 3.2: Boundary Conditions for both Triangular and Trapezoidal Valley.

3.2 Modelling Concrete Arch Dams with Single Curvature

First, we will concentrate on arch dams with single curvature that are built in a rectangular, triangular and trapezoidal valley (Fig. 3.1a-c) with the modelling incorporated using the *shell extrusion* technique. The horizontal bulge of the shell relative to the vertical plane linking the left and right abutments (Fig. 3.3) is referred to as the rise (h) of the shell. As illustrated in the 2013 paper by (Zingoni et al., 2013), the ratio b/a will be known as the aspect ratio of the dam, whilst the ratio h/a will be known as the rise ratio of the shell. For the single curvature buckling analysis, the shell's thickness is considered to be constant (triangular and trapezoidal valley) and also to vary linearly and quadratically (rectangular, triangular and trapezoidal valley).

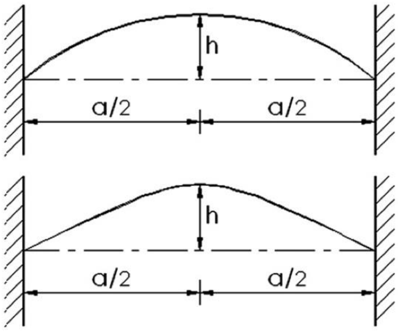

Figure 3.3 Circular and Parabolic arch plan view. (Zingoni et al., 2013).

In the 2013 paper by (Zingoni et al., 2013) Arch dams with single curvature built in rectangular valley (Fig. 3.1b) was only analysed for the shell having constant thickness. In this paper the study is carried further by analysing arch dams with single curvature built in rectangular valley with the shell thickness varying linearly and quadractically.

The dam is considered to be completely filled with water with a unit weight of 10 kN/m3. As stated previously, we wish to explore the dependence of shell curvature, shell geometry, and variation in shell thickness on the shell arch's buckling behavior.

Arch dams with single curvature having triangular or trapezoidal valley shape were modelled for constant, linear and quadratic varying thickness. A comprehensive numerical research was undertaken as a research study. With the parameter *a* fixed at 50m, The aspect ratio b/a for arch dams with constant and linearly varying thickness was varied from 0.25 to 2.0 in intervals of 0.25 and from 0.50 to 2.0 in intervals of 0.50 for the parameter *a* fixed at 100m, whereas the aspect ratio b/a for arch dams with quadratic varying thickness was varied from 0.50 to 2.0 in intervals of 0.50 with *a* fixed at 50m and 100m.

For arch dams with constant thickness, the critical buckling pressure was calculated for each aspect ratio using three different thickness parameter values (0.5 m, 1.0 m, 2.0 m) and three representative rise ratio values (5%, 10%, 25%) for a total of 144 cases.

Similarly, for arch dams with linearly varying thickness, the critical buckling pressure was calculated for each aspect ratio using a generic linear equation to get the thickness. First, two cases were assumed with t_1 = 0.5m at the top of the dam and t_2 = 1.0m at the base of the dam (see Fig 3.4) and the second case assumes t_1 = 1.0m at the top of the dam and t_2 = 2.0m at the base of the dam.

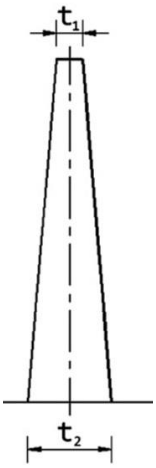

Figure 3.4: Linear varying thickness profile of the arch dam. (Zingoni et al., 2013).

The following single curvature linear equations were derived using ABAQUS model space in the z-y plane for each aspect ratio. The detailed derivation can be accessed in appendix A1.

Case 1 (a=50m): with $t_1 = 0.5m$ & with $t_2 = 1.0m$

- Aspect Ratio 0,25: $-0.04Z + 1.0$ …… (3.41a)
- Aspect Ratio 0,50: $-0.02Z + 1.0$ …… (3.42a)
- Aspect Ratio 0,75: $-(1/75)Z + 1.0$ …… (3.43a)
- Aspect Ratio 1,0: $-0.01Z + 1.0$ …… (3.44a)
- Aspect Ratio 1,25: $-0.008Z + 1.0$ …… (3.45a)
- Aspect Ratio 1,50: $-(1/150)Z + 1.0$ …… (3.46a)
- Aspect Ratio 1,75: $-(1/175)Z + 1.0$ …… (3.47a)
- Aspect Ratio 2,00: $-0.005Z + 1.0$ …… (3.48a)

Case 2(a=50m): with $t_1 = 1.0m$ & with $t_2 = 2.0m$

- Aspect Ratio 0,25: $-0.08Z + 2.0$ …… (3.41b)
- Aspect Ratio 0,50: $-0.04Z + 2.0$ …… (3.42b)
- Aspect Ratio 0,75: $-(2/75)Z + 2.0$ …… (3.43b)
- Aspect Ratio 1,0: $-0.02Z + 2.0$ …… (3.44b)
- Aspect Ratio 1,25: $-0.016Z + 2.0$ …… (3.45b)
- Aspect Ratio 1,50: $-(2/150)Z + 2.0$ …… (3.46b)
- Aspect Ratio 1,75: $-(2/175)Z + 2.0$ …… (3.47b)
- Aspect Ratio 2,00: $-0.01Z + 2.0$ …… (3.48b)

Case 1 (a=100m): with $t_1 = 0.5m$ & with $t_2 = 1.0m$

- Aspect Ratio 0,50: $-0.01Z + 1.0$ …… (3.41c)
- Aspect Ratio 1,00: $-0.005Z + 1.0$ …… (3.42c)
- Aspect Ratio 1,50: $-(1/300)Z + 1.0$ …… (3.43c)
- Aspect Ratio 2,00: $-0.0025Z + 1.0$ …… (3.44c)

Case 2 (a=100m): with $t_1 = 1.0m$ & with $t_2 = 2.0m$

- Aspect Ratio 0,50: $-0.02Z + 2.0$ …… (3.41d)
- Aspect Ratio 1,00: $-0.01Z + 2.0$ …… (3.42d)
- Aspect Ratio 1,50: $-(1/150)Z + 2.0$ …… (3.43d)
- Aspect Ratio 2,00: $-0.005Z + 2.0$ …… (3.44d)

For arch dams with quadratic varying thickness depicting a concave shape, the critical buckling pressure was computed for each aspect ratio using a quadratic equation in the z-y plane to determine the thickness expression. Similarly, two cases were assumed with t_1 = 0.5m at the dam's crest and t_2 = 1.0m at the dam's base (see Fig. 3.5), while the second case assumes t_1 = 1.0m at the dam's crest and t_2 = 2.0m at the dam's base.

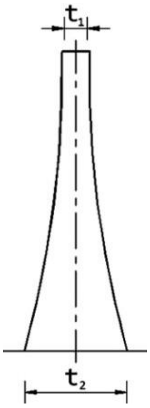

Figure 3.5: Quadratic varying thickness profile of the arch dam. (Zingoni et al., 2013).

For each aspect ratio, the following single curvature quadratic equations were derived using the ABAQUS model space in the z-y plane. The detailed derivation is available in appendix B1.

Case 1 (a=50m): with t_1 = 0.5m & with t_2 = 1.0m

- Aspect Ratio 0,50: $0.0008(Z-25)^2+0.5$………………………………………….…..(3.51a)
- Aspect Ratio 1,00: $0.0002(Z-50)^2+0.5$………………………………………….…..(3.52a)
- Aspect Ratio 1,50: $(1/11250)(Z-75)^2+0.5$……………………………………...(3.53a)
- Aspect Ratio 2,00: $0.00005(Z-100)^2+0.5$……………………………………….…..(3.54a)

Case 2 (a=50m): with t_1 = 1.0m & with t_2 = 2.0m

- Aspect Ratio 0,50: $2(0.0008(Z-25)^2+0.5)$………………………………………….…..(3.51b)
- Aspect Ratio 1,00: $2(0.0002(Z-50)^2+0.5)$………………………………………….…..(3.52b)
- Aspect Ratio 1,50: $2((1/11250)(Z-75)^2+0.5)$……………………………………...(3.53b)
- Aspect Ratio 2,00: $2(0.00005(Z-100)^2+0.5)$……………………………………….…..(3.54b)

Case 1 (a=100m): with t_1 = 0.5m & with t_2 = 1.0m

- Aspect Ratio 0,50: $0.0002(Z-50)^2+0.5$……………………………………….…….(3.51c)
- Aspect Ratio 1,00: $0.00005(Z-100)^2+0.5$………………………………………..(3.52c)
- Aspect Ratio 1,50: $(1/45000)(Z-150)^2+0.5$……………………………………...(3.53c)
- Aspect Ratio 2,00: $0.0000125(Z-200)^2+0.5$……………………………...…..(3.54c)

Case 2 (a=100m): with t_1 = 1.0m & with t_2 = 2.0m

- Aspect Ratio 0,50: $2(0.0002(Z - 50)^2 + 0.5)$…………………………………....…..(3.51d)
- Aspect Ratio 1,00: $2(0.00005(Z - 100)^2 + 0.5)$……………………………….…..(3.52d)
- Aspect Ratio 1,50: $2((1/45000)(Z - 150)^2 + 0.5)$…………………………………....(3.53d)
- Aspect Ratio 2,00: $2(0.0000125(Z - 200)^2 + 0.5)$………………………....……...(3.54d)

When encoding each linear and quadratic equation into the ABAQUS software, the thickness was assigned to each structural member using the expression field technique and the element distribution method with the Section thickness selected as one of the Field output requests.

3.3 Modelling Concrete Arch Dams with Double Curvature

To better interpret the effect of double curvature with shells depicting elliptical paraboloid and parabolic cylinder mathematical functions buckling analysis was also performed on arch dams that are constructed in a valley that is triangular and trapezoidal (Fig. 3.1a and c) using the *shell revolution* technique. For the double curvature buckling analysis, the shell's thickness is assumed to be constant and to vary both linearly and quadratically. Regarding this analysis, the parameter *a* was only fixed at 50m, with the aspect ratio b/a for arch dams with constant and linearly varying thickness varying from 0.25 to 2.0 in intervals of 0.25, and the aspect ratio b/a for arch dams with quadratic varying thickness varying from 0.50 to 2.0 in intervals of 0.50.

For arch dams with constant thickness, the critical buckling pressure was computed using similar three distinct thickness parameter values as in single curvature analysis (0.5 m, 1.0 m, 2.0 m) and three representative rise ratio values (5%, 10%, 25%).

The mathematical description for a general paraboloid (elliptic paraboloid) in a 3D quadratic surface is given by:

$$\frac{x^2}{a^2} + \frac{y^2}{b^2} = z \qquad (3)$$

where:

a & b = The radii in the *x* and *y* direction respectively for the arch.

For a paraboloid of revolution, a = b, therefore intersections of the surface with planes above and parallel to the x-y plane produce traces of circles. For a elliptic paraboloid, a ≠ b, which means intersections with planes parallel to the x-y plane form traces of ellipses, and the surface is an elliptical paraboloid.

The critical buckling pressure for arch dams with linear and quadratic varying thickness was determined for each aspect ratio using the respective conventional linear and quadratic equations to obtain the thickness expression. The first case assumes t_1 = 0.5m at the dam's crest and t_2 = 1.0m at the dam's base, whereas the second case assumes t_1 = 1.0m at the dam's crest and t_2 = 2.0m at the dam's base.

Using figure 3.4, the following double curvature linear equations were derived using ABAQUS model space in the z-y plane for each aspect ratio. The detailed derivation can be accessed in appendix A2.

Case 1 (a=50m): with t_1 = 0.5m & with t_2 = 1.0m

- Aspect Ratio 0,25: $-0.04Z + 0.75$……………………………………………… (3.41e)
- Aspect Ratio 0,50: $-0.02Z + 0.75$……………………………………………… (3.42e)
- Aspect Ratio 0,75: $-(1/75)Z + 0.75$…………………………………………..….(3.43e)
- Aspect Ratio 1,0: $-0.01Z + 0.75$………………………………..……………...(3.44e)
- Aspect Ratio 1,25: $-0.008Z + 0.75$…………………………..…………………(3.45e)
- Aspect Ratio 1,50: $-(1/150)Z + 0.75$………………………………..……....(3.46e)
- Aspect Ratio 1,75: $-(1/175)Z + 0.75$……………………………………………..(3.47e)
- Aspect Ratio 2,00: $-0.005Z + 0.75$……………………………………………….(3.48e)

Case 2(a=50m): with t_1 = 1.0m & with t_2 = 2.0m

- Aspect Ratio 0,25: $-0.08Z + 1.5$………………………………………………… (3.41f)
- Aspect Ratio 0,50: $-0.04Z + 1.5$………………………………………………… (3.42f)
- Aspect Ratio 0,75: $-(2/75)Z + 1.5$……………………………………………..(3.43f)
- Aspect Ratio 1,0: $-0.02Z + 1.5$…………………………………………………...(3.44f)
- Aspect Ratio 1,25: $-0.016Z + 1.5$…………………………………………………(3.45f)
- Aspect Ratio 1,50: $-(2/150)Z + 1.5$……………………………………………….(3.46f)
- Aspect Ratio 1,75: $-(2/175)Z + 1.5$……………………………………………….(3.47f)
- Aspect Ratio 2,00: $-0.01Z + 1.5$…………………………….....…………...(3.48f)

Using figure 3.5, the following double curvature quadratic equations were derived using ABAQUS model space in the z-y plane for each aspect ratio. The detailed derivation can be accessed in appendix B2.

Case 1 (a=50m): with t_1 = 0.5m & with t_2 = 1.0m

- Aspect Ratio 0,50: $0.0008(Z - 12.5)^2 + 0.5$……………………………………….…....(3.51e)
- Aspect Ratio 1,00: $0.0002(Z - 25)^2 + 0.5$…………………………………….……...(3.52e)
- Aspect Ratio 1,50: $(1/11250)(Z - 37.5)^2 + 0.5$…………………………………….…...(3.53e)
- Aspect Ratio 2,00: $0.00005(Z - 50)^2 + 0.5$……………………………………..........(3.54e)

Case 2 (a=50m): with t_1 = 1.0m & with t_2 = 2.0m

- Aspect Ratio 0,50: $2(0.0008(Z - 12.5)^2 + 0.5)$……………………………….….…..(3.51f)
- Aspect Ratio 1,00: $2(0.0002(Z - 25)^2 + 0.5)$……………………………………..…..(3.52f)
- Aspect Ratio 1,50: $2((1/11250)(Z - 37.5)^2 + 0.5)$…………………………………...(3.53f)
- Aspect Ratio 2,00: $2(0.00005(Z - 50)^2 + 0.5)$………………………..………..…..(3.54f)

3.4 Finite Element Model Calibration

Elastic linear buckling analysis was implemented to seek both model validation and mesh convergence. Table 3.1 and 3.2 compares the results with those obtained by (Zingoni et al., 2013) for various element sizes (quadrilateral shell elements with 8 nodes) and b/a aspect ratios. The created finite element model demonstrated convergence at element sizes of 1 m for single curvature analysis and 0.6 m for double curvature analysis, which were subsequently utilized for all models.

	b/a		
	0.50	1	1,5
Element Size(m)	**Load Factor (LF)**		
10	37,0	8,8	4,3
5	33,1	8	4
2.5	32.9	8	4
1	32.8	8	4
Zingoni et al.	32.8	8	4

Table 3.1: Mesh Sensitivity Analysis for Single Curvature

	b/a		
	0,50	0,75	1
Element Size(m)	**Load Factor (LF)**		
10	40,7	15,9	9,5
5	32,7	14,6	8,8
2.5	32,7	14,5	8,7
1	32,7	14,4	8,4
0,6	-	13,9	8,1
Zingoni et al.	32.8	13,8	8

Table 3.2: Mesh Sensitivity Analysis for Double Curvature

Figure 3.6a-c below shows the buckling modes and the mesh convergence modelling with the respective mesh sizes discussed in the above tables.

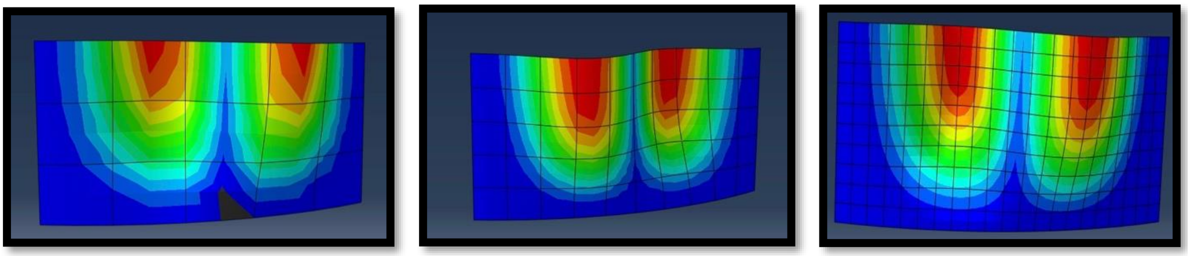

Figure 3.6a-c: (a) Element size 10, (b) Element size 5, (c) Element size 2.5

As depicted in Figure 3.7 and 3.8, the critical load factors generated by the current model were compared to those obtained from (Zingoni et al., 2013). This is accomplished over a useful range of aspect ratios, namely 0.5 ≤ b/a ≤ 1.5 for single curvature and 0.5 ≤ b/a ≤ 1.0 for double curvature. A 10% rise ratio is evaluated. Figure 3.7 and 3.8 illustrates results that are nearly identical to those reported by (Zingoni et al., 2013). The conclusions of this analysis are based on the premise that the dam’s wall thickness is 1 m along its height.

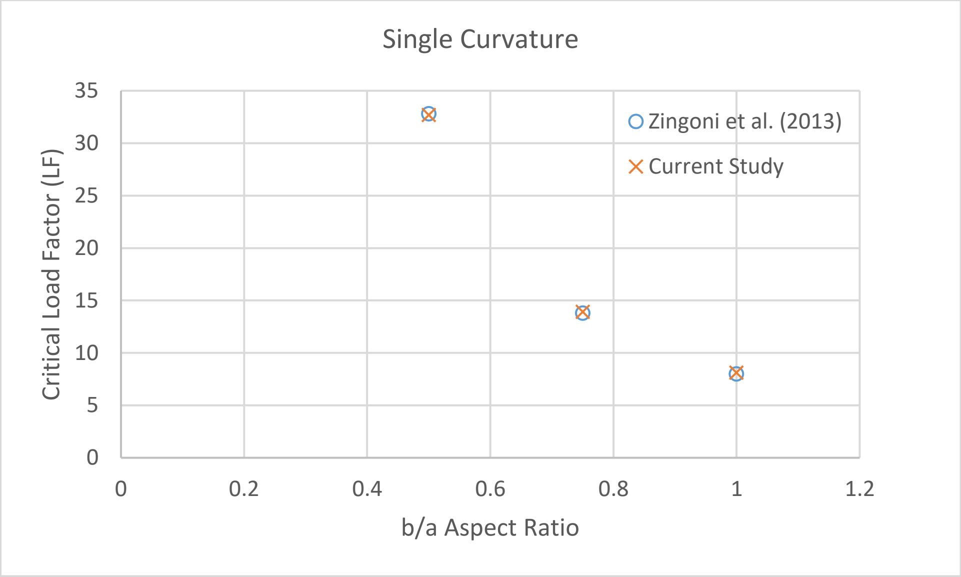

Figure 3.7: Critical Load Factor vs. b/a Aspect Ratio – Single Curvature.

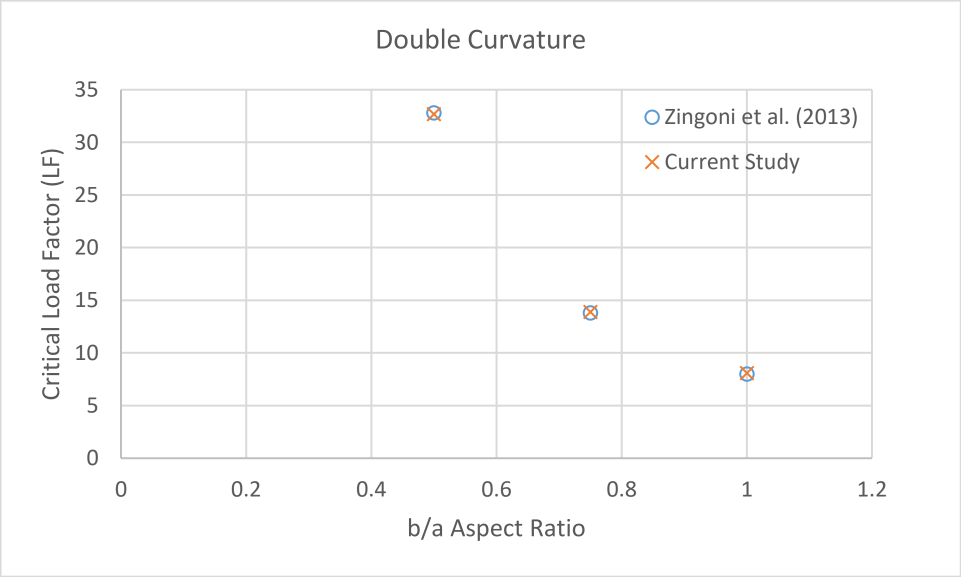

Figure 3.8: Critical Load Factor vs. b/a Aspect Ratio – Double Curvature.

3.5 Concluding Remarks

The comparison of critical load factors obtained from the current model and those obtained from Zingoni et al. (2013) was conducted, as depicted in Figure 3.7 and 3.8. Figure 3.7 and 3.8 illustrates similar findings to those found by Zingoni et al. (2013) with the difference margin less than 0.1%. The findings presented in this study are predicated on the assumption of a constant wall thickness across the vertical extent of the dam. Therefore, based on the successful calibration of the finite element model employed in the present study, it can be concluded that the findings reported in chapter 4 possess validity and can serve as a reliable set of design parameters for the purpose of thin concrete arch dam design.

4. Results and Analysis

4.1 Results for Single Curvature Modelling

4.1.1 Single Curvature Modelling with Constant Thickness

Figure 4.1 depicts typical mode shapes for the triangular circular and parabolic arch profile, while Figure 4.2 depicts mode shapes for the trapezoidal circular and parabolic arch profile. For trapezoidal and triangular arch dams, the results for the critical buckling pressures for the various cases that were analysed revealed that there is very little difference between the corresponding results for the parabolic and circular profiles, similar to the results published by Zingoni for rectangular arch dams.

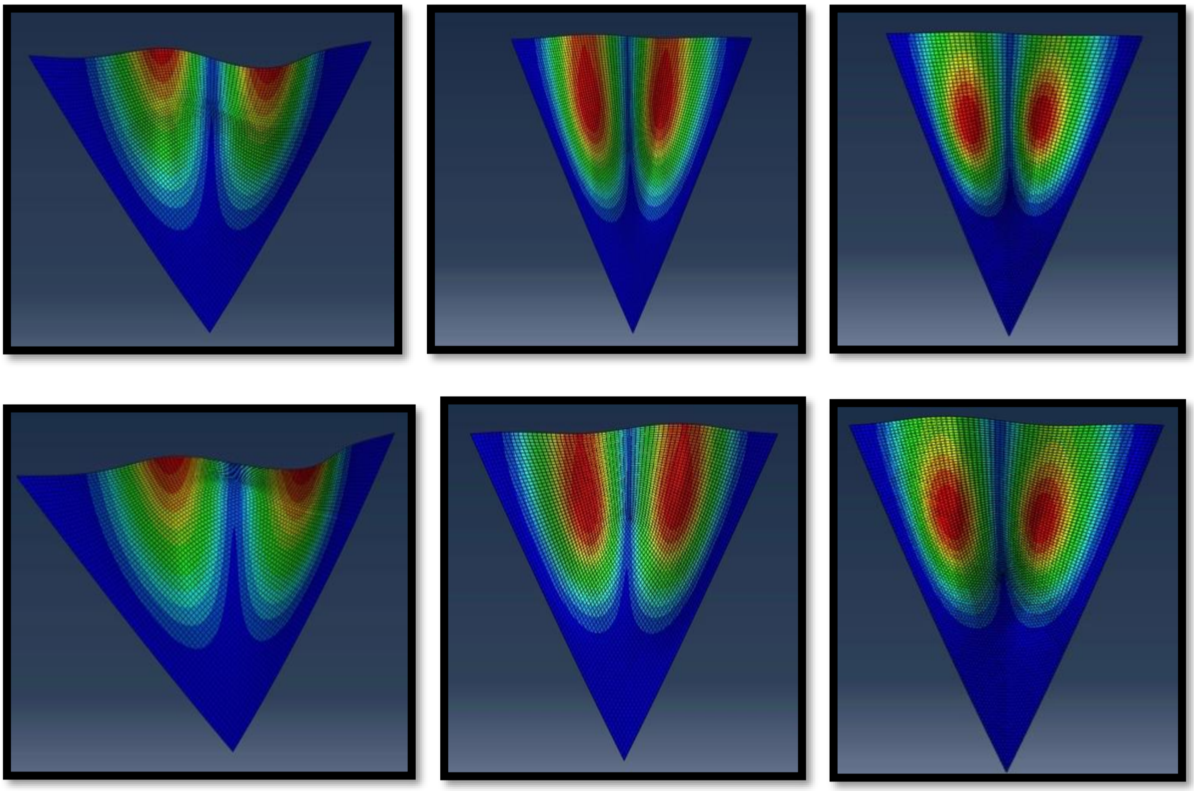

Figure 4.1: Triangular-valley arch dam buckling mode shapes for *a* = 50m, h=10% and t=1.0m for circular arch (first three mode shapes with b/a=0.50, 1.0, and 1.50 respectively) and parabolic arch (last three mode shapes with b/a=0.50, 1.0, and 1.50 respectively).

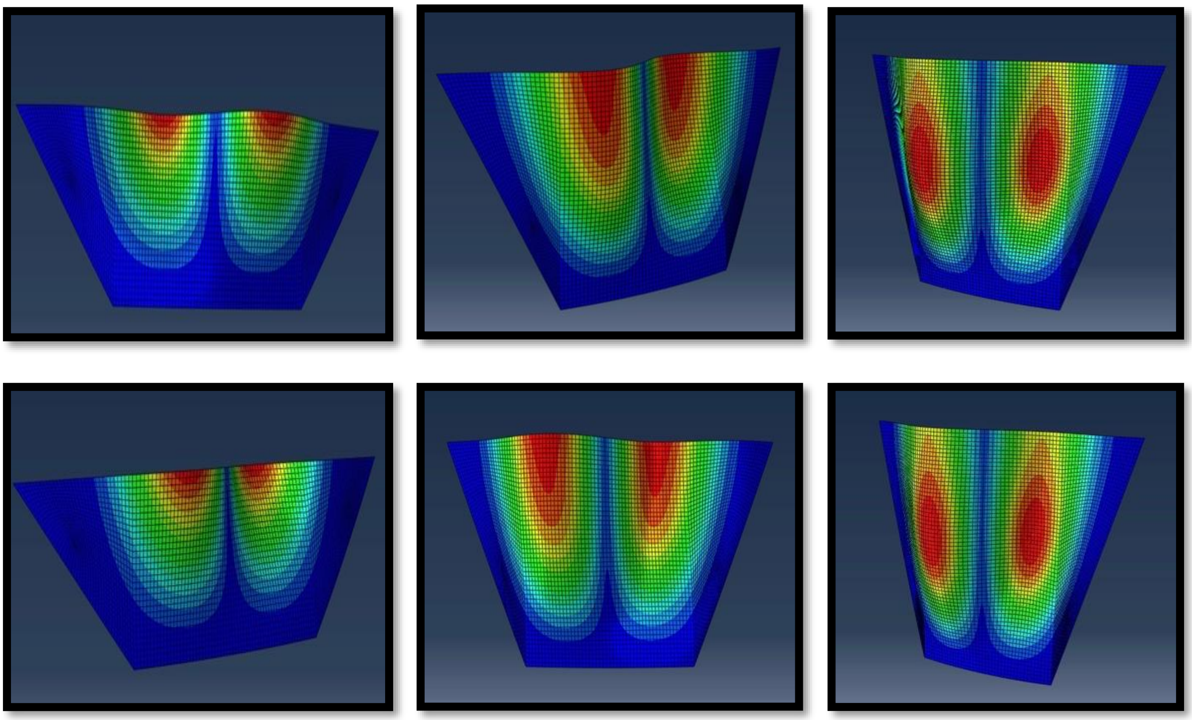

Figure 4.2: Trapezoidal-valley arch dam buckling mode shapes for *a* = 50m, h=10% and t=1.0m for circular arch (first three mode shapes with b/a=0.50, 1.0, and 1.50 respectively) and parabolic arch (last three mode shapes with b/a=0.50, 1.0, and 1.50 respectively).

The tables 4.11(a)-(i) and 4.12(a)-(i) compare the buckling pressures for the triangular and trapezoidal-valley arch dams respectively, between the circular and parabolic profiles, assuming t is constant (0.5m, t=1.0m, t=2.0m) for three representative rise ratio values (5%, 10%, 25%).

t=1.0m; h=10% - Triangular						
Critical Buckling Pressure Pcr (kN/m2)						
	a=100m			**a=50m**		
b/a	**Circular**	**Parabola**	**Diff. %**	**Circular**	**Parabola**	**Diff. %**
0,25	5850,5	5977,5	2,12	63963	64362	0,62
0,5	2957,1	3020,8	2,11	24062	24375	1,28
0,75	2118,6	2164,6	2,13	18010	18205	1,07
1	1755,5	1794,6	2,18	14978	15148	1,12
1,25	1517,5	1556	2,47	12865	13077	1,62
1,5	1400,7	1436,5	2,49	11876	12083	1,71
1,75	1322,9	1356,7	2,49	11228	11431	1,78
2	1267,8	1300,3	2,50	10775	10975	1,82

Table 4.11(a): Results of circular vs. parabolic arch for t=1m and h=10%

t=0.5m; h=10% - Triangular						
Critical Buckling Pressure Pcr (kN/m2)						
	a=100m			a=50m		
b/a	**Circular**	**Parabola**	**Diff. %**	**Circular**	**Parabola**	**Diff. %**
0,25	747,9	772,58	3,19	5850,3	5977,7	2,13
0,5	387,97	400,68	3,17	2957,1	3020,7	2,11
0,75	290,71	300,3	3,19	2118,6	2164,8	2,13
1	244,66	252,56	3,13	1755,6	1794,5	2,17
1,25	212,26	219,38	3,25	1517,4	1556,4	2,51
1,5	194,3	200,69	3,18	1400,7	1436,9	2,52
1,75	181,71	187,52	3,10	1322,9	1357,1	2,52
2	172,41	177,84	3,05	1267,8	1300,6	2,52

Table 4.11(b): Results of circular vs. parabolic arch for t=0.5m and h=10%

t=2.0m; h=10% - Triangular						
Critical Buckling Pressure Pcr (kN/m2)						
	a=100m			a=50m		
b/a	**Circular**	**Parabola**	**Diff. %**	**Circular**	**Parabola**	**Diff. %**
0,25	63973	64358	0,60	932444	925654	0,73
0,5	24063	24379	1,30	245326	245376	-0,02
0,75	18011	18205	1,07	169257	169819	-0,33
1	14978	15148	1,12	146077	146557	-0,33
1,25	12864	13073	1,60	129345	130315	-0,74
1,5	11876	12080	1,69	120961	121918	-0,78
1,75	11228	11428	1,75	114755	115693	-0,81
2	10775	10972	1,80	110036	110996	-0,86

Table 4.11(c): Results of circular vs. parabolic arch for t=2.0m and h=10%

t=1.0m; h=5% - Triangular						
Critical Buckling Pressure Pcr (kN/m2)						
	a=100m			a=50m		
b/a	**Circular**	**Parabola**	**Diff. %**	**Circular**	**Parabola**	**Diff. %**
0,25	4351,6	4358,7	0,16	75684	75471	0,28
0,5	1646,1	1651,9	0,35	17633	17693	0,34
0,75	1238,2	1241,8	0,29	12275	12292	0,14
1	1030,5	1033,7	0,31	10661	10676	0,14
1,25	913,82	916,87	0,33	9782,5	9795,3	0,13
1,5	843,02	846,04	0,36	9146,9	9159,6	0,14
1,75	796,5	799,57	0,38	8659,8	8672,5	0,15
2	764,05	767,04	0,39	8283,3	8296	0,15

Table 4.11(d): Results of circular vs. parabolic arch for t=1.0m and h=5%

t=0.5m; h=5% - Triangular						
Critical Buckling Pressure Pcr (kN/m2)						
a=100m				a=50m		
b/a	Circular	Parabola	Diff. %	Circular	Parabola	Diff. %
0,25	389,2	391,32	0,54	4351,3	4358,5	0,17
0,5	198,02	199,1	0,54	1633,5	1639,5	0,37
0,75	142,06	142,84	0,55	1228,2	1232,1	0,32
1	117,89	118,55	0,56	1021,9	1025,3	0,33
1,25	104,92	105,53	0,58	906,28	909,62	0,37
1,5	96,962	97,527	0,58	836,22	839,48	0,39
1,75	91,659	92,198	0,58	790,24	793,45	0,40
2	87,897	88,421	0,59	758,08	761,26	0,42

Table 4.11(e): Results of circular vs. parabolic arch for t=0.5m and h=5%

t=2.0m; h=5% - Triangular						
Critical Buckling Pressure Pcr (kN/m2)						
a=100m				a=50m		
b/a	Circular	Parabola	Diff. %	Circular	Parabola	Diff. %
0,25	75694	75472	0,29	1277520	1276030	0,12
0,5	17796	17853	0,32	258473	258394	0,03
0,75	12387	12400	0,10	150878	151068	0,13
1	10753	10765	0,11	123240	123463	0,18
1,25	9866,9	9876,7	0,10	112328	112550	0,20
1,5	9226,9	9236,6	0,11	106205	106417	0,20
1,75	8736	8746	0,11	101579	101759	0,18
2	8356	8366,3	0,12	97557	97721	0,17

Table 4.11(f): Results of circular vs. parabolic arch for t=2.0m and h=5%

t=1.0m; h=25% - Triangular						
Critical Buckling Pressure Pcr (kN/m2)						
a=100m				a=50m		
b/a	Circular	Parabola	Diff. %	Circular	Parabola	Diff. %
0,25	10989	13237	16,98	80391	92883	13,45
0,5	5625,6	6812,1	17,42	39983	45713	12,53
0,75	4224	5120,1	17,50	28621	32749	12,60
1	3556,9	4285,2	17,00	23629	26954	12,34
1,25	3145,9	3761	16,35	20824	23666	12,01
1,5	2862,1	3395,6	15,71	19035	21560	11,71
1,75	2654,4	3127,8	15,14	17804	20112	11,48
2	2496,7	2925	14,64	16913	19064	11,28

Table 4.11(g): Results of circular vs. parabolic arch for t=1.0m and h=25%

t=0.5m; h=25% - Triangular						
Critical Buckling Pressure Pcr (kN/m2)						
a=100m				a=50m		
b/a	Circular	Parabola	Diff. %	Circular	Parabola	Diff. %
0,25	1559,8	1941,4	19,66	10990	13237	16,98
0,5	848,6	1061,2	20,03	5625,6	6812	17,42
0,75	647,65	794,43	18,48	4224,5	5120	17,49
1	546,09	659,64	17,21	3557,4	4285	16,98
1,25	485,7	580,86	16,38	3146,3	3761	16,34
1,5	446,95	531,36	15,89	2862,2	3396	15,71
1,75	420,89	498,79	15,62	2654,5	3128	15,13
2	400,94	476,53	15,86	2497	2925	14,63

Table 4.11(h): Results of circular vs. parabolic arch for t=0.5m and h=25%

t=2.0m; h=25% - Triangular						
Critical Buckling Pressure Pcr (kN/m2)						
a=100m				a=50m		
b/a	Circular	Parabola	Diff. %	Circular	Parabola	Diff. %
0,25	80390	92898	13,46	713902	744752	4,14
0,5	39984	45715	12,54	290726	315673	7,90
0,75	28619	32750	12,61	210586	226116	6,87
1	23628	26955	12,34	172705	185987	7,14
1,25	20823	23666	12,01	152290	164620	7,49
1,5	19034	21560	11,72	139917	151695	7,76
1,75	17804	20111	11,47	131765	143158	7,96
2	16912	19065	11,29	126044	137172	8,11

Table 4.11(i): Results of circular vs. parabolic arch for t=2.0m and h=25%

t=1.0m; h=10% - Trapezoidal						
Critical Buckling Pressure Pcr (kN/m2)						
a=100m				a=50m		
b/a	Circular	Parabola	Diff. %	Circular	Parabola	Diff. %
0,25	2841,7	2897,4	1,92	23324	23517	0,82
0,5	1395,9	1423,5	1,94	10270	10349	0,76
0,75	952,19	971,75	2,01	7264,9	7336,1	0,97
1	775,88	792,56	2,10	6112,1	6183,7	1,16
1,25	690,37	705,61	2,16	5577,8	5647,5	1,23
1,5	642,71	657,05	2,18	5288,7	5356,5	1,27
1,75	613,28	626,9	2,17	5113,2	5179,2	1,27
2	593,65	606,9	2,18	4996,9	5061,4	1,27

Table 4.12(a): Results of circular vs. parabolic arch for t=1.0m and h=10%

t=0.5m; h=10% - Trapezoidal						
Critical Buckling Pressure Pcr (kN/m2)						
a=100m				a=50m		
b/a	Circular	Parabola	Diff. %	Circular	Parabola	Diff. %
0,25	408	418,45	2,50	2841,7	2894,9	1,84
0,5	195,59	200,69	2,54	1395,8	1422,8	1,90
0,75	146,72	150,86	2,74	952,1	971,02	1,95
1	127,32	131,03	2,83	775,83	791,63	2,00
1,25	108,18	111,18	2,70	690,34	704,54	2,02
1,5	96,18	98,78	2,63	642,7	655,88	2,01
1,75	88,39	90,74	2,59	613,28	625,76	1,99
2	83,12	85,3	2,56	593,66	605,62	1,97

Table 4.12(b): Results of circular vs. parabolic arch for t=0.5m and h=10%

t=2.0m; h=10% - Trapezoidal						
Critical Buckling Pressure Pcr (kN/m2)						
a=100m				a=50m		
b/a	Circular	Parabola	Diff. %	Circular	Parabola	Diff. %
0,25	23323	23538	0,91	278000	276287	0,62
0,5	10270	10364	0,91	90305	90407	0,11
0,75	7265	7351,4	1,18	71017	71084	0,09
1	6112,1	6198,5	1,39	61657	61737	0,13
1,25	5577,8	5662,4	1,49	56507	56600	0,16
1,5	5288,6	5371,4	1,54	53567	53674	0,20
1,75	5113,3	5194,3	1,56	51747	51863	0,22
2	4996,9	5076,6	1,57	50516	50638	0,24

Table 4.12(c): Results of circular vs. parabolic arch for t=2.0m and h=10%

t=1.0m; h=5% - Trapezoidal						
Critical Buckling Pressure Pcr (kN/m2)						
a=100m				a=50m		
b/a	Circular	Parabola	Diff. %	Circular	Parabola	Diff. %
0,25	1547,7	1551,7	0,26	19834	19809	0,13
0,5	687,13	689,09	0,28	6343,4	6349,6	0,10
0,75	486,46	488,28	0,37	5025,5	5030,7	0,10
1	409,73	411,52	0,43	4361,6	4366,8	0,12
1,25	374,21	375,96	0,47	3994	3999,2	0,13
1,5	354,98	356,71	0,48	3785,3	3790,7	0,14
1,75	343,33	345	0,48	3656,5	3664	0,20
2	335,6	337,26	0,49	3569,5	3575,1	0,16

Table 4.12(d): Results of circular vs. parabolic arch for t=1.0m and h=5%

t=0.5m; h=5% - Trapezoidal						
Critical Buckling Pressure Pcr (kN/m2)						
	a=100m			a=50m		
b/a	Circular	Parabola	Diff. %	Circular	Parabola	Diff. %
0,25	187,09	188,08	0,53	1548,1	1551,8	0,24
0,5	91,91	92,4	0,53	687,48	689,11	0,24
0,75	62,77	63,12	0,55	486,77	488,28	0,31
1	51,26	51,57	0,60	410,03	411,53	0,36
1,25	45,69	45,97	0,61	374,51	375,96	0,39
1,5	42,57	42,84	0,63	355,29	356,71	0,40
1,75	40,64	40,89	0,61	343,63	345,01	0,40
2	39,35	39,59	0,61	335,91	337,27	0,40

Table 4.12(e): Results of circular vs. parabolic arch for t=0.5m and h=5%

t=2.0m; h=5% - Trapezoidal						
Critical Buckling Pressure Pcr (kN/m2)						
	a=100m			a=50m		
b/a	Circular	Parabola	Diff. %	Circular	Parabola	Diff. %
0,25	19824	19809	0,08	378474	377264	0,32
0,5	6338,3	6349,6	0,18	80204	80332	0,16
0,75	5020,6	5030,7	0,20	58909	59046	0,23
1	4356,8	4366,7	0,23	52019	52117	0,19
1,25	3989,4	3999,2	0,25	47149	47213	0,14
1,5	3780,7	3790,6	0,26	43898	43956	0,13
1,75	3652	3662	0,27	41812	41870	0,14
2	3565	3575	0,28	40421	40481	0,15

Table 4.12(f): Results of circular vs. parabolic arch for t=2.0m and h=5%

t=1.0m; h=25%						
Critical Buckling Pressure Pcr (kN/m2)						
	a=100m			a=50m		
b/a	Circular	Parabola	Diff. %	Circular	Parabola	Diff. %
0,25	10989	13237	16,98	80391	92883	13,45
0,5	5625,6	6812,1	17,42	39983	45713	12,53
0,75	4224	5120,1	17,50	28621	32749	12,60
1	3556,9	4285,2	17,00	23629	26954	12,34
1,25	3145,9	3761	16,35	20824	23666	12,01
1,5	2862,1	3395,6	15,71	19035	21560	11,71
1,75	2654,4	3127,8	15,14	17804	20112	11,48
2	2496,7	2925	14,64	16913	19064	11,28

Table 4.12(g): Results of circular vs. parabolic arch for t=1.0m and h=25%

t=0.5m; h=25%						
Critical Buckling Pressure Pcr (kN/m2)						
	a=100m			a=50m		
b/a	Circular	Parabola	Diff. %	Circular	Parabola	Diff. %
0,25	989,14	1151	14,06	6520,2	7429,8	12,24
0,5	504,39	594	15,09	3105,8	3559,8	12,75
0,75	369,15	433	14,75	2236,9	2576,1	13,17
1	290,48	336	13,55	1897,9	2200,9	13,77
1,25	249,42	290	13,99	1738,2	2200	20,99
1,5	227,41	267	14,83	1557	1790,5	13,04
1,75	214,6	251	14,50	1404,6	1605	12,49
2	206,38	239	13,65	1296,5	1475,9	12,16

Table 4.12(h): Results of circular vs. parabolic arch for t=0.5m and h=25%.

t=2.0m; h=25%						
Critical Buckling Pressure Pcr (kN/m2)						
	a=100m			a=50m		
b/a	Circular	Parabola	Diff. %	Circular	Parabola	Diff. %
0,25	43543	48433	10,10	325431	349036	6,76
0,5	21108	23688	10,89	143391	151601	5,42
0,75	14941	16757	10,84	98433	105069	6,32
1	11900	13252	10,20	81132	87687	7,48
1,25	10308	11520	10,52	73039	79521	8,15
1,5	9396,7	10580	11,18	68658	75044	8,51
1,75	8834,1	9886	10,64	66011	72296	8,69
2	8463,9	9410	10,05	64264	70457	8,79

Table 4.12(i): Results of circular vs. parabolic arch for t=2.0m and h=25%.

The difference between circular and parabolic arch profile results for the triangular-valley arch dam is less than 0.45%, 2.6%, and 17.5% for the 5%, 10%, and 25% rise ratios regarding the 50 m wide dam respectively, and less than 0.60 %, 2.5 %, and 20.04% regarding the 100 m wide dam respectively. The same case applies to the trapezoidal-valley arch dam having similar arch profile differences regarding the three rise ratio parameters. With this being said , it is acceptable to only consider the results for the parabolic arch for rise ratio values lying below 10% for both geometric valleys.

Figures 4.3–4.8 represent the results obtained for the critical buckling pressure pcr (in kN/ m2) corresponding to the respective aspect ratio b/a values. The first three figures (Figs. 4.3-4.5) represent shell-thickness values of 0.5 m, 1.0 m, and 2.0 m for the triangular-valley arch dam with the *a* parameter fixed at 50m and 100m whereas the next three figures represent the trapezoidal-valley arch dam results with the same shell-thickness and *a* parameter values. Each plot contains three curves that correspond to the three h/a rising ratio values (5%, 10%, and 25%). The straight dashed line is the hydrostatic-pressure line representing the water pressure at the base of the dam wall corresponding to the respective b value, assuming a unit weight of water of 10 kN/m^3.

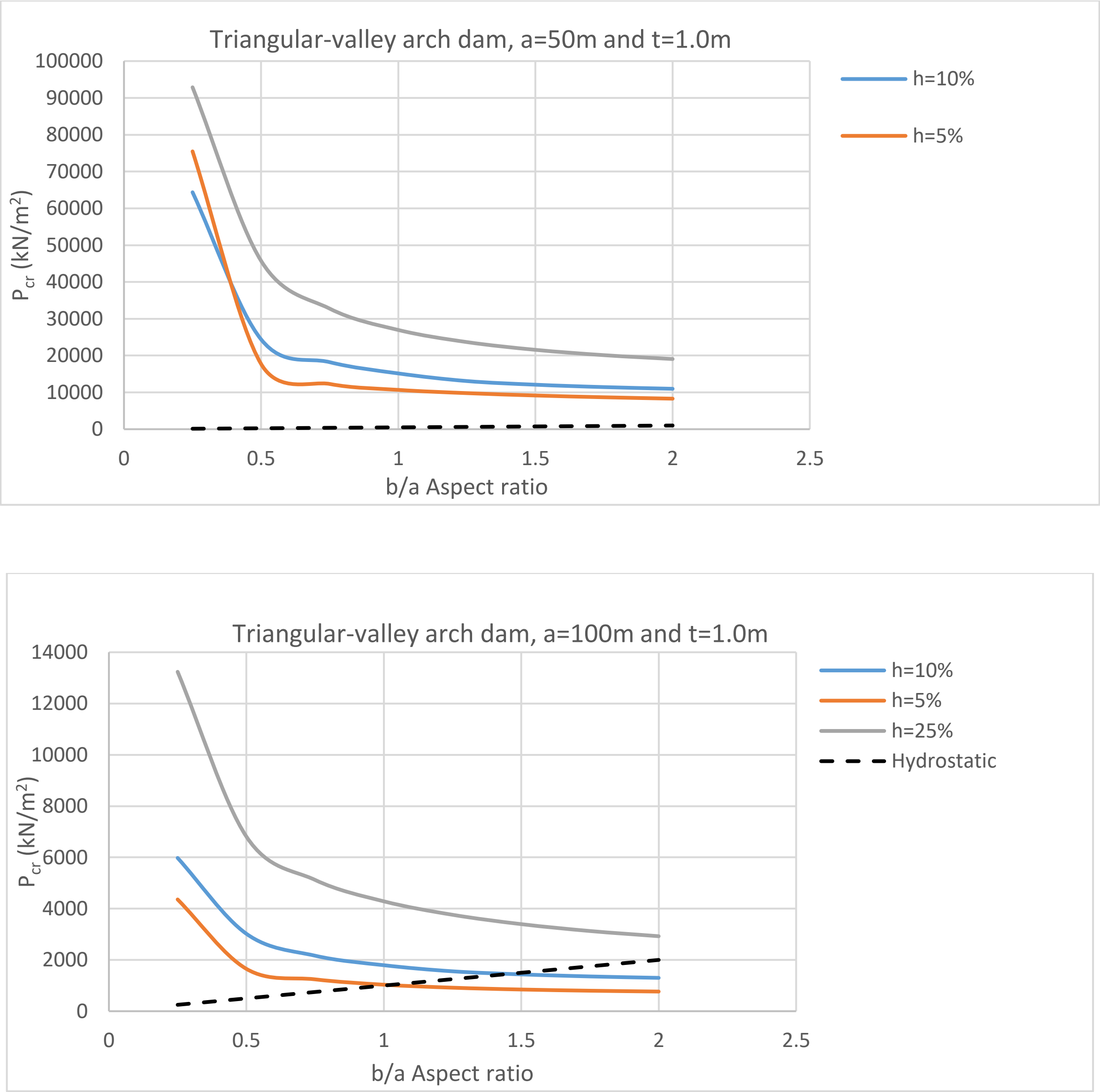

Figure 4.3: Critical buckling pressure plots for the parabolic arch dam of thickness 1.0m.

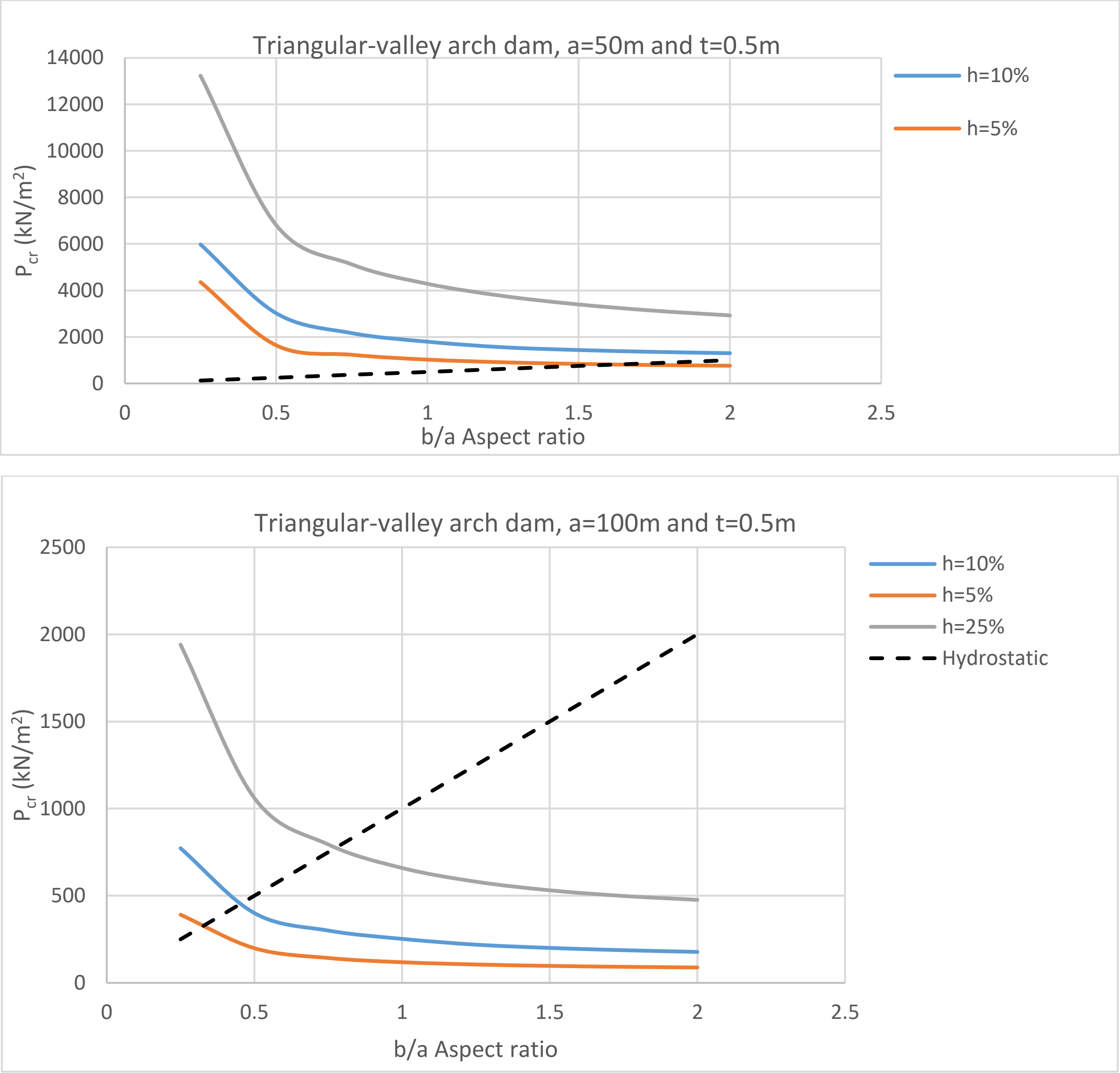

Figure 4.4: Critical buckling pressure plots for the parabolic arch dam of thickness 0.5m.

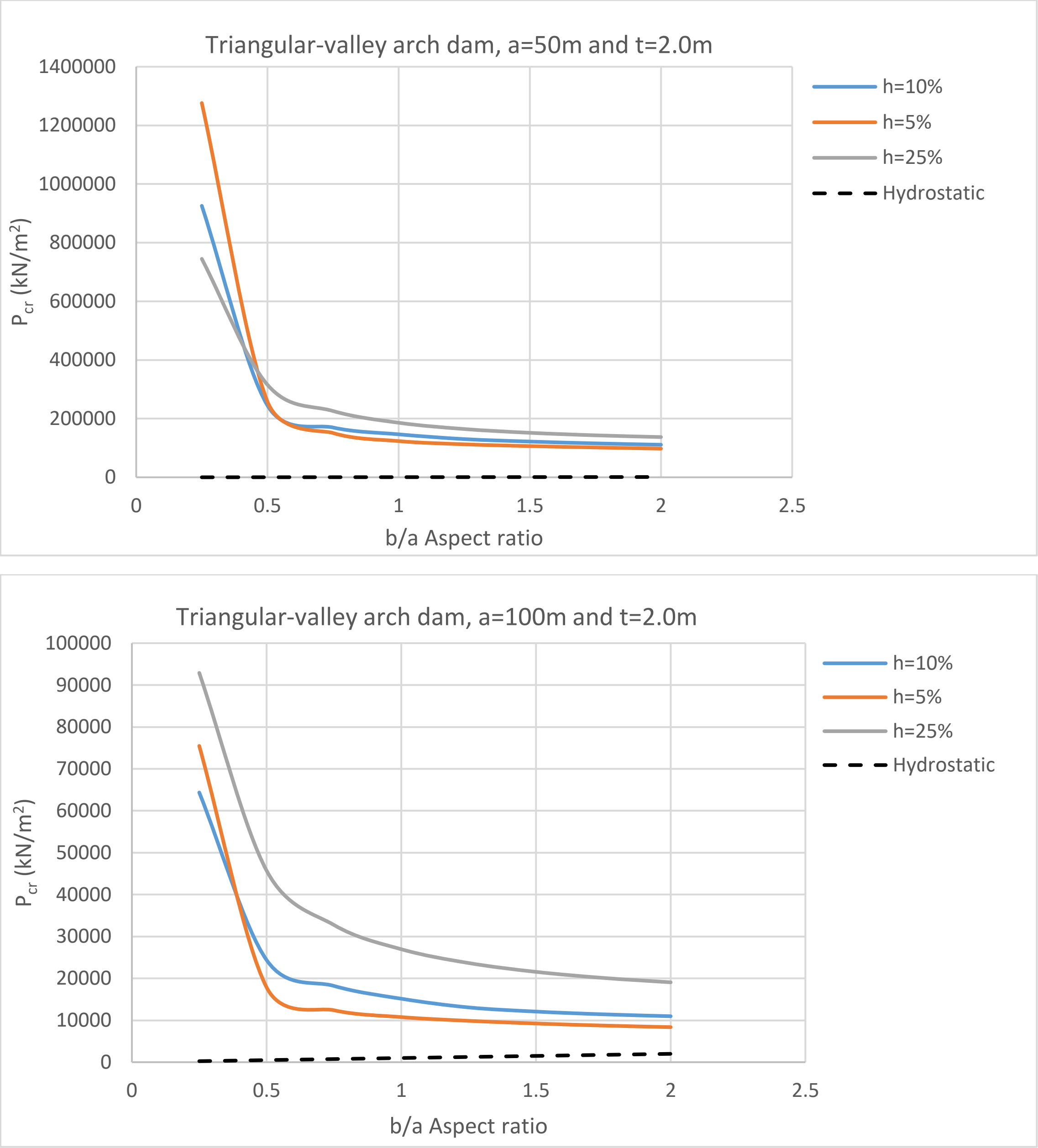

Figure 4.5: Critical buckling pressure plots for the parabolic arch dam of thickness 2.0m.

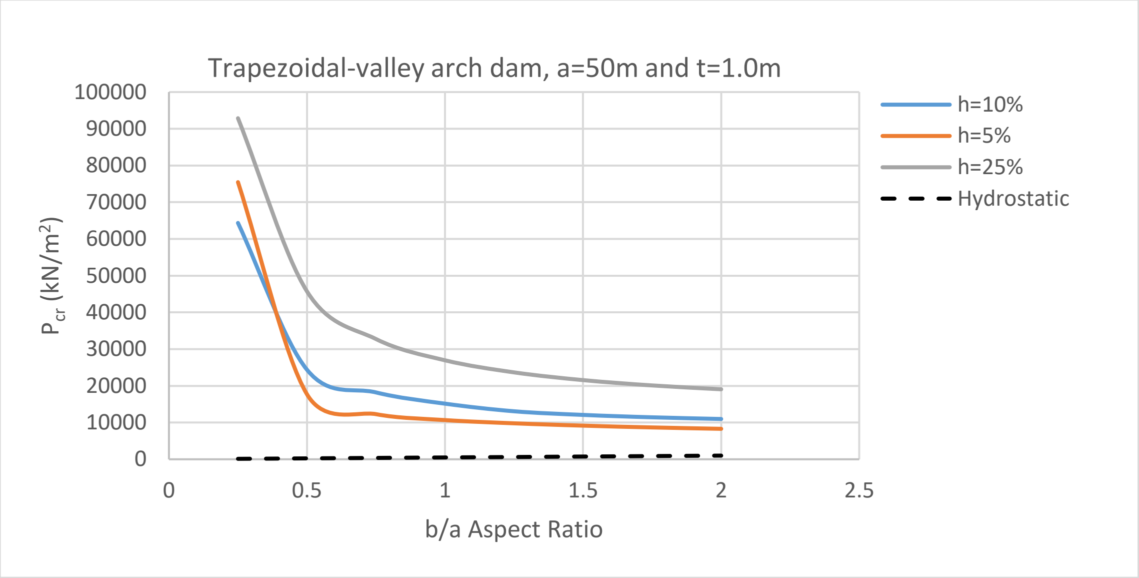

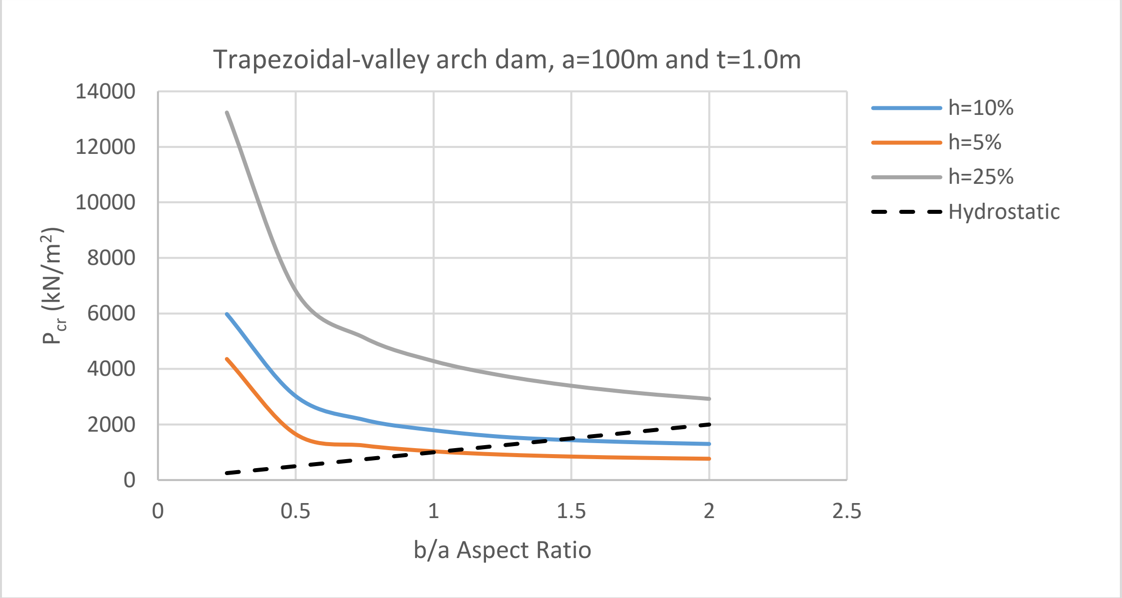

Figure 4.6: Critical buckling pressure plots for the parabolic arch dam of thickness 1.0m.

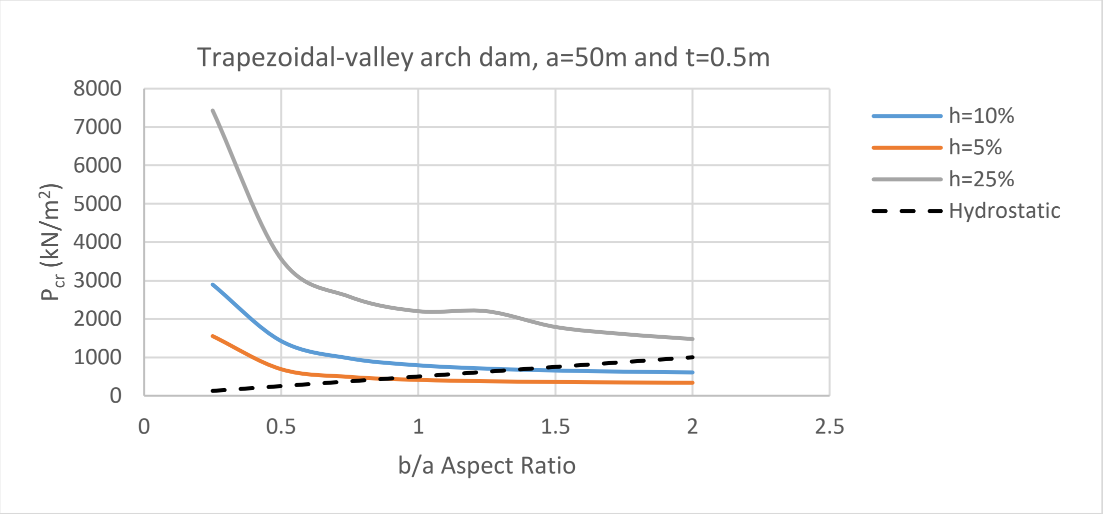

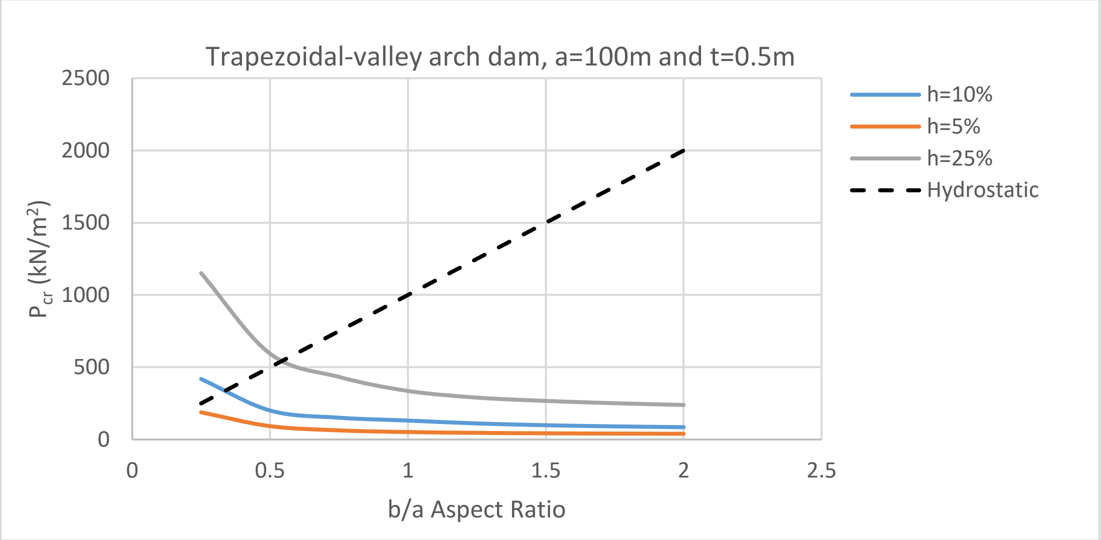

Figure 4.7: Critical buckling pressure plots for the parabolic arch dam of thickness 0.5m.

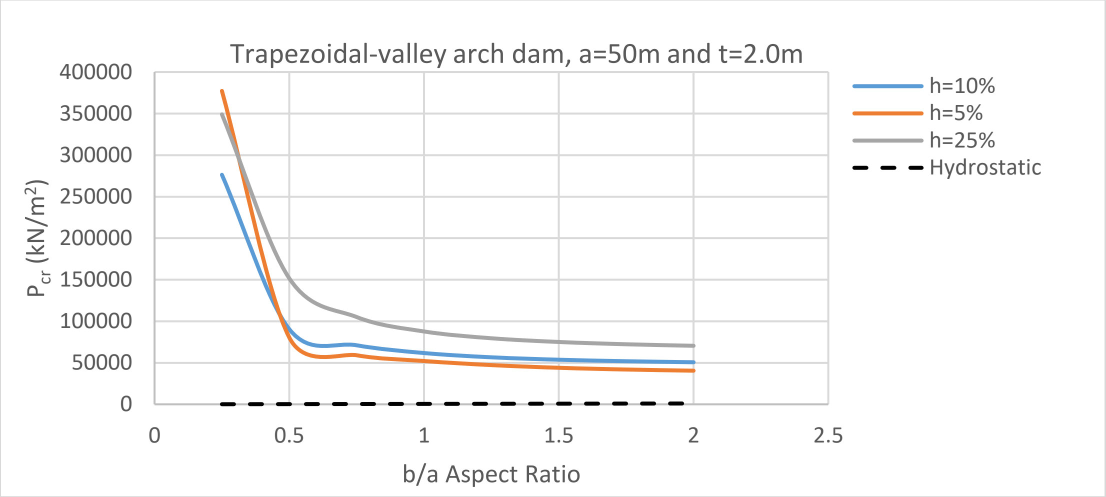

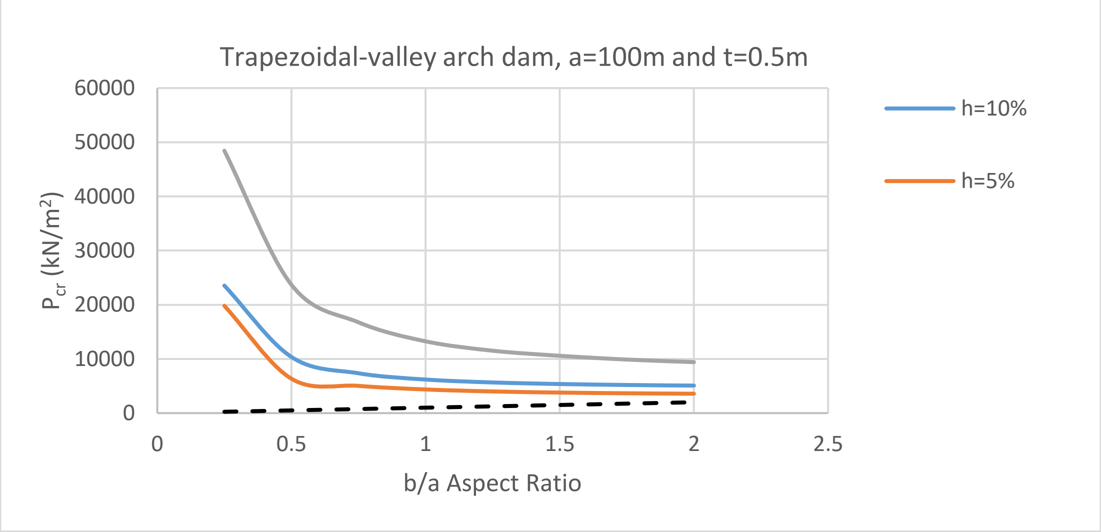

Figure 4.8: Critical buckling pressure plots for the parabolic arch dam of thickness 0.5m.

From Figures 4.3-4.8, it is evident that the buckling pressures for both triangular and trapezoidal-valley arch dams decrease quickly with increasing depth (aspect ratio), with the rate of decrease diminishing as the aspect ratio of the dam increases. The shell rise ratio h/a also has a significant impact on the buckling strength of the arch dam and can be utilized to enhance the buckling strength of an arch of a given dimension without increasing the shell thickness, therefore economising on the amount of concrete required for construction.

One of the significant factors discovered in this research is the effect that the arch dam base width ratio (c/a) has on the buckling strength. It can be seen that when the base width ratio (c/a) is zero (triangular-valley arch dam), the buckling strength increases significantly when compared with the base width ratio (c/a) of 50% (trapezoidal-valley arch dam), similarly when comparing the buckling strength of the trapezoidal-valley arch dam with 50% base width ratio to the rectangular-valley arch with 100% base width ratio. Thus, it can be concluded that the buckling strength increases with a decrease in arch dam base width ratio (c/a).

The dashed hydrostatic pressure line in Figures 4.3 to 4.8 has significant design implications. If a point on the plots lies above this boundary line, it indicates that the shell buckles at a pressure greater than the applied water pressure, indicating that the dam is safe. The intersection of the hydrostatic pressure line and the dam wall depth indicates the depth at which the applied water pressure causes the dam wall to buckle. This depth is referred to as the critical depth which can be used in calculation of a critical load factor. For points that lie underneath the boundary line, the applied water pressure exceeds the buckling strength of the arch dam, causing the dam to buckle under the water load (Zingoni et al., 2013).

4.1.2 Single Curvature Modelling with Linear Varying Thickness

Figure 4.9-4.11 show typical mode shapes for the triangular, trapezoidal and rectangular circular and parabolic arch profile respectively with linear varying thickness. Similarly, the results for the critical buckling pressures for the various cases that were analysed revealed that there is very little difference between the corresponding results for the parabolic and circular profiles.

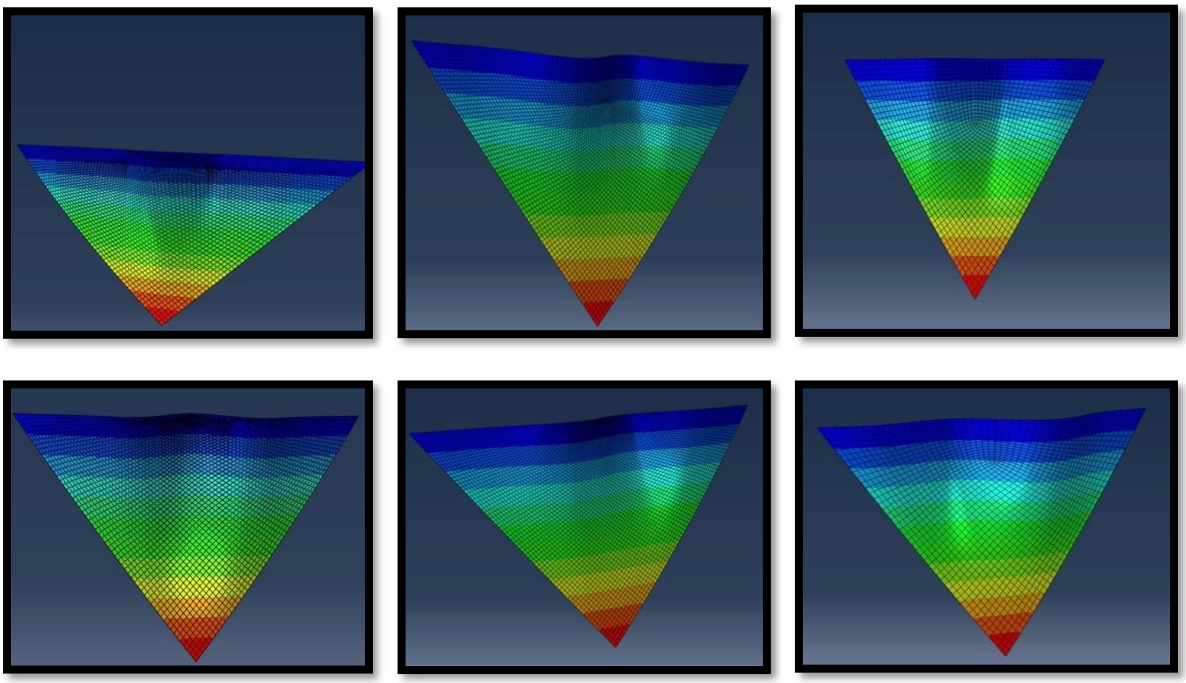

Figure 4.9: Triangular-valley arch dam buckling mode shapes for *a* = 50m, h=10%, t_1=0.5m t_2=1.0m for circular arch (first three mode shapes with b/a=0.25, 0.50 and 0.75 respectively) and parabolic arch (last three mode shapes with b/a=0.25, 0.50 and 0.75 respectively).

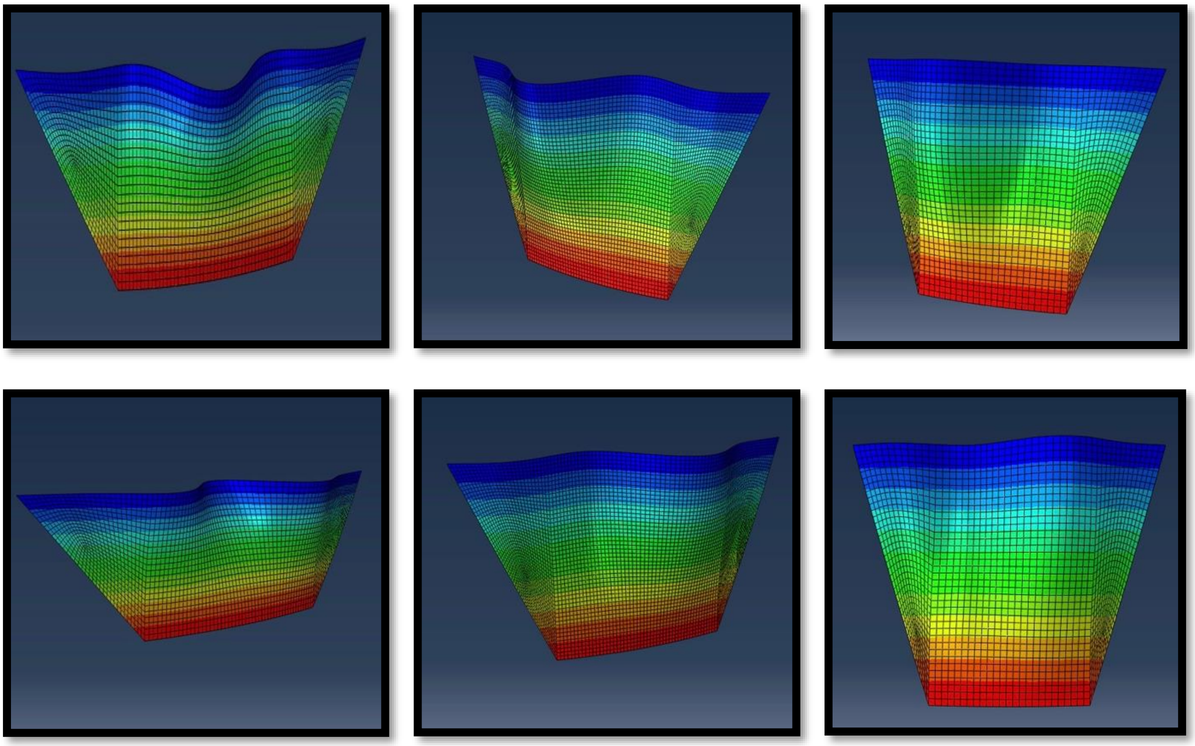

Figure 4.10: Trapezoidal-valley arch dam buckling mode shapes for *a* = 50m, h=10%, t_1=0.5m t_2=1.0m for circular arch (first three mode shapes with b/a=0.25, 0.50 and 0.75 respectively) and parabolic arch (last three mode shapes with b/a=0.25, 0.50 and 0.75 respectively).

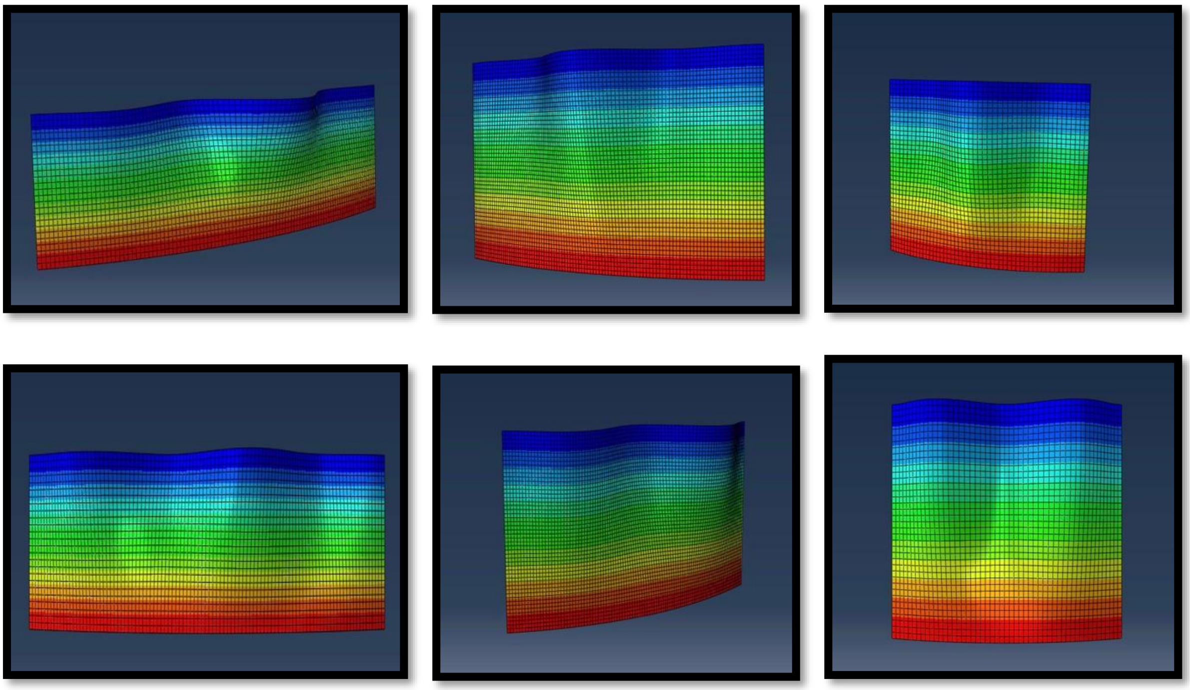

Figure 4.11: Rectangular-valley arch dam buckling mode shapes for *a* = 50m, h=10%, t_1=0.5m t_2=1.0m for circular arch (first three mode shapes with b/a=0.25, 0.50 and 0.75 respectively) and parabolic arch (last three mode shapes with b/a=0.25, 0.50 and 0.75 respectively).

The tables below, 4.13(a)-(c), 4.14(a)-(c) and 4.15(a)-(c), compare the buckling pressures for the triangular, trapezoidal and rectangular-valley arch dams respectively, between the circular and parabolic profiles, assuming the thickness *t* varies linearly in two cases namely, t_1=0.5m & t_2=1.0m and t_1=1.0m & t_2=2.0m for three representative rise ratio values (5%, 10%, 25%).

t1=0.5m & t2=1.0m; h=10%							t1=1.0m & t2=2.0m; h=10%						
Critical Buckling Pressure Pcr (kN/m2)							Critical Buckling Pressure Pcr (kN/m2)						
a=100m				a=50m			a=100m				a=50m		
b/a	Circular	Parabola	Diff. %	Circular	Parabola	Diff. %	b/a	Circular	Parabola	Diff. %	Circular	Parabola	Diff. %
0,25	-	-	-	16859	17017	0,93	0,25	-	-	-	258553	255982	-1,00
0,5	909	935	2,78	6438	6579	2,14	0,5	6438	6579	2,14	53197	53649	0,84
0,75	-	-	-	4820	4909	1,81	0,75	-	-	-	36363	36737	1,02
1	589	605	2,64	4012	4082	1,71	1	4012	4082	1,71	30767	31038	0,87
1,25	-	-	-	3477	3542	1,84	1,25	-	-	-	27506	27762	0,92
1,5	480	492	2,44	3241	3296	1,67	1,5	3241	3296	1,67	25336	25580	0,95
1,75	-	-	-	2971	3079	3,51	1,75	-	-	-	23824	24065	1,00
2	420	429	2,10	2872	2919	1,61	2	2872	2919	1,61	22261	22967	3,07

Table 4.13(a): Triangular-valley arch dam results of circular vs. parabolic arch for h=10%.

t1=0.5m & t2=1.0m; h=5%							t1=1.0m & t2=2.0m; h=5%						
Critical Buckling Pressure Pcr (kN/m2)							Critical Buckling Pressure Pcr (kN/m2)						
a=100m				a=50m			a=100m				a=50m		
b/a	Circular	Parabola	Diff. %	Circular	Parabola	Diff. %	b/a	Circular	Parabola	Diff. %	Circular	Parabola	Diff. %
0,25	-	-	-	18304	18253	0,28	0,25	-	-	-	392732	390873	-0,48
0,5	433	436	-0,69	3652	3660	0,22	0,5	3652	3660	0,22	49588	49593	0,01
0,75	-	-	-	2518	2510	-0,32	0,75	-	-	-	26090	26092	0,01
1	272	273	0,37	2146	2152	0,28	1	2146	2151	0,23	20308	20322	0,07
1,25	-	-	-	1925	1930	0,26	1,25	-	-	-	18166	18183	0,09
1,5	220	221	0,45	1776	1781	0,28	1,5	1776	1781	0,28	17102	17119	0,10
1,75	-	-	-	1672	1676	0,24	1,75	-	-	-	16425	16442	0,10
2	196	196	0,00	1596	1600	0,25	2	1596	1600	0,25	15915	15932	0,11

Table 4.13(b): Triangular-valley arch dam results of circular vs. parabolic arch for h=5%.

t1=0.5m & t2=1.0m; h=25%							t1=1.0m & t2=2.0m; h=25%						
Critical Buckling Pressure Pcr (kN/m2)							Critical Buckling Pressure Pcr (kN/m2)						
a=100m				a=50m			a=100m				a=50m		
b/a	**Circular**	**Parabola**	**Diff. %**	**Circular**	**Parabola**	**Diff. %**	**b/a**	**Circular**	**Parabola**	**Diff. %**	**Circular**	**Parabola**	**Diff. %**
0,25	-	-	-	25248	29977	15,78	0,25	-	-	-	217928	236169	7,72
0,5	2007	2398	16,31	13076	15279	14,42	0,5	13076	15279	14,42	87485	98907	11,55
0,75	-	-	-	9846	11402	13,65	0,75	-	-	-	64062	71159	9,97
1	1263	1457	13,32	8354	9524	12,28	1	8354	9524	12,28	53048	58268	8,96
1,25	-	-	-	7445	8445	11,84	1,25	-	-	-	46610	50685	8,04
1,5	1004	1134	11,46	6803	7713	11,80	1,5	6803	7713	11,80	42289	45612	7,29
1,75	-	-	-	6311	7091	11,00	1,75	-	-	-	39152	41968	6,71
2	872	979	10,93	5916	6593	10,27	2	5916	6593	10,27	36762	39227	6,28

Table 4.13(c): Triangular-valley arch dam results of circular vs. parabolic arch for h=25%.

t1=0.5m & t2=1.0m; h=10%							t1=1.0m & t2=2.0m; h=10%						
Critical Buckling Pressure Pcr (kN/m2)							Critical Buckling Pressure Pcr (kN/m2)						
a=100m				a=50m			a=100m				a=50m		
b/a	**Circular**	**Parabola**	**Diff. %**	**Circular**	**Parabola**	**Diff. %**	**b/a**	**Circular**	**Parabola**	**Diff. %**	**Circular**	**Parabola**	**Diff. %**
0,25	-	-	-	8295	8400	1,25	0,25	-	-	-	100077	99836	-0,24
0,5	561	573	2,09	3825	3886	1,57	0,5	3825	3886	1,57	27047	27267	0,81
0,75	-	-	-	2848	2885	1,28	0,75	-	-	-	20959	21103	0,68
1	379	386	1,81	2432	2468	1,46	1	2436	2467	1,26	18488	18586	0,53
1,25	-	-	-	2218	2245	1,20	1,25	-	-	-	17139	17281	0,82
1,5	307	312	1,60	2075	2106	1,47	1,5	2080	2101	1,00	16279	16424	0,88
1,75	-	-	-	1979	2009	1,49	1,75	-	-	-	15676	15822	0,92
2	273	277	1,44	1909	1937	1,45	2	1913	1933	1,03	15187	15377	1,24

Table 4.14(a): Trapezoidal-valley arch dam results of circular vs. parabolic arch for h=10%.

t1=0.5m & t2=1.0m; h=5%							t1=1.0m & t2=2.0m; h=5%						
Critical Buckling Pressure Pcr (kN/m2)							Critical Buckling Pressure Pcr (kN/m2)						
a=100m				a=50m			a=100m				a=50m		
b/a	**Circular**	**Parabola**	**Diff. %**	**Circular**	**Parabola**	**Diff. %**	**b/a**	**Circular**	**Parabola**	**Diff. %**	**Circular**	**Parabola**	**Diff. %**
0,25	-	-	-	6746	6742	0,06	0,25	-	-	-	131166	130759	-0,31
0,5	255	256	0,39	1832	1836	0,22	0,5	1832	1836	0,22	18997	18996	-0,01
0,75	-	-	-	1437	1440	0,21	0,75	-	-	-	13090	13091	0,01
1	163	164	0,61	1274	1276	0,16	1	1274	1276	0,16	11908	11919	0,09
1,25	-	-	-	1183	1186	0,25	1,25	-	-	-	11388	11409	0,18
1,5	140	141	0,71	1125	1128	0,27	1,5	1125	1128	0,27	11039	11050	0,10
1,75	-	-	-	1085	1087	0,18	1,75	-	-	-	10744	10756	0,11
2	129	130	0,77	1054	1057	0,28	2	1053	1057	0,38	10494	10506	0,11

Table 4.14(b): Trapezoidal-valley arch dam results of circular vs. parabolic arch for h=5%.

t1=0.5m & t2=1.0m; h=25%							t1=1.0m & t2=2.0m; h=25%						
Critical Buckling Pressure Pcr (kN/m2)							Critical Buckling Pressure Pcr (kN/m2)						
a=100m				a=50m			a=100m				a=50m		
b/a	**Circular**	**Parabola**	**Diff. %**	**Circular**	**Parabola**	**Diff. %**	**b/a**	**Circular**	**Parabola**	**Diff. %**	**Circular**	**Parabola**	**Diff. %**
0,25	-	-	-	16778	19072	12,03	0,25	-	-	-	121933	132216	7,78
0,5	1365	1544	11,59	8508	9420	9,68	0,5	8507	9420	9,69	56080	61534	8,86
0,75	-	-	-	6432	7074	9,08	0,75	-	-	-	41332	44409	6,93
1	828	911	9,11	5540	6100	9,18	1	5504	6100	9,77	34699	36813	5,74
1,25	-	-	-	5062	5598	9,57	1,25	-	-	-	30936	32599	5,10
1,5	655	732	10,52	4645	5010	7,29	1,5	4643	5029	7,68	28485	29911	4,77
1,75	-	-	-	4298	4613	6,83	1,75	-	-	-	26743	28033	4,60
2	599	665	9,92	4033	4302	6,25	2	4031	4302	6,30	25428	26643	4,56

Table 4.14(c): Trapezoidal-valley arch dam results of circular vs. parabolic arch for h=25%.

t1=0.5m & t2=1.0m; h=10%							t1=1.0m & t2=2.0m; h=10%						
Critical Buckling Pressure Pcr (kN/m2)							Critical Buckling Pressure Pcr (kN/m2)						
a=100m				a=50m			a=100m				a=50m		
b/a	Circular	Parabola	Diff. %	Circular	Parabola	Diff. %	b/a	Circular	Parabola	Diff. %	Circular	Parabola	Diff. %
0,25	-	-	-	7115	7164	0,68	0,25	-	-	-	79833	79796	-0,05
0,5	472	474	0,42	2982	2994	0,40	0,5	2982	2994	0,40	21171	21131	-0,19
0,75	-	-	-	2247	2270	1,01	0,75	-	-	-	14501	14443	-0,40
1	277	279	0,72	1870	1861	-0,48	1	1870	1860	-0,54	11905	11887	-0,15
1,25	-	-	-	1596	1588	-0,50	1,25	-	-	-	10695	10698	0,03
1,5	238	241	1,24	1434	1429	-0,35	1,5	1434	1429	-0,35	10029	10042	0,13
1,75	-	-	-	1332	1329	-0,23	1,75	-	-	-	9614	9634	0,21
2	209	208	-0,48	1263	1261	-0,16	2	1263	1261	-0,16	9333	9356	0,25

Table 4.15(a): Rectangular-valley arch dam results of circular vs. parabolic arch for h=10%.

t1=0.5m & t2=1.0m; h=5%							t1=1.0m & t2=2.0m; h=5%						
Critical Buckling Pressure Pcr (kN/m2)							Critical Buckling Pressure Pcr (kN/m2)						
a=100m				a=50m			a=100m				a=50m		
b/a	Circular	Parabola	Diff. %	Circular	Parabola	Diff. %	b/a	Circular	Parabola	Diff. %	Circular	Parabola	Diff. %
0,25	-	-	-	5379	5378	0,02	0,25	-	-	-	100029	99926	-0,10
0,5	199	200	-0,50	1426	1425	-0,07	0,5	1426	1425	-0,07	12276	12269	-0,06
0,75	-	-	-	987	986	-0,10	0,75	-	-	-	8057	8056	-0,01
1	125	125	0,00	815	814	-0,12	1	815	814	-0,12	7095	7096	0,01
1,25	-	-	-	734	734	0,00	1,25	-	-	-	6595	6597	0,03
1,5	97	96	-1,04	689	689	0,00	1,5	689	689	0,00	6282	6285	0,05
1,75	-	-	-	661	661	0,00	1,75	-	-	-	6078	6081	0,05
2	85	85	0,00	642	642	0,00	2	642	642	0,00	5939	5942	0,05

Table 4.15(b): Rectangular-valley arch dam results of circular vs. parabolic arch for h=5%.

t1=0.5m & t2=1.0m; h=25%							t1=1.0m & t2=2.0m; h=25%						
Critical Buckling Pressure Pcr (kN/m2)							Critical Buckling Pressure Pcr (kN/m2)						
	a=100m			a=50m				a=100m			a=50m		
b/a	Circular	Parabola	Diff. %	Circular	Parabola	Diff. %	b/a	Circular	Parabola	Diff. %	Circular	Parabola	Diff. %
0,25	-	-	-	15165	14637	-3,61	0,25	-	-	-	105961	109821	3,51
0,5	1151	1098	-4,83	6958	6917	-0,59	0,5	6958	6917	-0,59	43824	43607	-0,50
0,75	-	-	-	5068	4927	-2,86	0,75	-	-	-	30275	31408	3,61
1	657	674	2,52	3942	3977	0,88	1	3942	3977	0,88	25771	27511	6,32
1,25	-	-	-	3416	3567	4,23	1,25	-	-	-	23775	23245	-2,28
1,5	489	492	0,61	3147	3351	6,09	1,5	3147	3351	6,09	21057	20186	-4,31
1,75	-	-	-	2992	3218	7,02	1,75	-	-	-	18905	18256	-3,55
2	410	432	5,09	2889	3125	7,55	2	2889	3125	7,55	17410	16980	-2,53

Table 4.15(c): Rectangular-valley arch dam results of circular vs. parabolic arch for h=25%.

The difference between circular and parabolic arch profile results for the triangular-valley arch dam is less than 0.49 %, 3.5 %, and 15.8 % for the 5%, 10%, and 25% rise ratios for the 50 m wide dam respectively, and less than 0.70 %, 2.8 %, and 16.3 % for the 100 m wide dam respectively. Similar variations exist between the rectangular and trapezoidal-valley arch dams in terms of the three rise ratio parameters.

Another significant observation made is the relationship between the change in arch dam base width ratio c/a and the difference of the buckling strength between circular and parabolic arch profiles. The observation made is that, an increase in base width ratio c/a leads to a decrease in the difference between buckling strength results between circular and parabolic arch profiles with linear varying thickness.

Figures 4.12 - 4.17 illustrate the numerical results obtained for the critical buckling pressure corresponding to the respective aspect ratios b/a. The first two figures (Figs. 4.12-4.13) represent shell-thickness expressions for two cases, namely t1=0.5m & t2=1.0m and t1=1.0m & t2=2.0m, for the triangular-valley arch dam with the a parameter fixed at 50m and 100m, whereas the next four figures represent the trapezoidal and rectangular-valley arch dam results for the same shell-thickness expressions and a parameter values.

Three curves in each plot correspond to the three h/a rise ratio values (5%, 10%, and 25%). Similarly, the straight dashed line emerging from the origin is the hydrostatic-pressure line indicating the water pressure at the base of the dam wall for each b value.

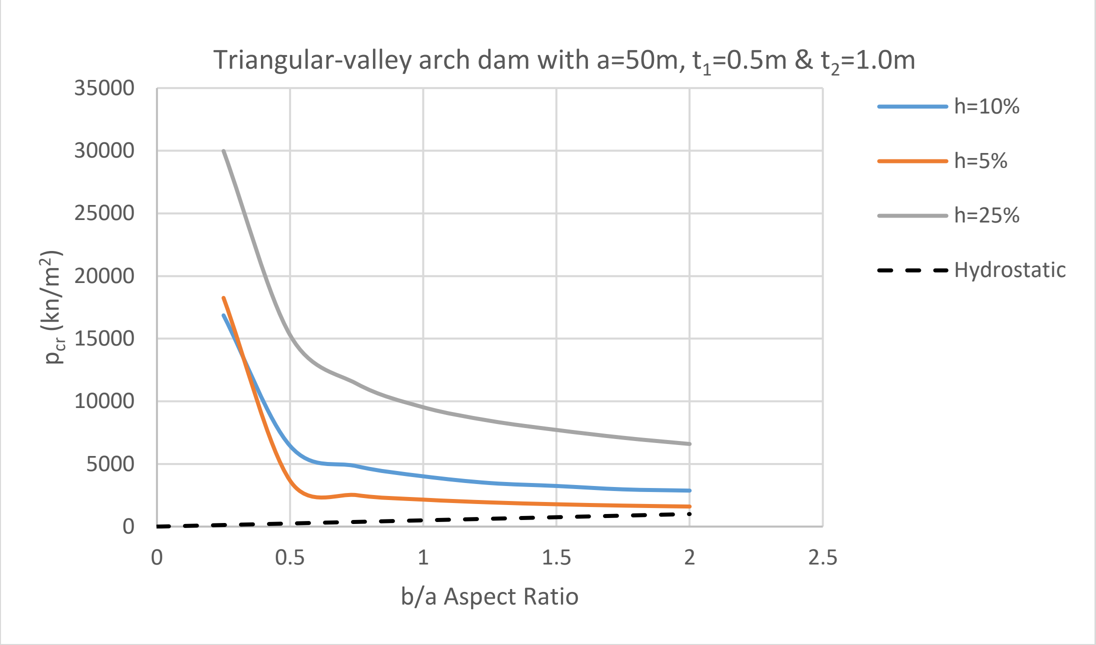

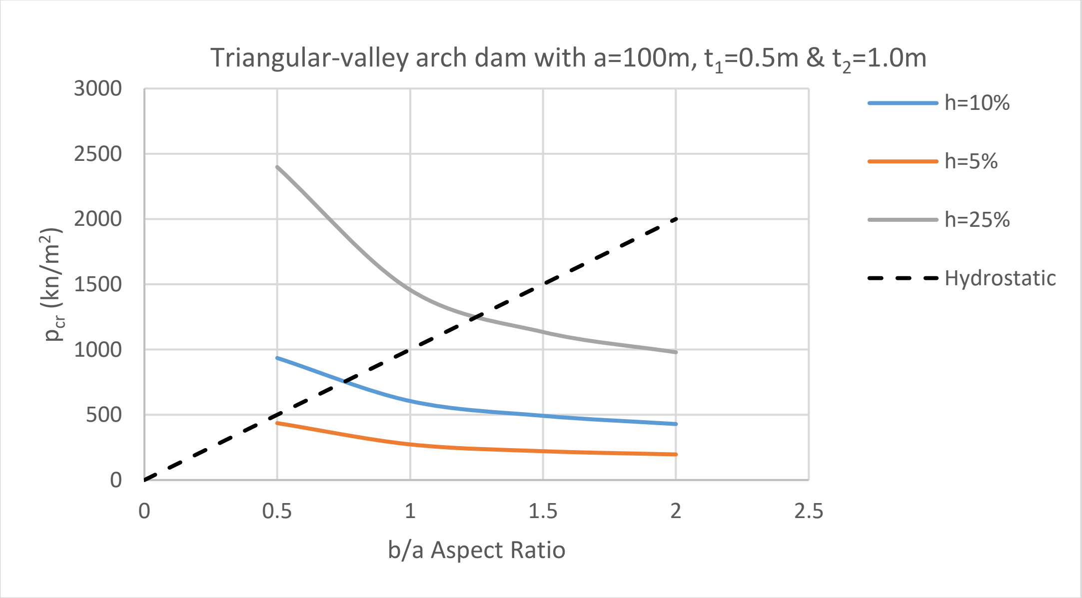

Figure 4.12: Critical buckling pressure plots for the parabolic arch dam of thickness expression t_1=0.5m & t_2=1.0m.

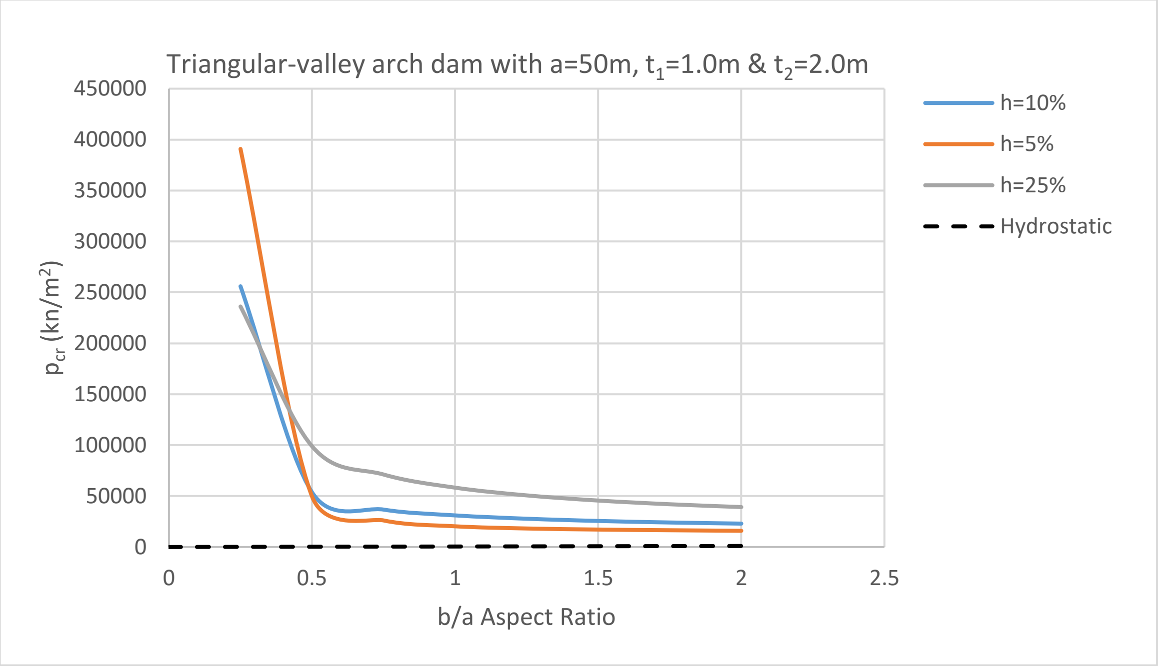

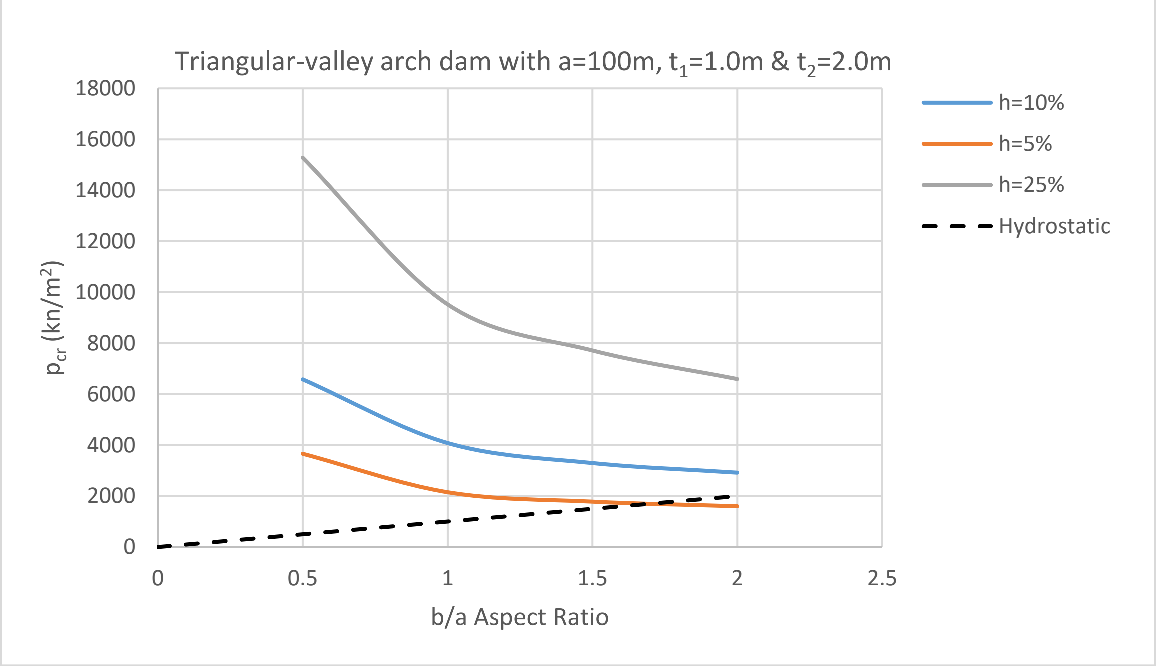

Figure 4.13: Critical buckling pressure plots for the parabolic arch dam of thickness expression t_1=1.0m & t_2=2.0m.

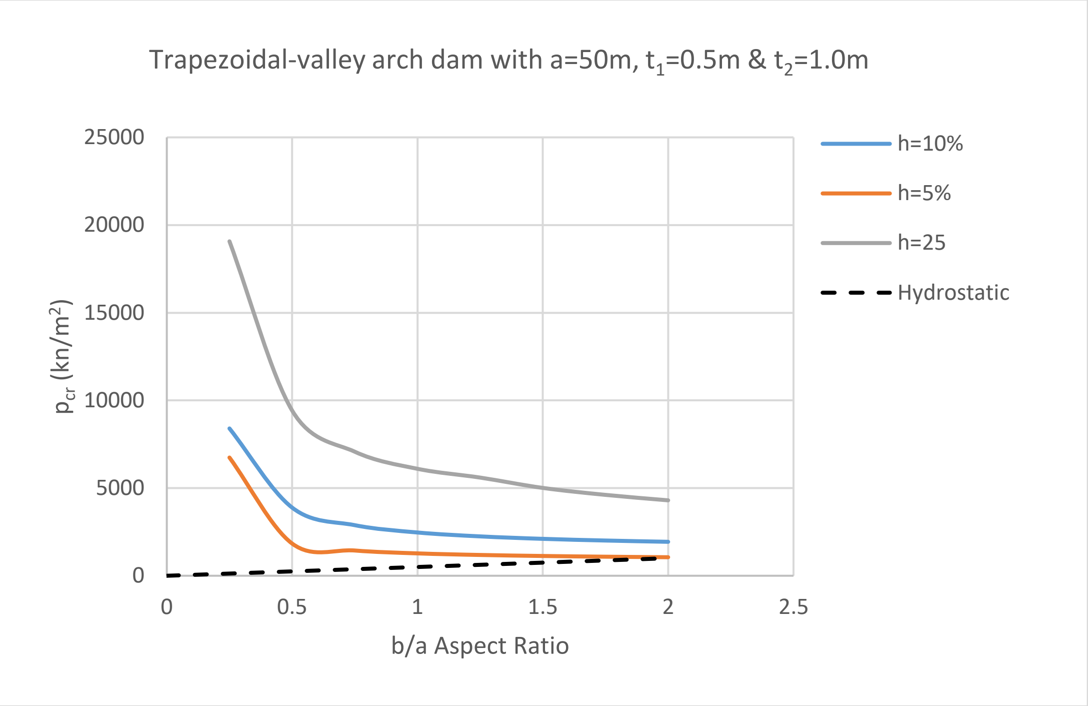

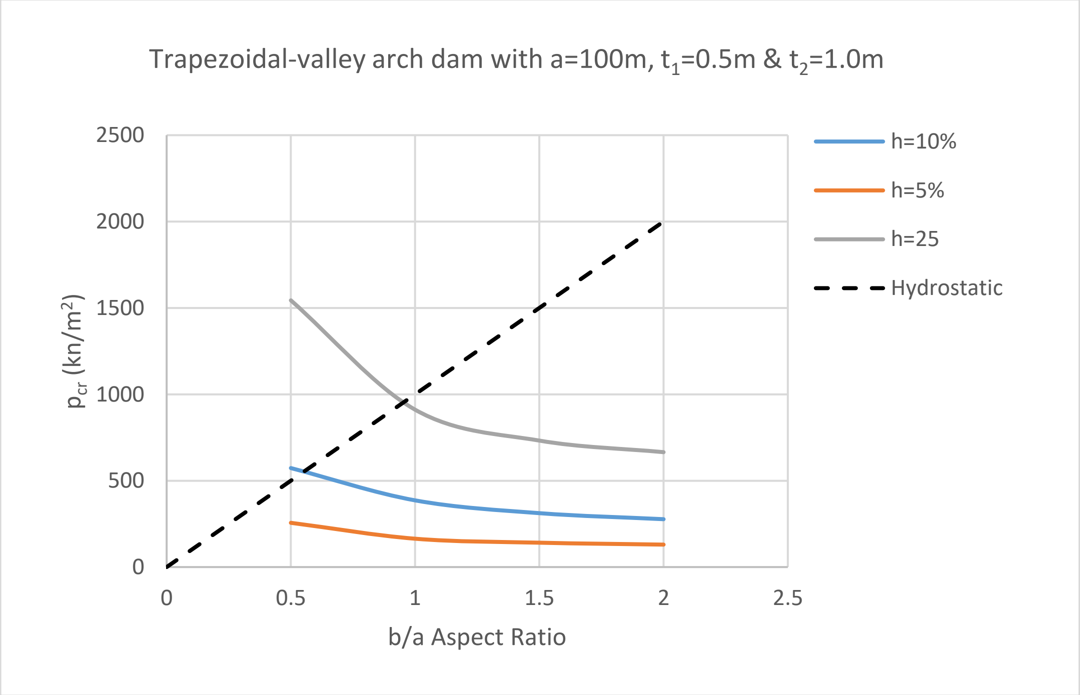

Figure 4.14: Critical buckling pressure plots for the parabolic arch dam of thickness expression t_1=0.5m & t_2=1.0m.

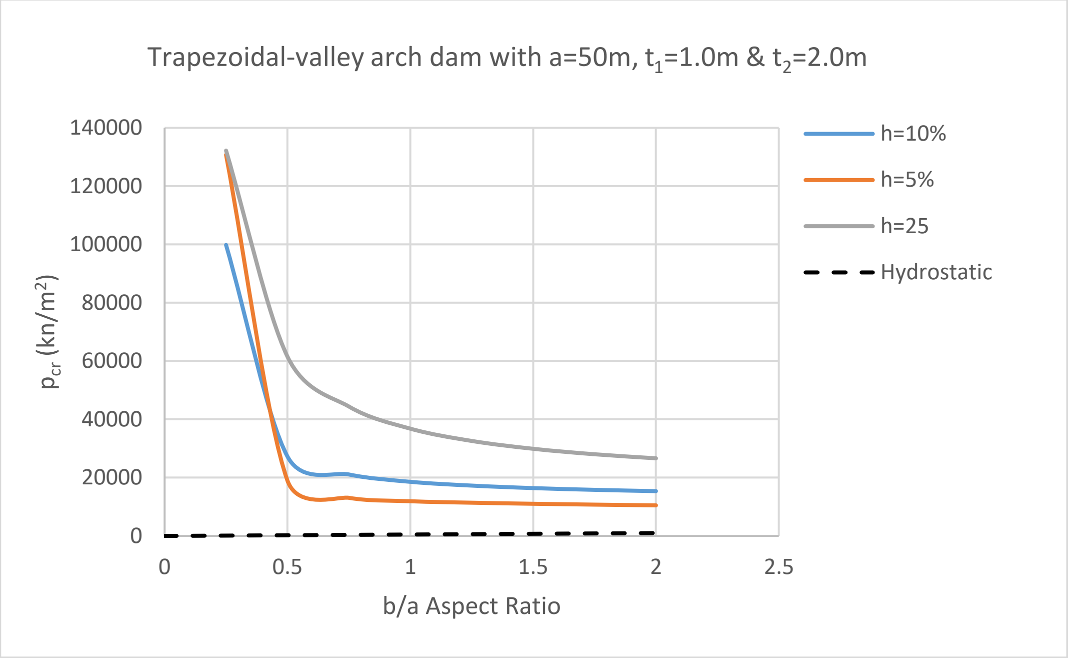

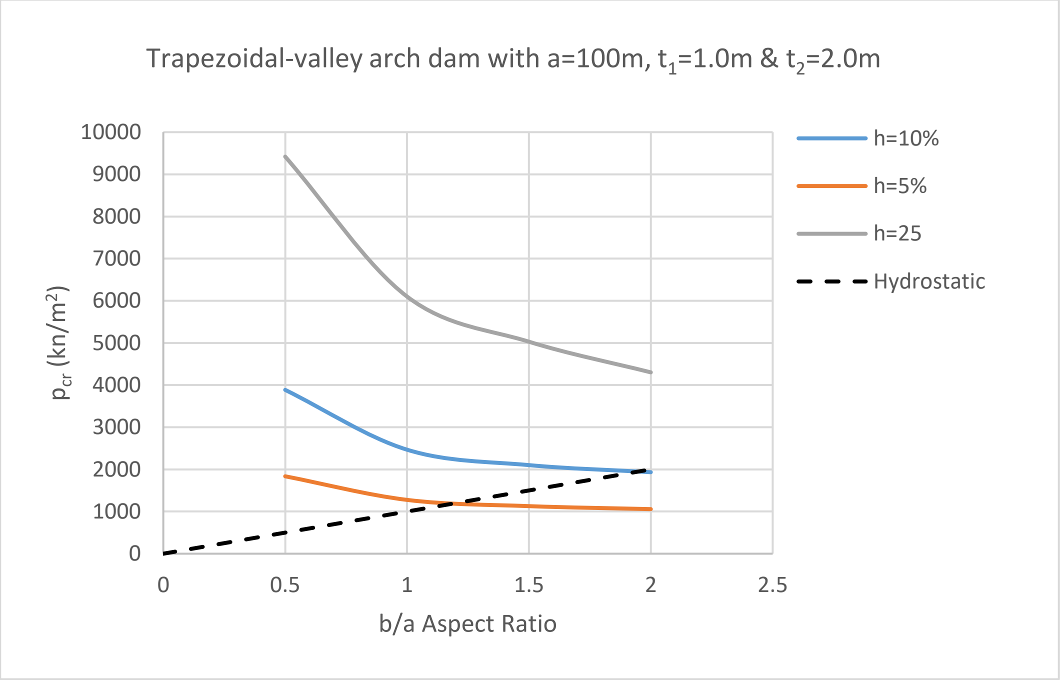

Figure 4.15: Critical buckling pressure plots for the parabolic arch dam of thickness expression t_1=1.0m & t_2=2.0m.

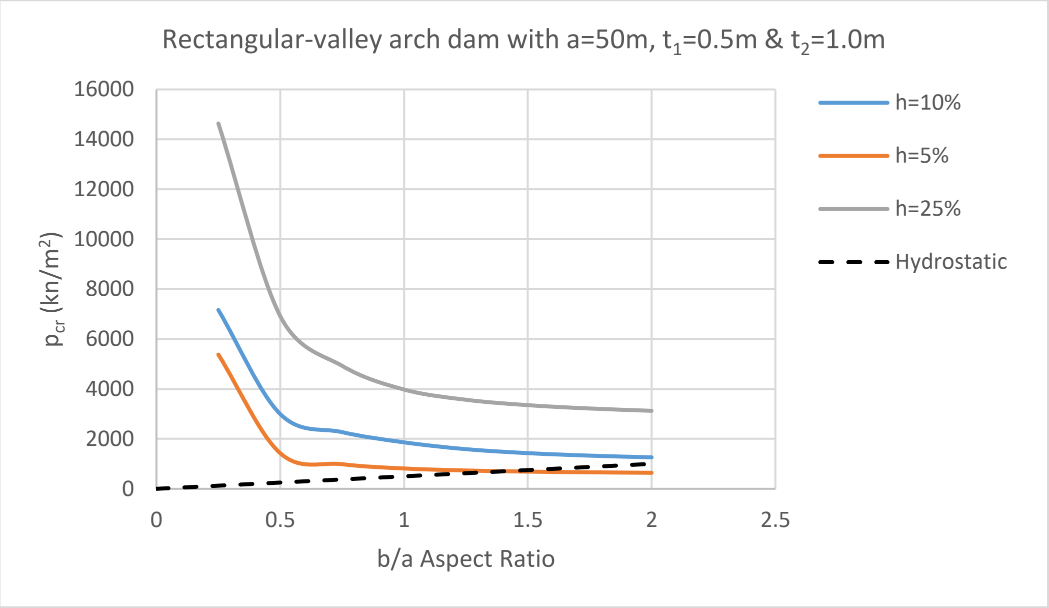

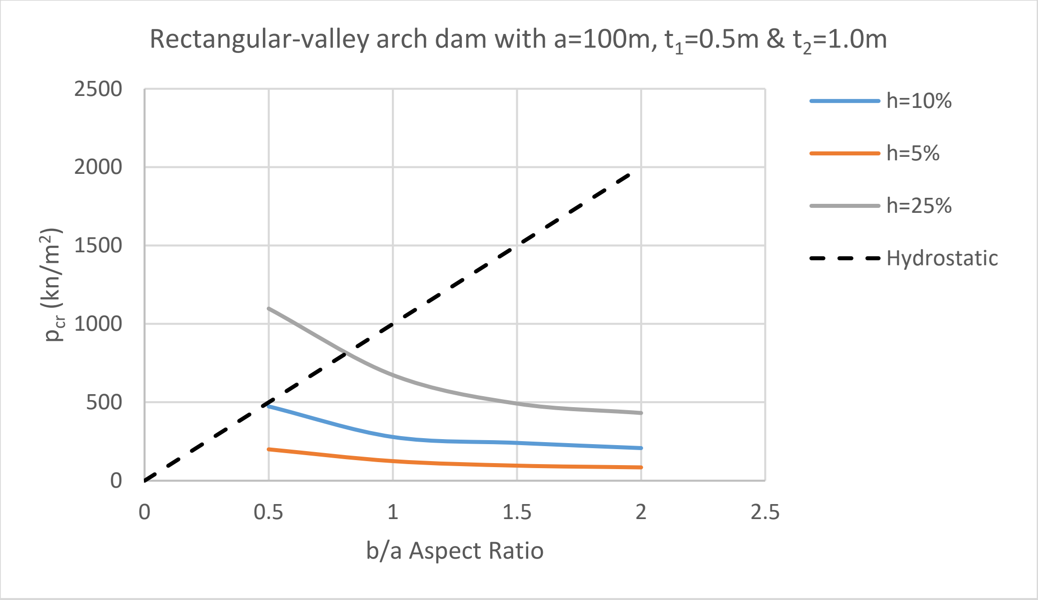

Figure 4.16: Critical buckling pressure plots for the parabolic arch dam of thickness expression t_1=0.5m & t_2=1.0m.

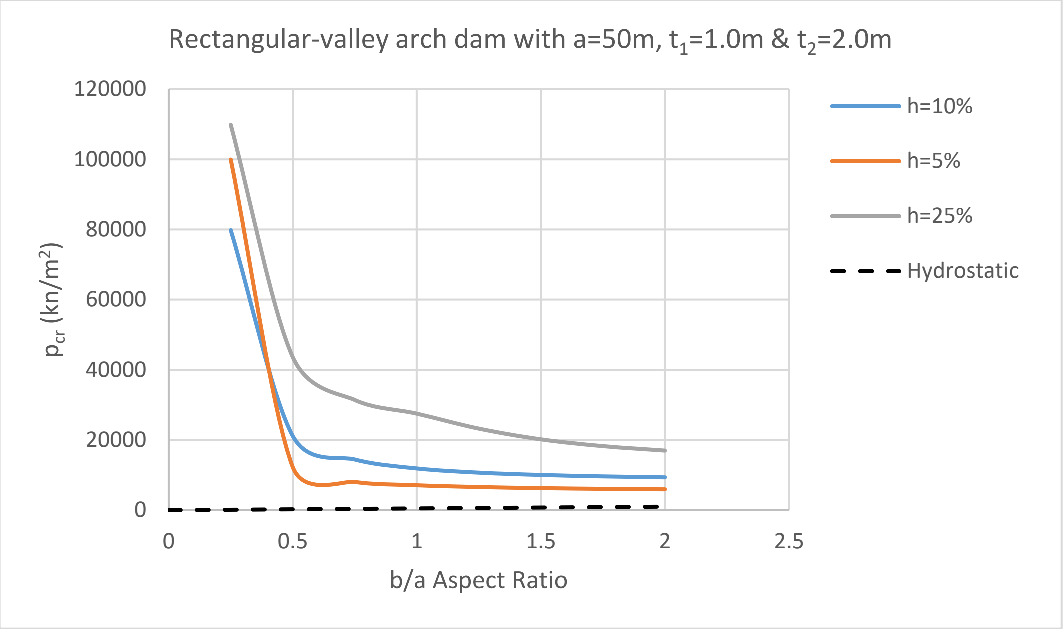

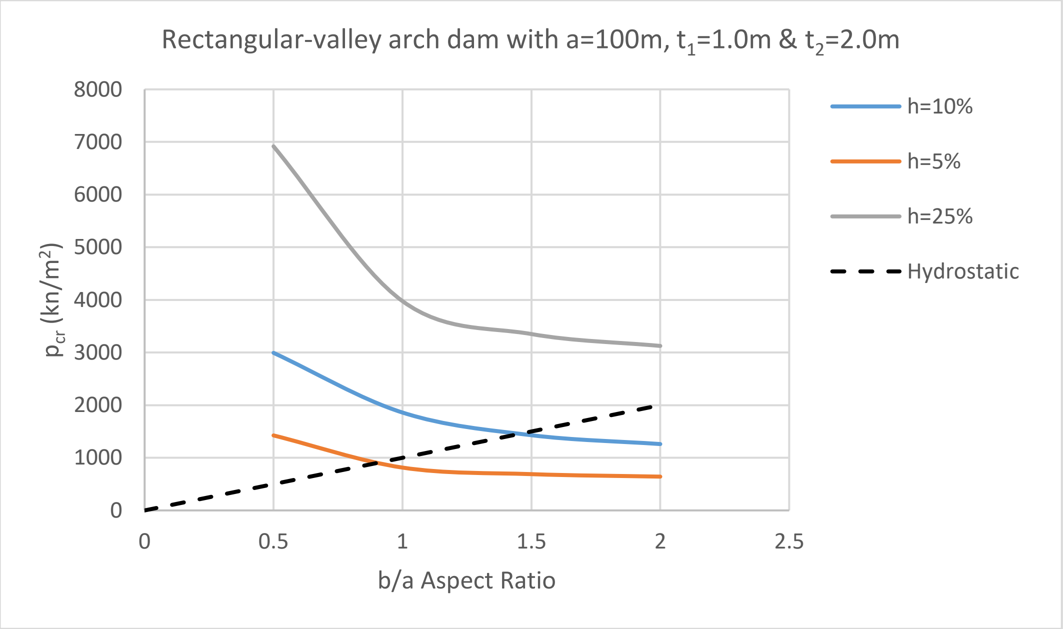

Figure 4.17: Critical buckling pressure plots for the parabolic arch dam of thickness expression t_1=1.0m & t_2=2.0m.

It is evident from Figures 4.12-4.17 that linear buckling analysis for triangular, trapezoidal, and rectangular-valley arch dams follow the same trend as constant-thickness arch dam buckling analysis, where the buckling pressures decrease rapidly with increasing depth (aspect ratio), with the rate of decrease diminishing as the aspect ratio of the dam increases. Similarly, the shell rise ratio h/a has a major effect on the arch dam's buckling strength.

The effect the constant and linear varying thickness has on the 50m wide arch dam's buckling strength was further investigated. Tables 4.16-4.18 below show the difference in buckling strength between the 50m wide triangular-valley arch dam with constant thickness 1m & 2m and the linear varying thickness expressions t_1=0.5m & t_2=1.0m and t_1=1.0m & t_2=2.0m. It is clear that the 50m wide arch dam with constant thickness, 1m, performs better than the arch dam with the thickness expression t_1=0.5m & t_2=1.0m by a margin of 80%, 73% and 65% for the 5%, 10%, and 25% rise ratios respectively. Whereas, the 50m wide arch dam with constant thickness, 2m, performs better than the arch dam with the thickness expression t_1=1.0m & t_2=2.0m by a margin of 81%, 78% and 69% for the 5%, 10%, and 25% rise ratios respectively.

a=50m: h=5%						
t_1=0.5m & t_2=1.0m vs constant thickness 1m				**t_1=1.0m & t_2=2.0m vs constant thickness 2m**		
b/a	**linear**	**constant**	**Diff %**	**linear**	**constant**	**Diff%**
0,25	18253	75471	75,81	1276030	390873	69,37
0,5	3660	17693	79,31	258394	49593	80,81
0,75	2510	12292	79,58	151068	26092	82,73
1	2152	10676	79,84	123463	20322	83,54
1,25	1930	9795,3	80,30	112550	18183	83,84
1,5	1781	9159,6	80,56	106417	17119	83,91
1,75	1676	8672,5	80,67	101759	16442	83,84
2	1600	8296	80,71	97721	15932	83,70
		Average	**80**		**Average**	**81**

Table 4.16: Constant thickness vs linear varying thickness buckling strength results, h=5%.

a= 50m: h=10%						
t_1=0.5m & t_2=1.0m vs. constant thickness 1m				**t_1=1.0m & t_2=2.0m vs. constant thickness 2m**		
b/a	**linear**	**constant**	**Diff %**	**linear**	**constant**	**Diff%**
0,25	17017	64362	73,56	255982	925654	72,35
0,5	6579	24375	73,01	53649	245376	78,14
0,75	4909	18205	73,03	36737	169819	78,37
1	4082	15148	73,05	31038	146557	78,82
1,25	3542	13077	72,91	27762	130315	78,70
1,5	3296	12083	72,72	25580	121918	79,02
1,75	3079	11431	73,06	24065	115693	79,20
2	2919	10975	73,40	22967	110996	79,31
		Average	**73**		**Average**	**78,0**

Table 4.17: Constant thickness vs linear varying thickness buckling strength results, h=10%.

a=50m: h=25%						
t_1=0.5m & t_2=1.0m vs constant thickness 1m				t_1=1.0m & t_2=2.0m vs constant thickness 2m		
b/a	**linear**	**constant**	**Diff %**	**linear**	**constant**	**Diff%**
0,25	29977	92883	67,73	236169	744752	68,29
0,5	15279	45713	66,58	98907	315673	68,67
0,75	11402	32749	65,18	71159	226116	68,53
1	9524	26954	64,67	58268	185987	68,67
1,25	8445	23666	64,32	50685	164620	69,21
1,5	7713	21560	64,23	45612	151695	69,93
1,75	7091	20112	64,74	41968	143158	70,68
2	6593	19064	65,42	39227	137172	71,40
		Average	**65**		**Average**	**69**

Table 4.18: Constant thickness vs linear varying thickness buckling strength results, h=25%.

4.1.3 Single Curvature Modelling with Quadratic Varying Thickness

Figures 4.18 – 4.20 depict the typical mode shapes for the triangular, trapezoidal, and rectangular circular and parabolic arch profiles with quadratic thickness variation. Similarly, the results for the critical buckling pressures for the various analysed cases revealed that there is minimal difference between the results for the parabolic and circular profiles.

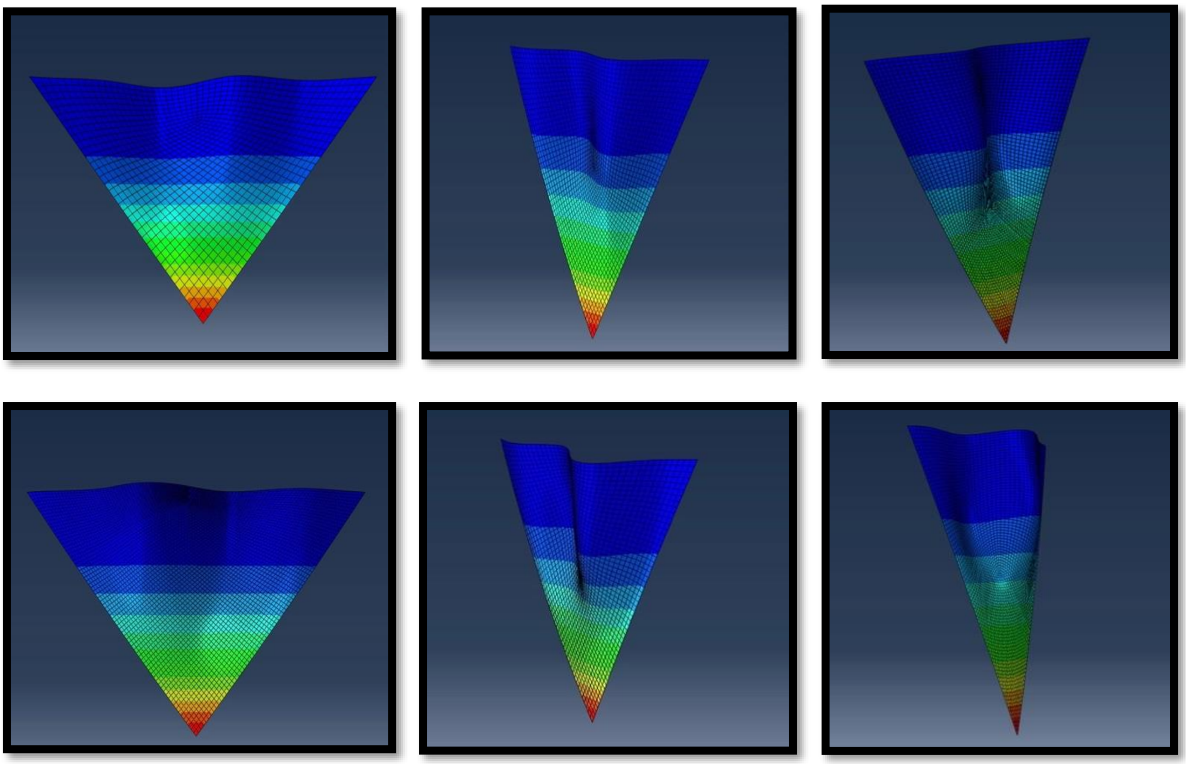

Figure 4.18: Triangular-valley arch dam buckling mode shapes for *a* = 50m, h=10%, t_1=0.5m t_2=1.0m for circular arch (first three mode shapes with b/a=0.50, 1.0 and 1.50 respectively) and parabolic arch (last three mode shapes with b/a=0.50, 1.0 and 1.50 respectively).

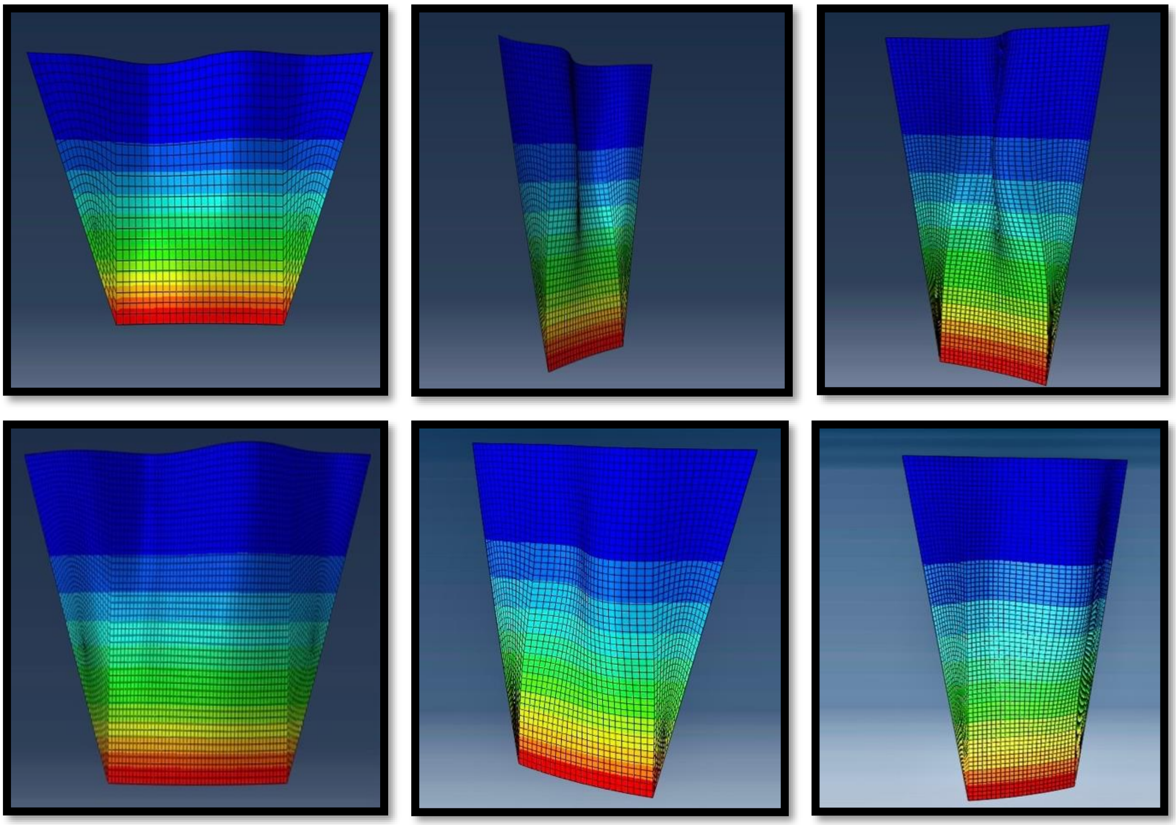

Figure 4.19: Trapezoidal-valley arch dam buckling mode shapes for *a* = 50m, h=10%, t_1=0.5m t_2=1.0m for circular arch (first three mode shapes with b/a=0.50, 1.0 and 1.50 respectively) and parabolic arch (last three mode shapes with b/a=0.50, 1.0 and 1.50 respectively).

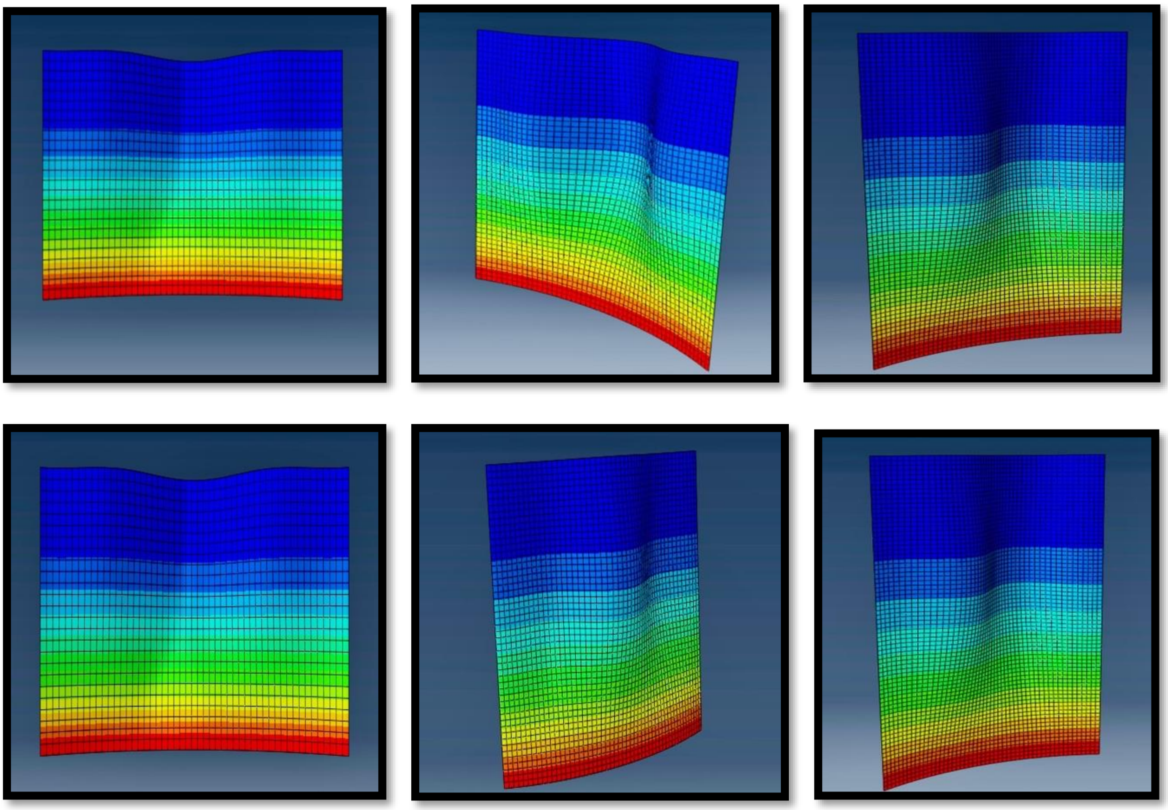

Figure 4.20: Rectangular-valley arch dam buckling mode shapes for *a* = 50m, h=10%, t_1=0.5m t_2=1.0m for circular arch (first three mode shapes with b/a=0.50, 1.0 and 1.50 respectively) and parabolic arch (last three mode shapes with b/a=0.50, 1.0 and 1.50 respectively).

The following tables, 4.19(a)-(c), 4.20(a)-(c), and 4.21(a)-(c), compare the buckling pressures for triangular, trapezoidal, and rectangular-valley arch dams between circular and parabolic arch profiles, assuming the thickness t varies quadratically in two cases, namely t_1=0.5m & t_2=1.0m and t_1=1.0m & t_2=2.0m, for three representative rise ratio values (5%, 10%, 25%).

t1=0.5m & t2=1.0m; h=10%							**t1=1.0m & t2=2.0m; h=10%**						
Critical Buckling Pressure Pcr (kN/m2)							**Critical Buckling Pressure Pcr (kN/m2)**						
a=100m				**a=50m**			**a=100m**				**a=50m**		
b/a	**Circular**	**Parabola**	**Diff. %**	**Circular**	**Parabola**	**Diff. %**	**b/a**	**Circular**	**Parabola**	**Diff. %**	**Circular**	**Parabola**	**Diff. %**
0,5	604	622	2,89	4190	4285	2,22	0,5	4359	4456	2,18	32683	33070	1,17
1	384	395	2,78	2531	2582	1,98	1	2581	2633	1,97	19841	20039	0,99
1,5	309	317	2,52	2033	2074	1,98	1,5	2061	2102	1,95	16048	16247	1,22
2	268	274	2,19	1801	1837	1,96	2	1819	1855	1,94	14362	14557	1,34

Table 4.19(a): Triangular-valley arch dam results of circular vs. parabolic arch for h=10%.

t1=0.5m & t2=1.0m; h=5%							t1=1.0m & t2=2.0m; h=5%						
Critical Buckling Pressure Pcr (kN/m2)							Critical Buckling Pressure Pcr (kN/m2)						
a=100m				a=50m			a=100m				a=50m		
b/a	Circular	Parabola	Diff. %	Circular	Parabola	Diff. %	b/a	Circular	Parabola	Diff. %	Circular	Parabola	Diff. %
0,5	292	294	0,68	2231	2238	0,31	0,5	2328	2335	0,30	26698	26678	-0,07
1	174	175	0,57	1380	1375	-0,36	1	1398	1402	0,29	13153	13073	-0,61
1,5	139	140	0,71	1110	1114	0,36	1,5	1126	1129	0,27	11226	11239	0,12
2	123	124	0,81	994	997	0,30	2	1004	1008	0,40	10242	10255	0,13

Table 4.19(b): Triangular-valley arch dam results of circular vs. parabolic arch for h=5%.

t1=0.5m & t2=1.0m; h=25%							t1=1.0m & t2=2.0m; h=25%						
Critical Buckling Pressure Pcr (kN/m2)							Critical Buckling Pressure Pcr (kN/m2)						
a=100m				a=50m			a=100m				a=50m		
b/a	Circular	Parabola	Diff. %	Circular	Parabola	Diff. %	b/a	Circular	Parabola	Diff. %	Circular	Parabola	Diff. %
0,5	1344	1627	17,39	8436	9955	15,26	0,5	8781	10357	15,22	57641	65464	11,95
1	833	977	14,74	5416	6215	12,86	1	5519	6329	12,80	34565	38610	10,48
1,5	655	752	12,90	4435	5095	12,95	1,5	4490	5158	12,95	27414	30137	9,04
2	567	648	12,50	3836	4356	11,94	2	3872	4396	11,92	23787	25921	8,23

Table 4.19(c): Triangular-valley arch dam results of circular vs. parabolic arch for h=25%.

t1=0.5m & t2=1.0m; h=10%							t1=1.0m & t2=2.0m; h=10%						
Critical Buckling Pressure Pcr (kN/m2)							Critical Buckling Pressure Pcr (kN/m2)						
a=100m				a=50m			a=100m				a=50m		
b/a	Circular	Parabola	Diff. %	Circular	Parabola	Diff. %	b/a	Circular	Parabola	Diff. %	Circular	Parabola	Diff. %
0,5	378	386	2,07	2550	2595	1,73	0,5	2646	2690	1,64	17824	17977	0,85
1	254	260	2,31	1559	1581	1,39	1	1588	1611	1,43	11388	11494	0,92
1,5	204	208	1,92	1297	1315	1,37	1,5	1314	1333	1,43	9813	9922	1,10
2	178	180	1,11	1178	1195	1,42	2	1190	1207	1,41	9106	9212	1,15

Table 4.20(a): Trapezoidal-valley arch dam results of circular vs. parabolic arch for h=10%.

t1=0.5m & t2=1.0m; h=5%							t1=1.0m & t2=2.0m; h=5%						
Critical Buckling Pressure Pcr (kN/m2)							Critical Buckling Pressure Pcr (kN/m2)						
a=100m				a=50m			a=100m				a=50m		
b/a	Circular	Parabola	Diff. %	Circular	Parabola	Diff. %	b/a	Circular	Parabola	Diff. %	Circular	Parabola	Diff. %
0,5	176	176	0,00	1201	1204	0,25	0,5	1246	1249	0,24	11154	11160	0,05
1	106	106	0,00	775	777	0,26	1	792	793	0,13	7295	7303	0,11
1,5	88	88	0,00	670	672	0,30	1,5	680	682	0,29	6499	6508	0,14
2	80	80	0,00	622	624	0,32	2	629	631	0,32	6038	6042	0,07

Table 4.20(b): Trapezoidal-valley arch dam results of circular vs. parabolic arch for h=5%.

t1=0.5m & t2=1.0m; h=25%							t1=1.0m & t2=2.0m; h=25%						
Critical Buckling Pressure Pcr (kN/m2)							Critical Buckling Pressure Pcr (kN/m2)						
a=100m				a=50m			a=100m				a=50m		
b/a	Circular	Parabola	Diff. %	Circular	Parabola	Diff. %	b/a	Circular	Parabola	Diff. %	Circular	Parabola	Diff. %
0,5	938	1059	11,43	5637	6280	10,24	0,5	5849	6511	10,17	37017	40455	8,50
1	556	617	9,89	3547	3916	9,42	1	3566	3965	10,06	23090	24769	6,78
1,5	428	480	10,83	3004	3360	10,60	1,5	2995	3410	12,17	18508	19601	5,58
2	377	425	11,29	2676	2886	7,28	2	2678	2898	7,59	16278	17219	5,46

Table 4.20(c): Trapezoidal-valley arch dam results of circular vs. parabolic arch for h=25%.

t1=0.5m & t2=1.0m; h=10%							t1=1.0m & t2=2.0m; h=10%						
Critical Buckling Pressure Pcr (kN/m2)							Critical Buckling Pressure Pcr (kN/m2)						
a=100m				a=50m			a=100m				a=50m		
b/a	Circular	Parabola	Diff. %	Circular	Parabola	Diff. %	b/a	Circular	Parabola	Diff. %	Circular	Parabola	Diff. %
0,5	322	325	0,92	1997	2002	0,25	0,5	2070	2075	0,24	14588	14703	0,78
1	186	187	0,53	1262	1276	1,10	1	1287	1300	1,00	7768	7748	-0,26
1,5	154	155	0,65	968	963	-0,52	1,5	978	973	-0,51	6327	6328	0,02
2	140	142	1,41	831	829	-0,24	2	838	836	-0,24	5779	5787	0,14

Table 4.21(a): Rectangular-valley arch dam results of circular vs. parabolic arch for h=10%.

t1=0.5m & t2=1.0m; h=5%							t1=1.0m & t2=2.0m; h=5%						
Critical Buckling Pressure Pcr (kN/m2)							Critical Buckling Pressure Pcr (kN/m2)						
a=100m				a=50m			a=100m				a=50m		
b/a	Circular	Parabola	Diff. %	Circular	Parabola	Diff. %	b/a	Circular	Parabola	Diff. %	Circular	Parabola	Diff. %
0,5	138	138	0,00	990	990	0,00	0,5	1023	1023	0,00	7816	7811	-0,06
1	86	87	1,15	526	526	0,00	1	536	536	0,00	4350	4350	0,00
1,5	65	65	0,00	431	431	0,00	1,5	437	437	0,00	3645	3646	0,03
2	56	56	0,00	394	394	0,00	2	398	399	0,25	3377	3379	0,06

Table 4.21(b): Rectangular -valley arch dam results of circular vs. parabolic arch for h=5%.

t1=0.5m & t2=1.0m; h=25%							t1=1.0m & t2=2.0m; h=25%						
Critical Buckling Pressure Pcr (kN/m2)							Critical Buckling Pressure Pcr (kN/m2)						
a=100m				a=50m			a=100m				a=50m		
b/a	Circular	Parabola	Diff. %	Circular	Parabola	Diff. %	b/a	Circular	Parabola	Diff. %	Circular	Parabola	Diff. %
0,5	808	744	-8,60	4731	4581	-3,27	0,5	4896	4751	-3,05	30356	30016	-1,13
1	449	448	-0,22	2722	2697	-0,93	1	2763	2740	-0,84	16964	17816	4,78
1,5	343	341	-0,59	2081	2175	4,32	1,5	2105	2201	4,36	14423	14209	-1,51
2	278	288	3,47	1857	1975	5,97	2	1874	1995	6,07	11978	11603	-3,23

Table 4.21(c): Rectangular -valley arch dam results of circular vs. parabolic arch for h=25%.

The distinction between circular and parabolic arch profile results for the triangular-valley arch dam is less than 0.40 %, 2.30 %, and 15.30 % for the 5%, 10%, and 25% rise ratios for the 50 m wide dam respectively, and less than 0.80 %, 2.90 %, and 17.40 % for the 100 m wide dam respectively. Quadratic thickness variation also exhibit similar differences that exist between the rectangular and trapezoidal-valley arch dams in terms of the three rise ratio parameters.

Figures 4.21-4.26 depict the critical buckling pressure results corresponding to the various aspect ratios b/a. The first two figures (Figs. 4.21-4.22) depict shell-thickness expressions for two cases, namely t1=0.5m & t2=1.0m and t1=1.0m & t2=2.0m, for the triangular-valley arch dam with the parameter *a* fixed at 50m and 100m, while the following four figures depict the trapezoidal and rectangular-valley arch dam results for the same shell-thickness expressions and *a* parameter values.

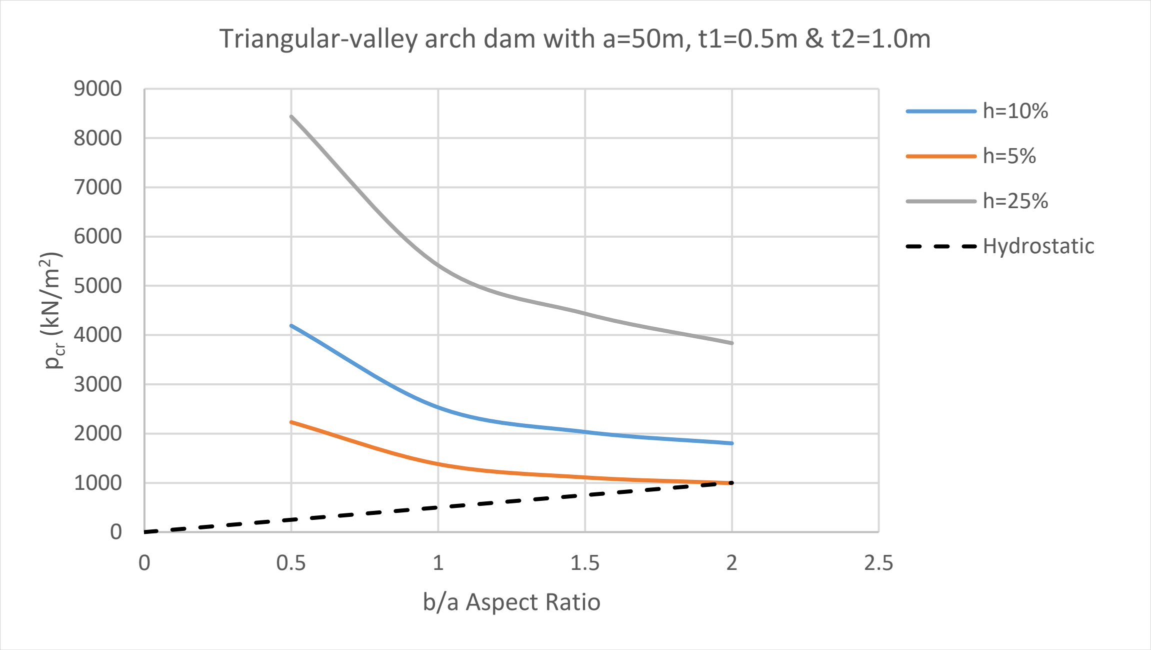

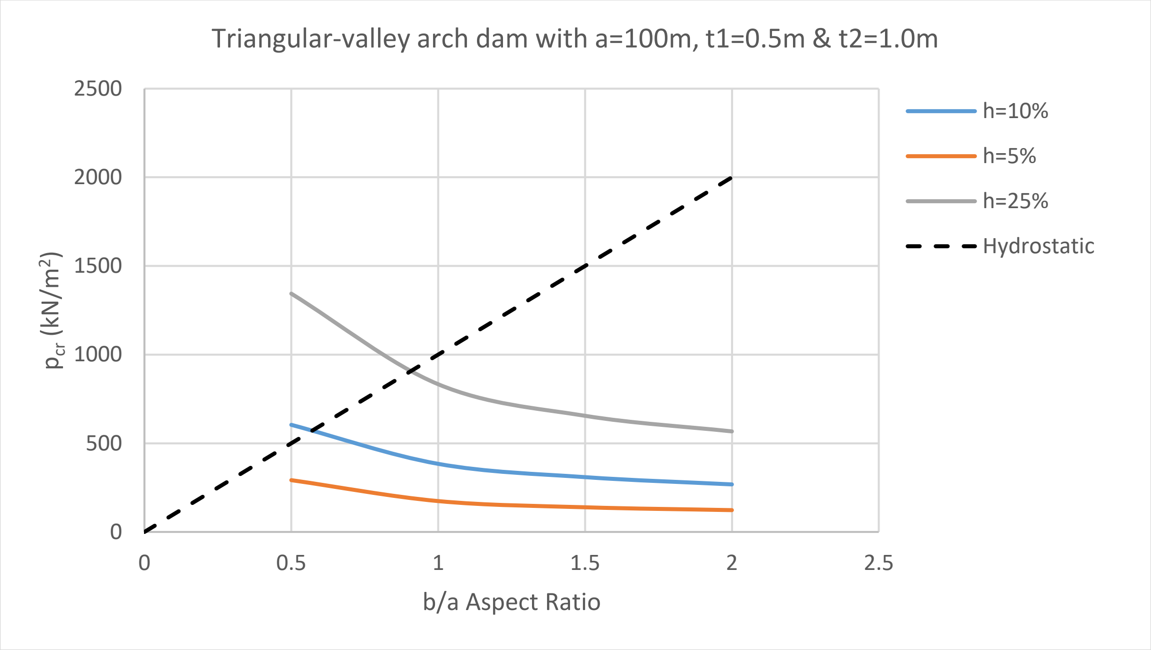

Figure 4.21: Critical buckling pressure plots for the parabolic arch dam of thickness expression t_1=0.5m & t_2=1.0m.

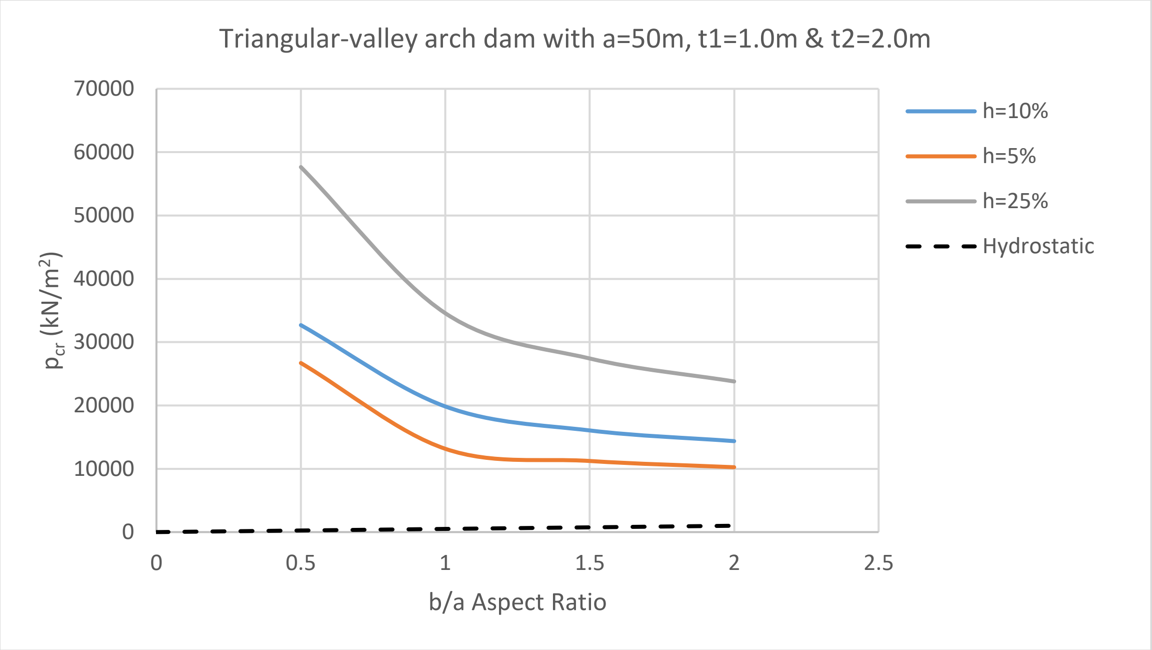

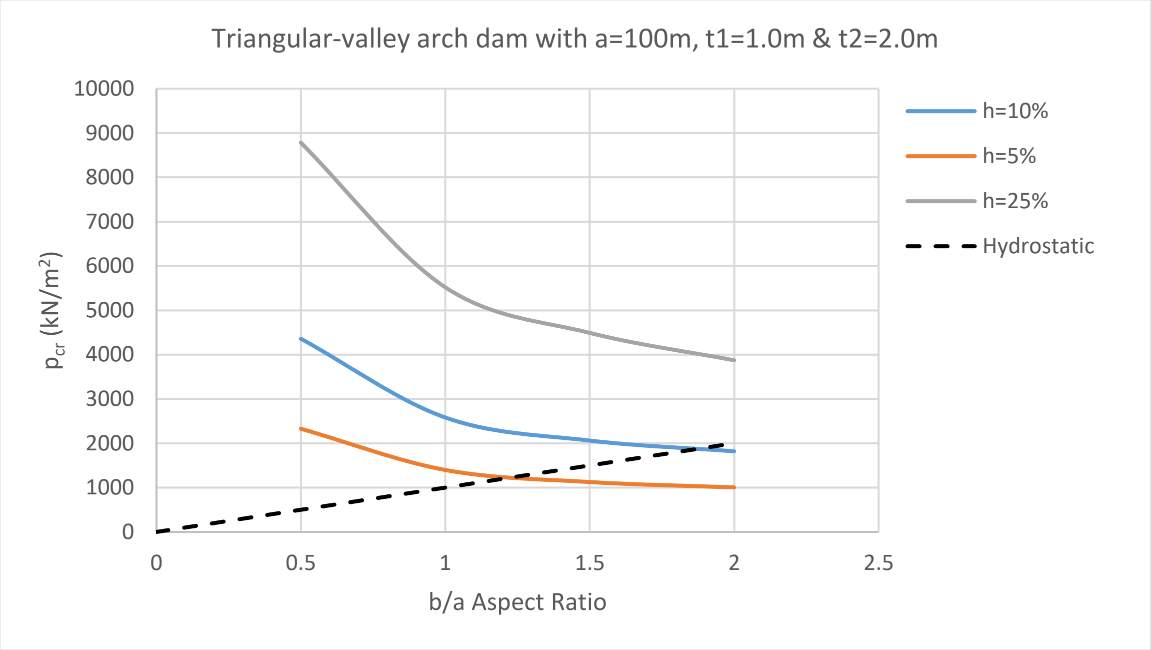

Figure 4.22: Critical buckling pressure plots for the parabolic arch dam of thickness expression t_1=1.0m & t_2=2.0m.

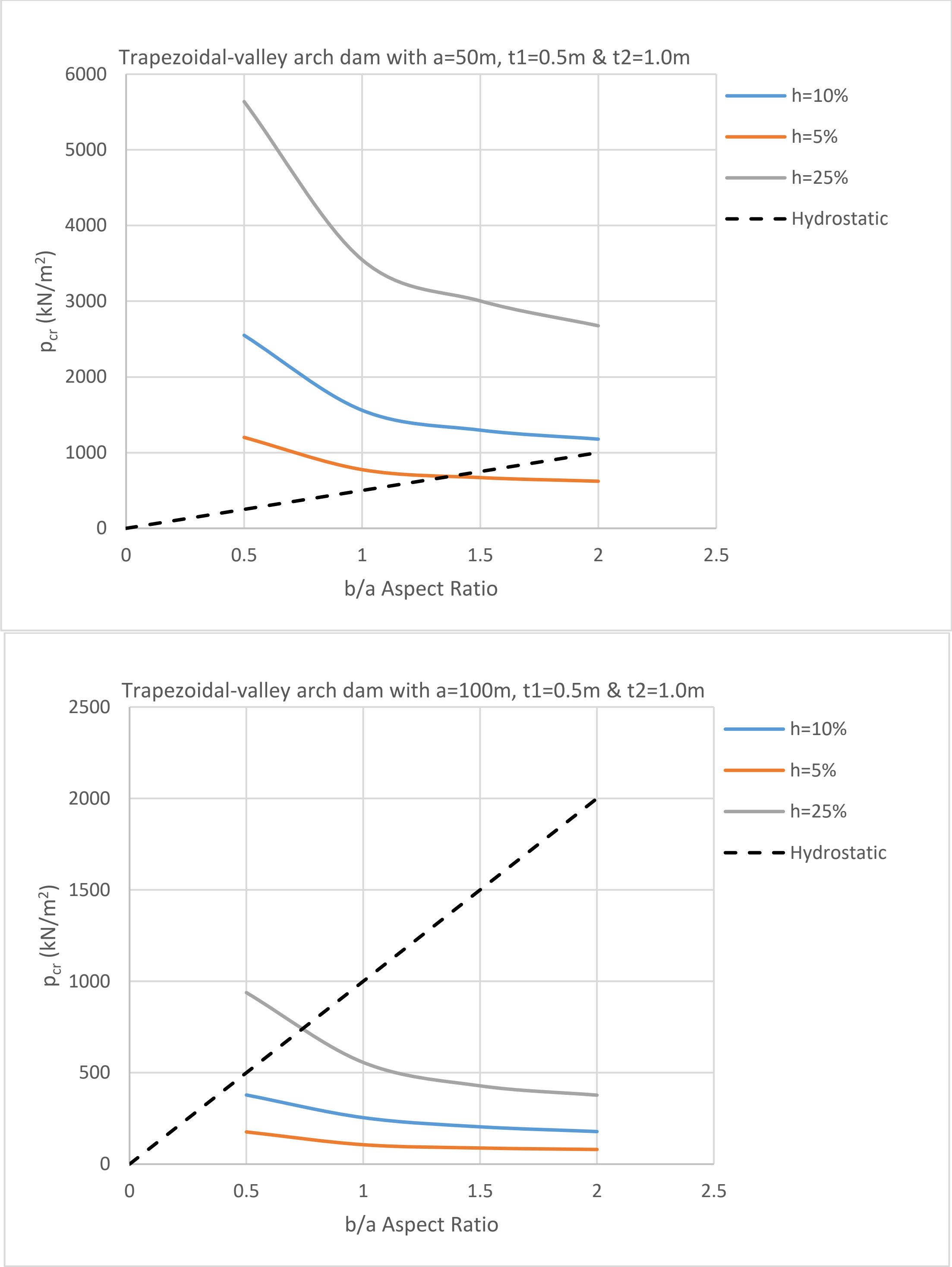

Figure 4.23: Critical buckling pressure plots for the parabolic arch dam of thickness expression t_1=0.5m & t_2=1.0m.

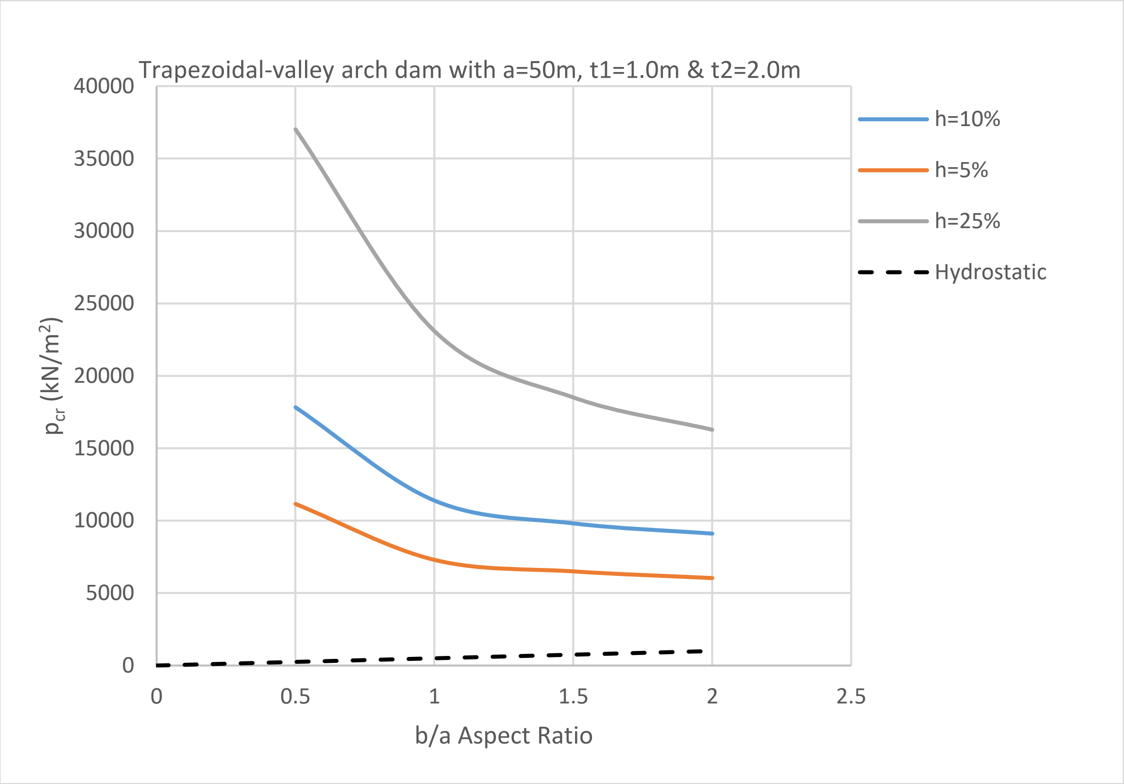

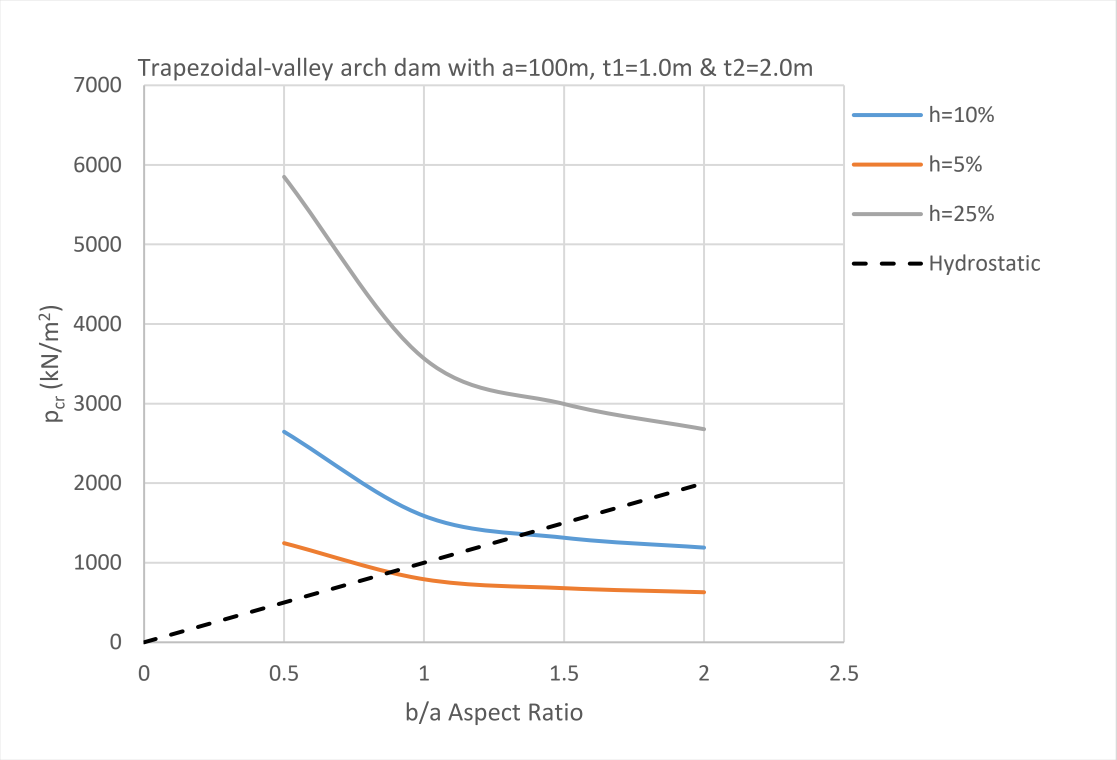

Figure 4.24: Critical buckling pressure plots for the parabolic arch dam of thickness expression t_1=1.0m & t_2=2.0m.

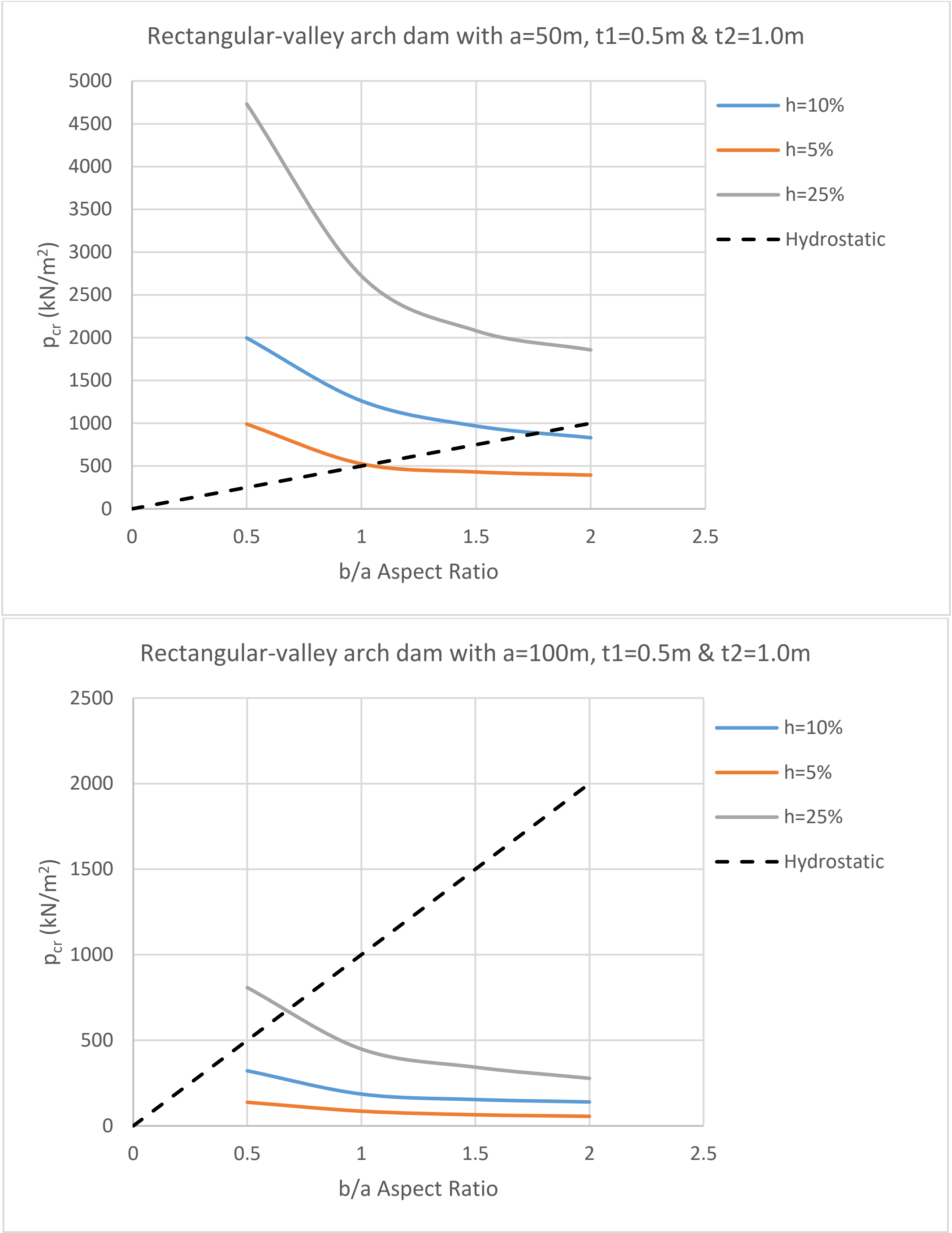

Figure 4.25: Critical buckling pressure plots for the parabolic arch dam of thickness expression t_1=0.5m & t_2=1.0m.

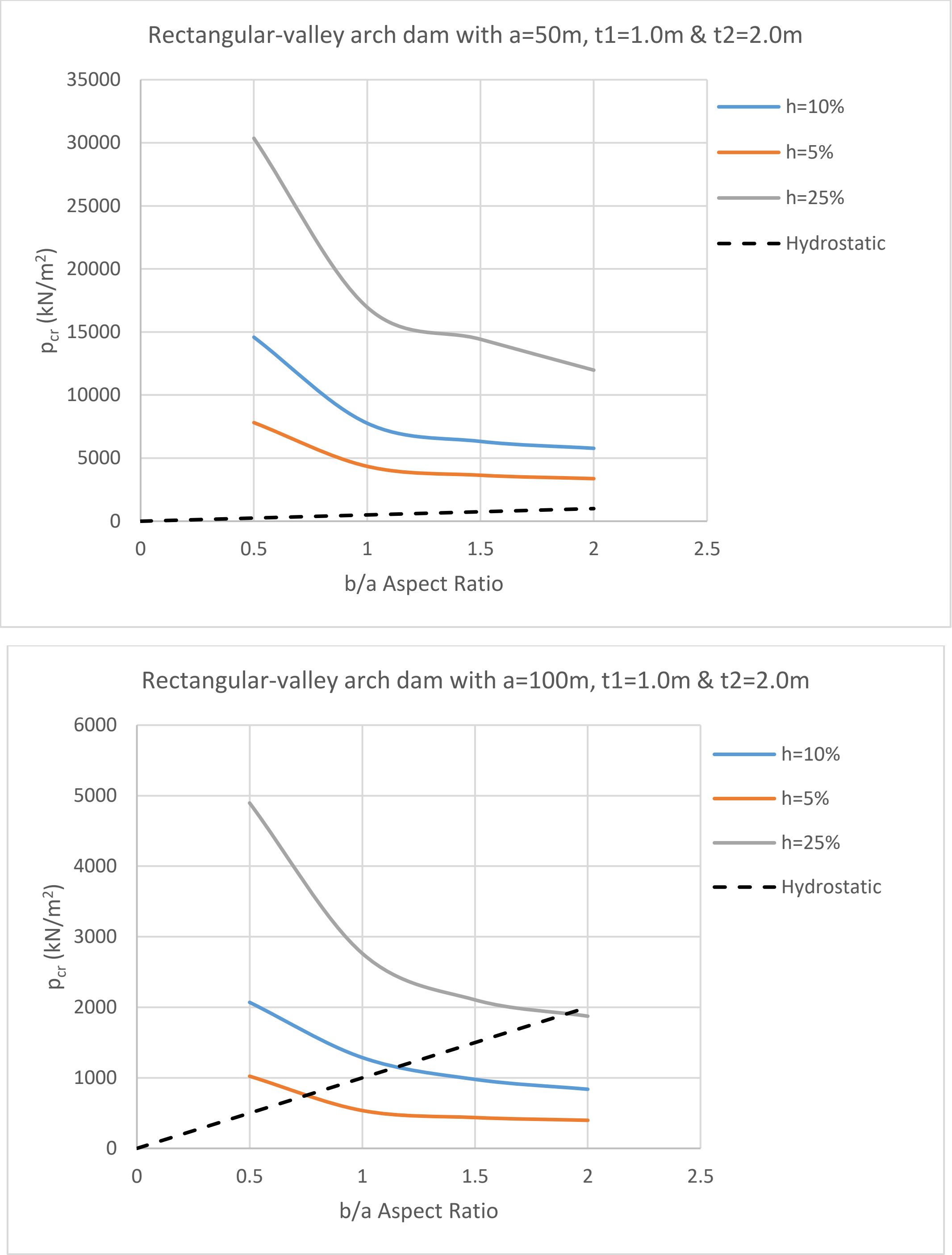

Figure 4.26: Critical buckling pressure plots for the parabolic arch dam of thickness expression t_1=1.0m & t_2=2.0m.

Figures 4.21-4.26 demonstrate that linear buckling analysis for triangular, trapezoidal, and rectangular-valley arch dams follows the same trend as constant and linear-thickness arch dam buckling analysis, where the buckling pressures decrease rapidly with increasing depth (aspect ratio), with the rate of decrease reducing as the aspect ratio of the dam increases. Conversely, the shell rise ratio h/a has a significant impact on the buckling strength of an arch dam.

The buckling strength comparison due to constant, linear and quadratic varying thickness for the 50m wide arch dam was further investigated. Tables 4.22-4.24 below show the difference in buckling strength between the 50m wide triangular-valley arch dam with constant thickness (1m & 2m), linear and quadratic varying thickness. It is clear that the 50m wide arch dam with constant thickness (1m and 2m), performs better than both linear and quadratic arch dams with the thickness expressions t_1=0.5m & t_2=1.0m and t_1=1.0m & t_2=2.0m.

When comparing the buckling strength between arch dams with linear and quadratic varying thickness with the thickness- expression, t_1=0.5m & t_2=1.0m, arch dams with linear varying thickness out-perform quadratic varying thickness arch dams by an average margin of 38%, 36% and 34% for the 5%, 10%, and 25% rise ratios respectively. Whereas, arch dam with linear varying thickness-expression t_1=1.0m & t_2=2.0m, performs better than quadratic varying thickness arch dam by an average margin of 38%, 37% and 34% for the 5%, 10%, and 25% rise ratios respectively.

h=5%								
t1=0.5m & t2=1.0m vs constant thickness 1m					t1=1.0m & t2=2.0m vs constant thickness 2m			
b/a	**linear**	**Quadratic**	**constant**	**Diff %**	**linear**	**Quadratic**	**constant**	**Diff%**
0,25	18253	-	75471	-	390873	-	1276030	-
0,5	3660	2238	17693	38,85	49593	26678	258394	46,21
0,75	2510	-	12292	-	26092	-	151068	-
1	2152	1375	10676	36,11	20322	13073	123463	35,67
1,25	1930	-	9795,3	-	18183	-	112550	-
1,5	1781	1114	9159,6	37,45	17119	11239	106417	34,35
1,75	1676	-	8672,5	-	16442	-	101759	-
2	1600	997	8296	37,69	15932	10255	97721	35,63
			Average	**38**			**Average**	**38**

Table 4.22: Constant thickness vs linear and quadratic varying thickness buckling strength results, h=5%.

h=10%								
t1=0.5m & t2=1.0m vs. constant thickness 1m					t1=1.0m & t2=2.0m vs. constant thickness 2m			
b/a	linear	Quadratic	constant	Diff %	linear	Quadratic	constant	Diff%
0,25	17017	-	64362	-	255982	-	925654	-
0,5	6579	4285	24375	34,87	53649	33070	245376	38,36
0,75	4909	-	18205	-	36737	-	169819	-
1	4082	2582	15148	36,75	31038	20039	146557	35,44
1,25	3542	-	13077	-	27762	-	130315	-
1,5	3296	2074	12083	37,08	25580	16247	121918	36,49
1,75	3079	-	11431	-	24065	-	115693	-
2	2919	1837	10975	37,07	22967	14557	110996	36,62
			Average	**36**			**Average**	**37**

Table 4.23: Constant thickness vs linear and quadratic varying thickness buckling strength results, h=10%.

h=25%								
t1=0.5m & t2=1.0m vs constant thickness 1m					t1=1.0m & t2=2.0m vs constant thickness 2m			
b/a	linear	Quadratic	constant	Diff %	linear	Quadratic	constant	Diff%
0,25	29977	-	92883	-	236169	-	744752	-
0,5	15279	9955	45713	34,85	98907	65464	315673	33,81
0,75	11402	-	32749	-	71159	-	226116	-
1	9524	6215	26954	34,74	58268	38610	185987	33,74
1,25	8445	-	23666	-	50685	-	164620	-
1,5	7713	5095	21560	33,94	45612	30137	151695	33,93
1,75	7091	-	20112	-	41968	-	143158	-
2	6593	4356	19064	33,93	39227	25921	137172	33,92
			Average	**34**			**Average**	**34**

Table 4.24: Constant thickness vs linear and quadratic varying thickness buckling strength results, h=25%.

4.2 Results for Double Curvature Modelling

4.2.1 Double Curvature Modelling with Constant Thickness

Figure 4.27 and 4.28 illustrates double-curvature mode shapes for the triangular and trapezoidal parabolic cylinder and elliptic paraboloid arch profiles respectively, having constant thickness, 0.5m, 1.0m, and 2.0m.

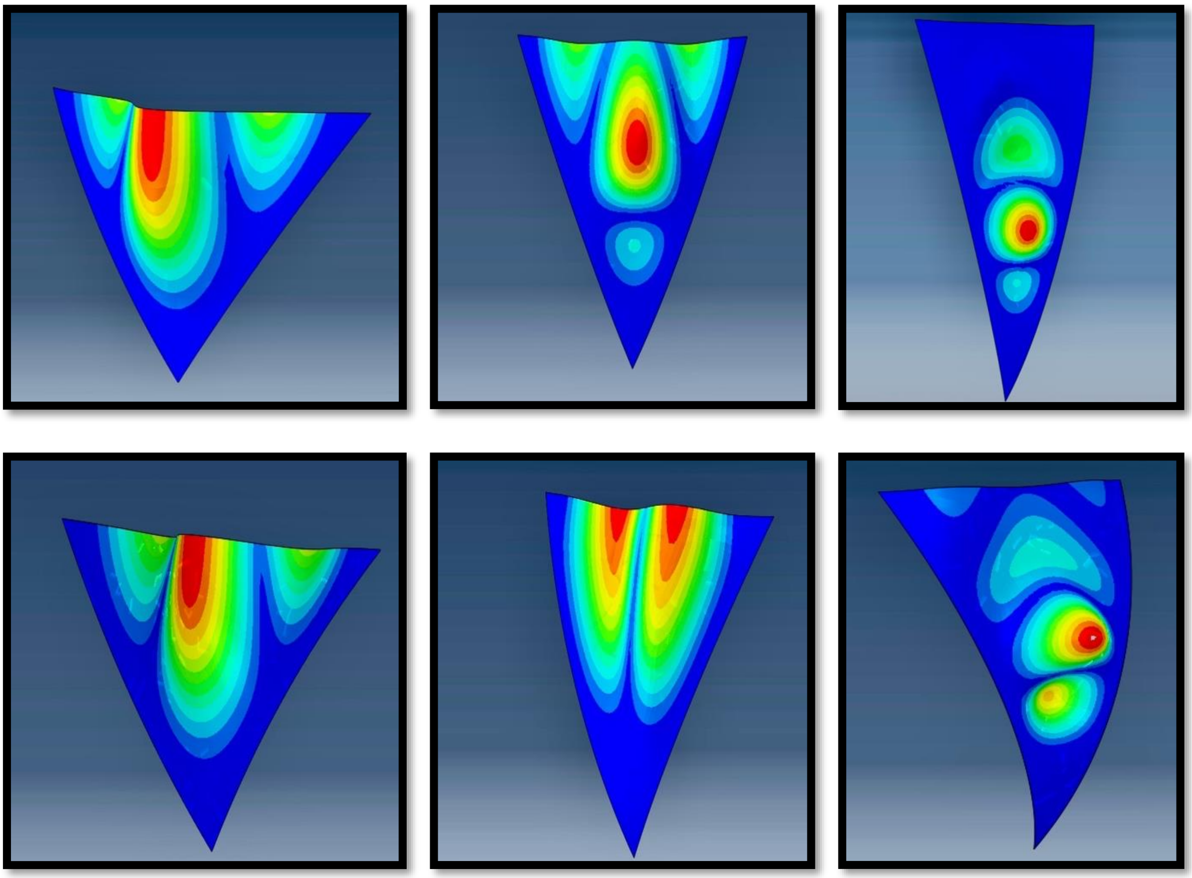

Figure 4.27: Triangular-valley arch dam buckling mode shapes for *a* = 50m, h=10% and t=1.0m for parabolic cylinder arch (first three mode shapes with b/a=0.50, 1.0, and 1.50 respectively) and elliptic paraboloid arch (last three mode shapes with b/a=0.50, 1.0, and 1.50 respectively).

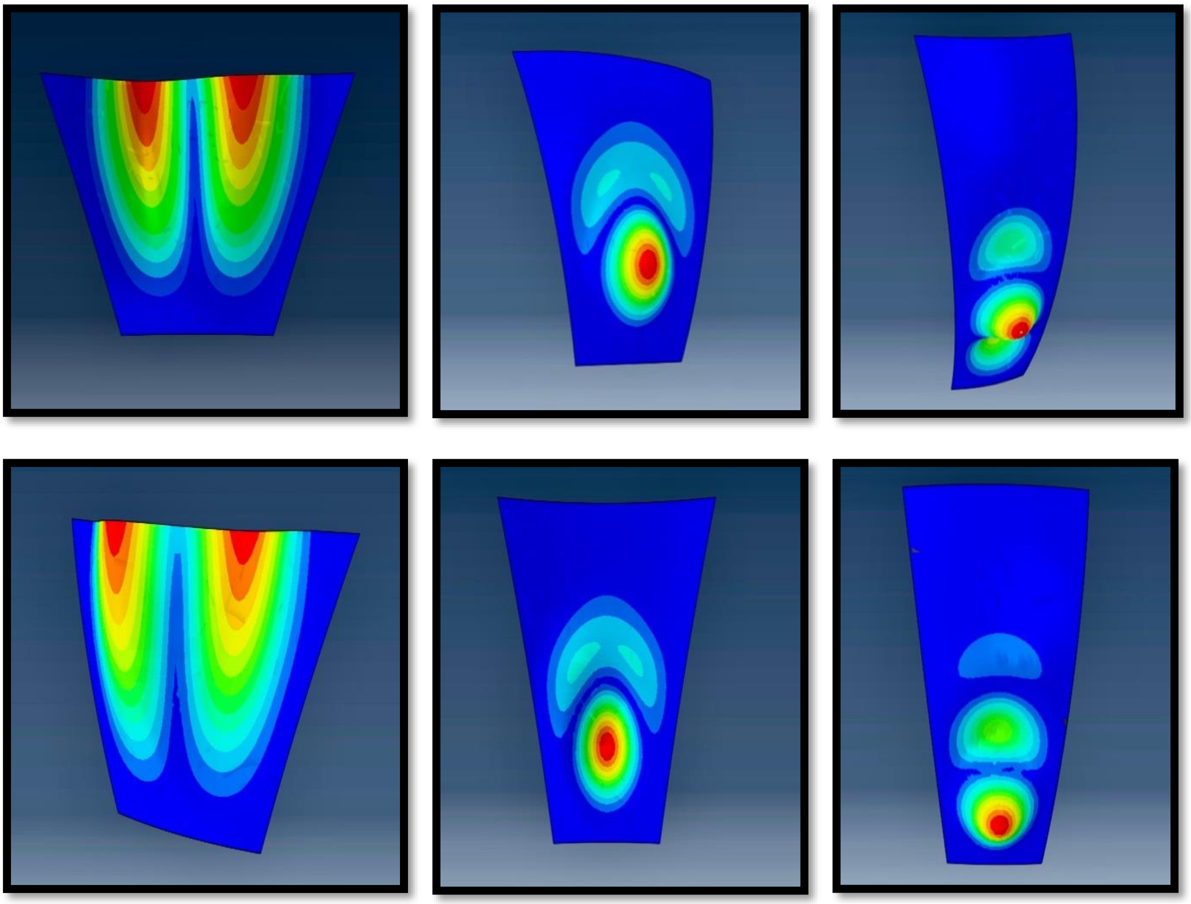

Figure 4.28: Trapezoidal-valley arch dam buckling mode shapes for *a* = 50m, h=10% and t=1.0m for parabolic cylinder arch (first three mode shapes with b/a=0.50, 1.0, and 1.50 respectively) and elliptic paraboloid arch (last three mode shapes with b/a=0.50, 1.0, and 1.50 respectively).

The tables, 4.25 (a)-(c) and 4.26 (a)-(c) compare the buckling pressures for the triangular and trapezoidal-valley arch dams, with parabolic cylinder and elliptical paraboloid profiles assuming t is constant (0.5m, t=1.0m, t=2.0m) for three representative rise ratio values (5%, 10%, 25%).

t=0.5m; h=10%				t=1.0m; h=10%				t=2.0m; h=10%			
Critical Buckling Pressure Pcr (kN/m2)				Critical Buckling Pressure Pcr (kN/m2)				Critical Buckling Pressure Pcr (kN/m2)			
a=50m				a=50m				a=50m			
b/a	PC	EP	ξ	b/a	PC	EP	ξ	b/a	PC	EP	ξ
0,25	6167	6105	0,99	0,25	69293	69475	1,00	0,25	1040500	1030550	0,99
0,5	4344	4436	1,02	0,5	29035	29467	1,01	0,5	278159	279599	1,01
0,75	5079	5536	1,09	0,75	27231	28320	1,04	0,75	204802	208898	1,02
1	4934	5279	1,07	1	29418	31477	1,07	1	186925	192533	1,03
1,25	4667	4881	1,05	1,25	27774	28607	1,03	1,25	184647	188340	1,02
1,5	4425	4613	1,04	1,5	26178	26663	1,02	1,5	182291	182291	1,00
1,75	4247	4416	1,04	1,75	24799	25257	1,02	1,75	170661	167247,8	0,98
2	4123	4268	1,04	2	23808	24161	1,01	2	162651	156651	0,96

Table 4.25(a): Triangular-valley arch dam results of parabolic cylinder vs. elliptic paraboloid for h=10%.

t=0.5m; h=5%				t=1.0m; h=5%				t=2.0m; h=5%			
Critical Buckling Pressure Pcr (kN/m2)				Critical Buckling Pressure Pcr (kN/m2)				Critical Buckling Pressure Pcr (kN/m2)			
a=50m				a=50m				a=50m			
b/a	PC	EP	ξ	b/a	PC	EP	ξ	b/a	PC	EP	ξ
0,25	4572	5948	1,30	0,25	82087	71797	0,87	0,25	1375550	1056180	0,77
0,5	1950	2738	1,40	0,5	19427	23211	1,19	0,5	292808	284003	0,97
0,75	1838	2210	1,20	0,75	14515	17191	1,18	0,75	171733	188193	1,10
1	1956	2051	1,05	1	13303	15169	1,14	1	138675	153606	1,11
1,25	1876	2015	1,07	1,25	13003	14237	1,09	1,25	123519	134787	1,09
1,5	1771	2019	1,14	1,5	12793	13710	1,07	1,5	114521	122592	1,07
1,75	1684	2012	1,19	1,75	12036	13335	1,11	1,75	108713	114213	1,05
2	1615	1965	1,22	2	11443	12913	1,13	2	104528	107445	1,03

Table 4.25(b): Triangular-valley arch dam results of parabolic cylinder vs. elliptic paraboloid for h=5%.

t=0.5m; h=25%				t=1.0m; h=25%				t=2.0m; h=25%			
Critical Buckling Pressure Pcr (kN/m2)				Critical Buckling Pressure Pcr (kN/m2)				Critical Buckling Pressure Pcr (kN/m2)			
a=50m				a=50m				a=50m			
b/a	PC	EP	ξ	b/a	PC	EP	ξ	b/a	PC	EP	ξ
0,25	15689	16598	1,06	0,25	110675	106977	0,97	0,25	894164	881683	0,99
0,5	8372	14988	1,79	0,5	50096	76305	1,52	0,5	352379	425613	1,21
0,75	7153	14331	2,00	0,75	38812	71548	1,84	0,75	259642	360447	1,39
1	7157	13314	1,86	1	35617	63383	1,78	1	227315	318506	1,40
1,25	7655	12017	1,57	1,25	35303	53320	1,51	1,25	214188	279737	1,31
1,5	8074	10217	1,27	1,5	36019	44080	1,22	1,5	208642	246182	1,18
1,75	7563	7910	1,05	1,75	36098	36562	1,01	1,75	204210	217076	1,06
2	7078	6107	0,86	2	34816	30560	0,88	2	197946	191004	0,96

Table 4.25(c): Triangular-valley arch dam results of parabolic cylinder vs. elliptic paraboloid for h=25%.

t=0.5m; h=10%				t=1.0m; h=10%				t=2.0m; h=10%			
Critical Buckling Pressure Pcr (kN/m2)				Critical Buckling Pressure Pcr (kN/m2)				Critical Buckling Pressure Pcr (kN/m2)			
a=50m				a=50m				a=50m			
b/a	PC	EP	ξ	b/a	PC	EP	ξ	b/a	PC	EP	ξ
0,25	2953	1595	0,54	0,25	23549	20959	0,89	0,25	531041	286762	0,54
0,5	2967	3768	1,27	0,5	14872	19334	1,30	0,5	84964	93460	1,10
0,75	2920	4789	1,64	0,75	16174	24261	1,50	0,75	63983	83178	1,30
1	2854	5052	1,77	1	15405	20643	1,34	1	55259	66311	1,20
1,25	2761	4142	1,50	1,25	14056	15462	1,10	1,25	49914	48916	0,98
1,5	2620	3537	1,35	1,5	12877	12233	0,95	1,5	45524	34143	0,75
1,75	2478	3246	1,31	1,75	12069	10983	0,91	1,75	42735	27778	0,65
2	2358	3065	1,30	2	11463	9858	0,86	2	41647	24988	0,60

Table 4.26(a): Trapezoidal-valley arch dam results of parabolic cylinder vs. elliptic paraboloid for h=10%.

t=0.5m; h=5%				t=1.0m; h=5%				t=2.0m; h=5%			
Critical Buckling Pressure Pcr (kN/m2)				Critical Buckling Pressure Pcr (kN/m2)				Critical Buckling Pressure Pcr (kN/m2)			
a=50m				a=50m				a=50m			
b/a	PC	EP	ξ	b/a	PC	EP	ξ	b/a	PC	EP	ξ
0,25	1553	2332	1,50	0,25	20521	21000	1,02	0,25	399455	293231	0,73
0,5	1002	1691	1,69	0,5	7537	9798	1,30	0,5	88405	97322	1,10
0,75	1086	1635	1,51	0,75	7204	11166	1,55	0,75	64856	86740	1,34
1	1040	1370	1,32	1	6694	10494	1,57	1	56831	84370	1,48
1,25	954	1082	1,13	1,25	5972	8579	1,44	1,25	52719	71968	1,37
1,5	880	932	1,06	1,5	5487	7229	1,32	1,5	48653	63365	1,30
1,75	830	849	1,02	1,75	5165	6437	1,25	1,75	45749	58080	1,27
2	795	799	1,01	2	4946	5896	1,19	2	43787	54383	1,24

Table 4.26(b): Trapezoidal-valley arch dam results of parabolic cylinder vs. elliptic paraboloid for h=5%.

t=0.5m; h=25%				t=1.0m; h=25%				t=2.0m; h=25%			
Critical Buckling Pressure Pcr (kN/m2)				Critical Buckling Pressure Pcr (kN/m2)				Critical Buckling Pressure Pcr (kN/m2)			
a=50m				a=50m				a=50m			
b/a	PC	EP	ξ	b/a	PC	EP	ξ	b/a	PC	EP	ξ
0,25	7966	9812	1,23	0,25	48686	51403	1,06	0,25	344404	353184	1,03
0,5	6327	9491	1,50	0,5	32048	49953	1,56	0,5	187009	229024	1,22
0,75	5577	9481	1,70	0,75	29234	48714	1,67	0,75	170685	249293	1,46
1	3768	6153	1,63	1	23012	34290	1,49	1	157779	220891	1,40
1,25	2965	3948	1,33	1,25	17362	22050	1,27	1,25	123595	150273	1,22
1,5	2566	2662	1,04	1,5	14434	15156	1,05	1,5	105574	115587	1,09
1,75	2348	1882	0,80	1,75	12848	11697	0,91	1,75	96539	96169	1,00
2	2154	1341	0,62	2	11972	9361	0,78	2	89891	85147	0,95

Table 4.26(c): Trapezoidal-valley arch dam results of parabolic cylinder vs. elliptic paraboloid for h=25%.

The parameter ξ specifies the factor that increases the critical buckling pressure of the parabolic cylinder by giving it the elliptic paraboloid's double curvature while preserving the same aspect ratio and rise ratio. It is the ratio of the elliptic paraboloid's critical buckling pressures to that of the corresponding parabolic cylinder.

The beneficial effect of double curvature (as determined by the value of the parameter ξ) for triangular and trapezoidal-valley arch dam increases as the shell becomes thinner, as shown in Fig. 4.29-34. This beneficial effect also increases as the aspect ratio is increased from 0.25 to a peak of b/a = 0.50 for the thinner shell and b/a = 1.0 for the thicker shell of both geometric entities with a 5% rise ratio.

The beneficial effect of the shell with a 10% rise ratio peaks at b/a = 0.75 (triangular-valley arch dam) and 1.0 (trapezoidal-valley arch dam) for the thinner shell and at b/a = 1.0 (triangular-valley arch dam) and 0.75 (trapezoidal-valley arch dam) for the thicker shell. Whereas, the beneficial effect of the 25% rise ratio peaks at b/a = 0.75 (for geometric entities) for the thinner shell and at b/a = 1.0 (triangular-valley arch dam) and 0.75 (trapezoidal-valley arch dam) for the thicker shell.

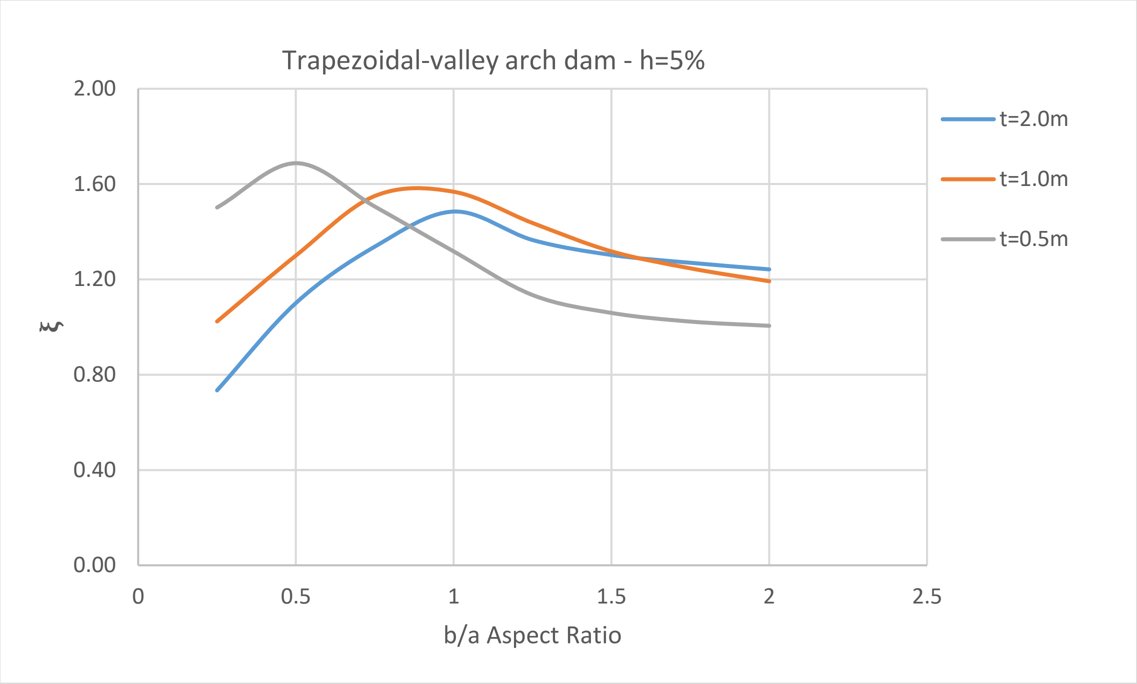

Figure 4.29: Variation of ξ and b/a with 5% rise ratio for various shell thicknesses (ratio of critical buckling pressure for elliptic paraboloid to critical buckling pressure for parabolic cylinder).

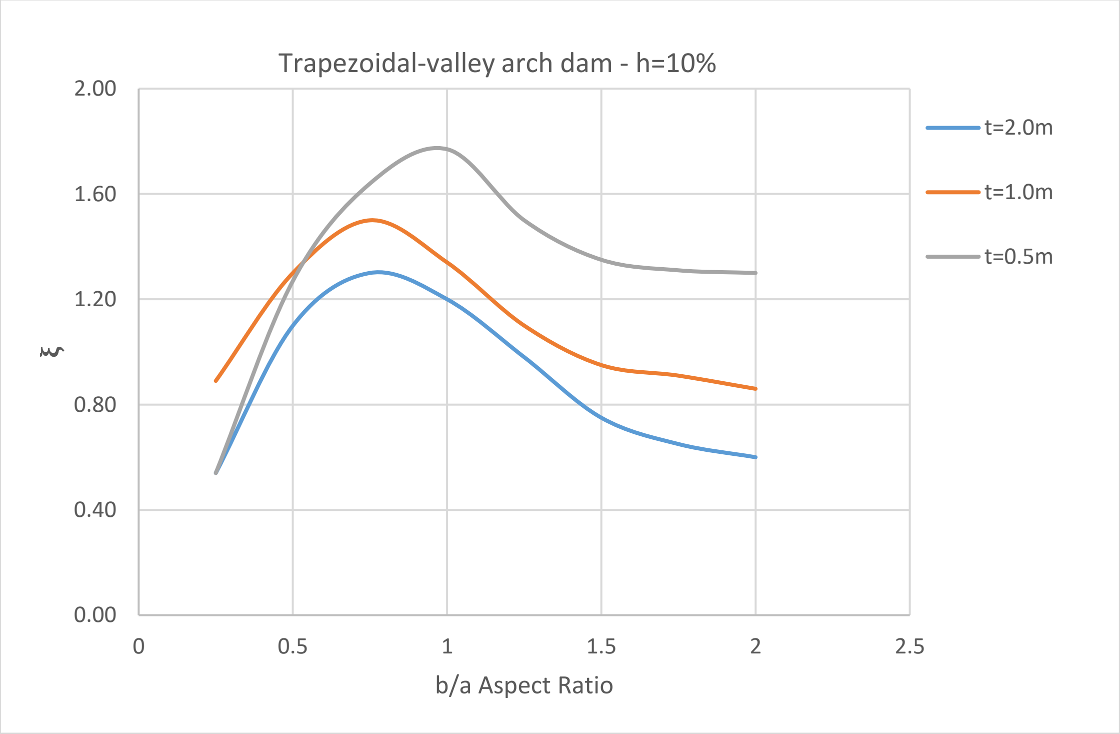

Figure 4.30: Variation of ξ and b/a with 10% rise ratio for various shell thicknesses (ratio of critical buckling pressure for elliptic paraboloid to critical buckling pressure for parabolic cylinder).

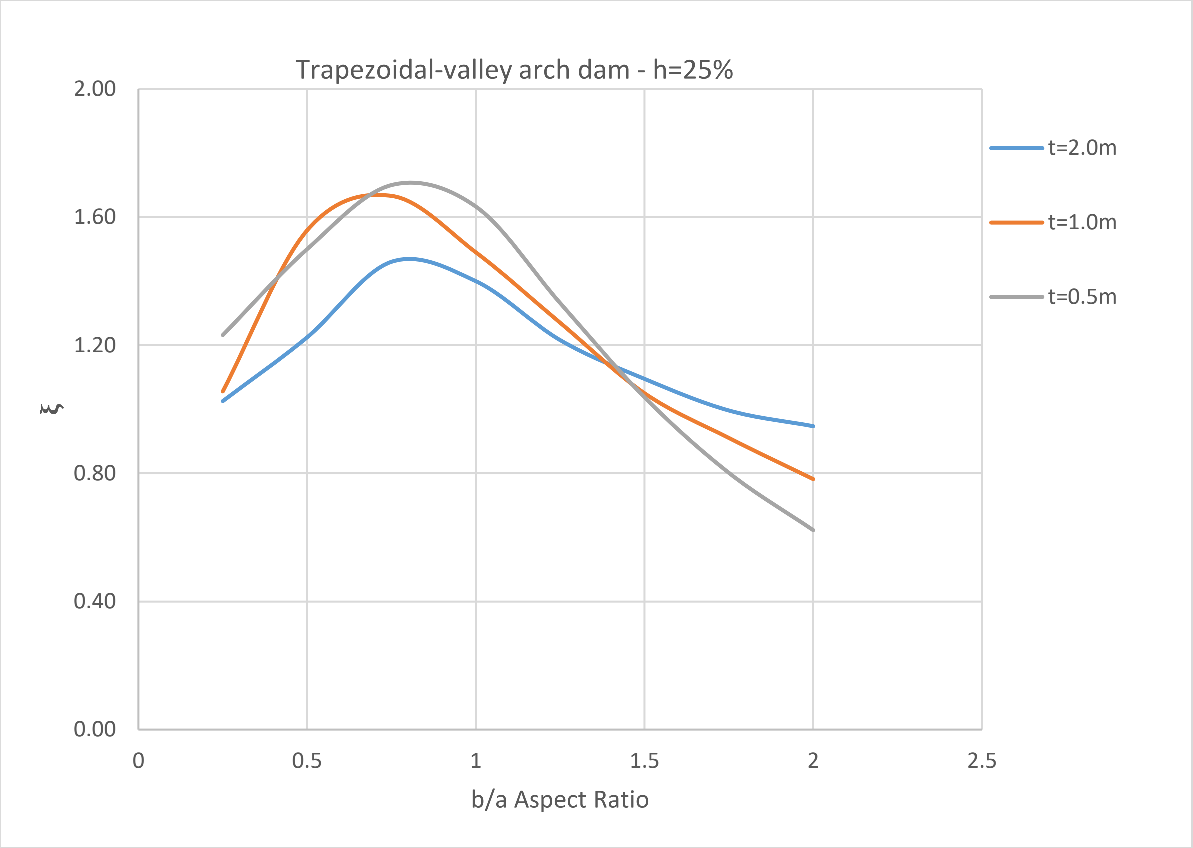

Figure 4.31: Variation of ξ and b/a with 25% rise ratio for various shell thicknesses (ratio of critical buckling pressure for elliptic paraboloid to critical buckling pressure for parabolic cylinder).

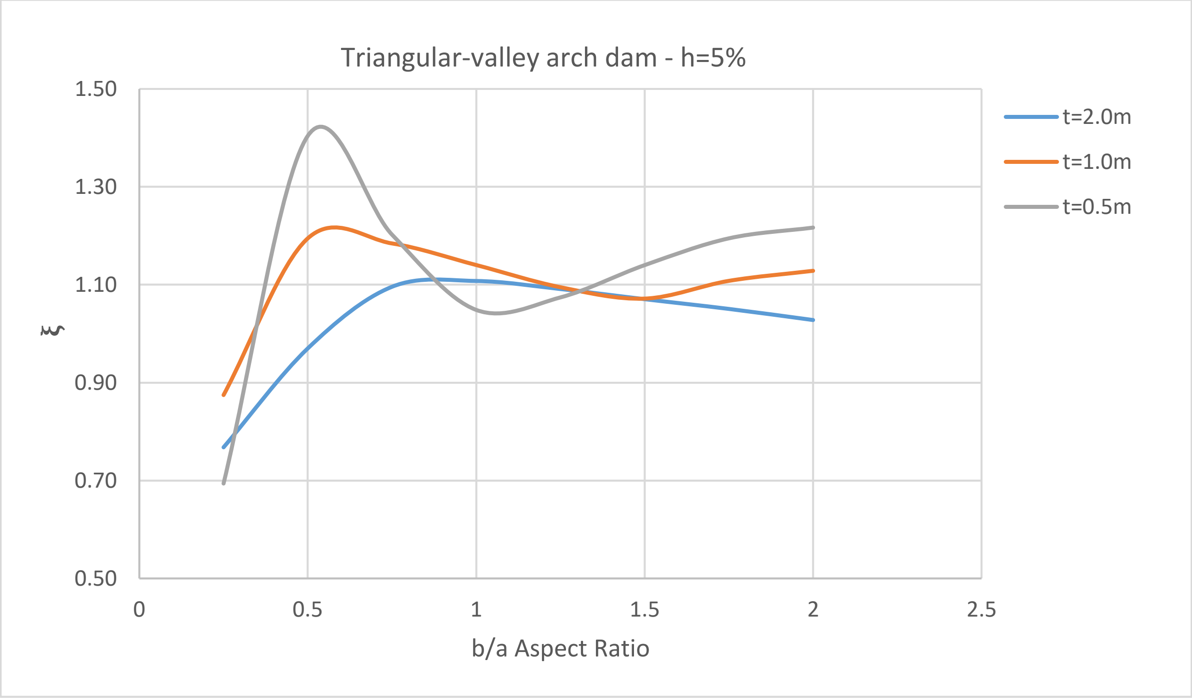

Figure 4.32: Variation of ξ and b/a with 5% rise ratio for various shell thicknesses (ratio of critical buckling pressure for elliptic paraboloid to critical buckling pressure for parabolic cylinder).

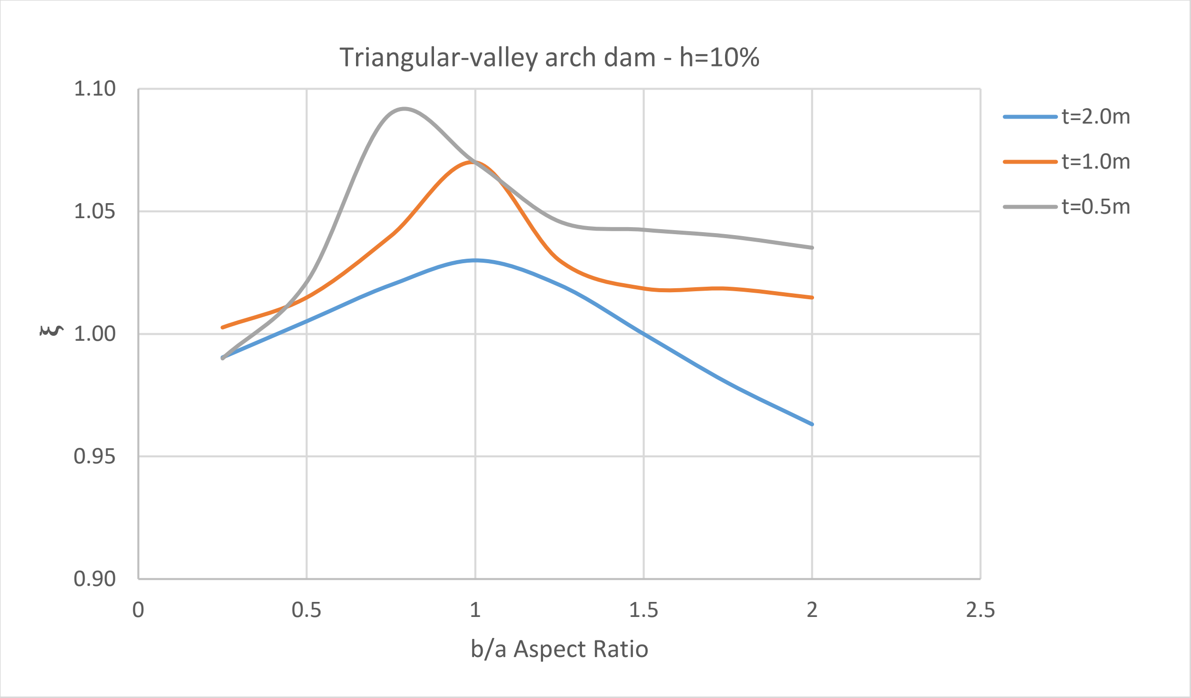

Figure 4.33: Variation of ξ and b/a with 10% rise ratio for various shell thicknesses (ratio of critical buckling pressure for elliptic paraboloid to critical buckling pressure for parabolic cylinder).

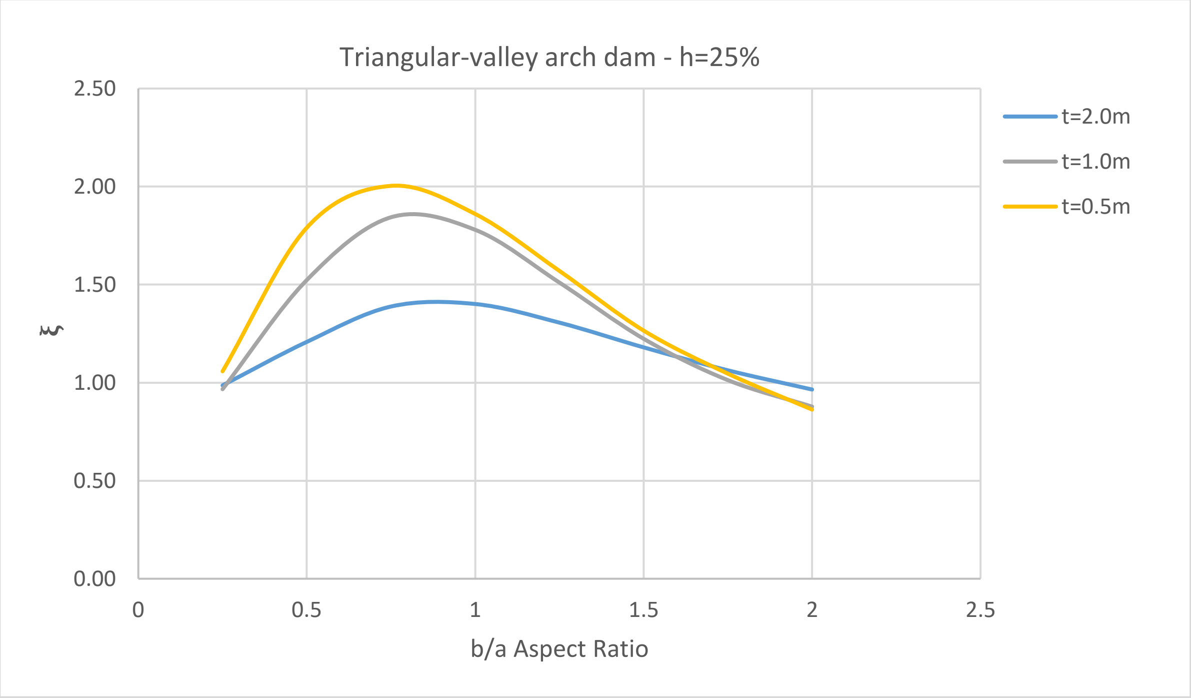

Figure 4.34: Variation of ξ and b/a with 25% rise ratio for various shell thicknesses (ratio of critical buckling pressure for elliptic paraboloid to critical buckling pressure for parabolic cylinder).

4.2.2 Double Curvature Modelling with Linear Varying Thickness

Figures 4.35-4.36 depict typical mode shapes for triangular and trapezoidal parabolic cylinder and elliptic paraboloid arch profiles with linear varying thickness.

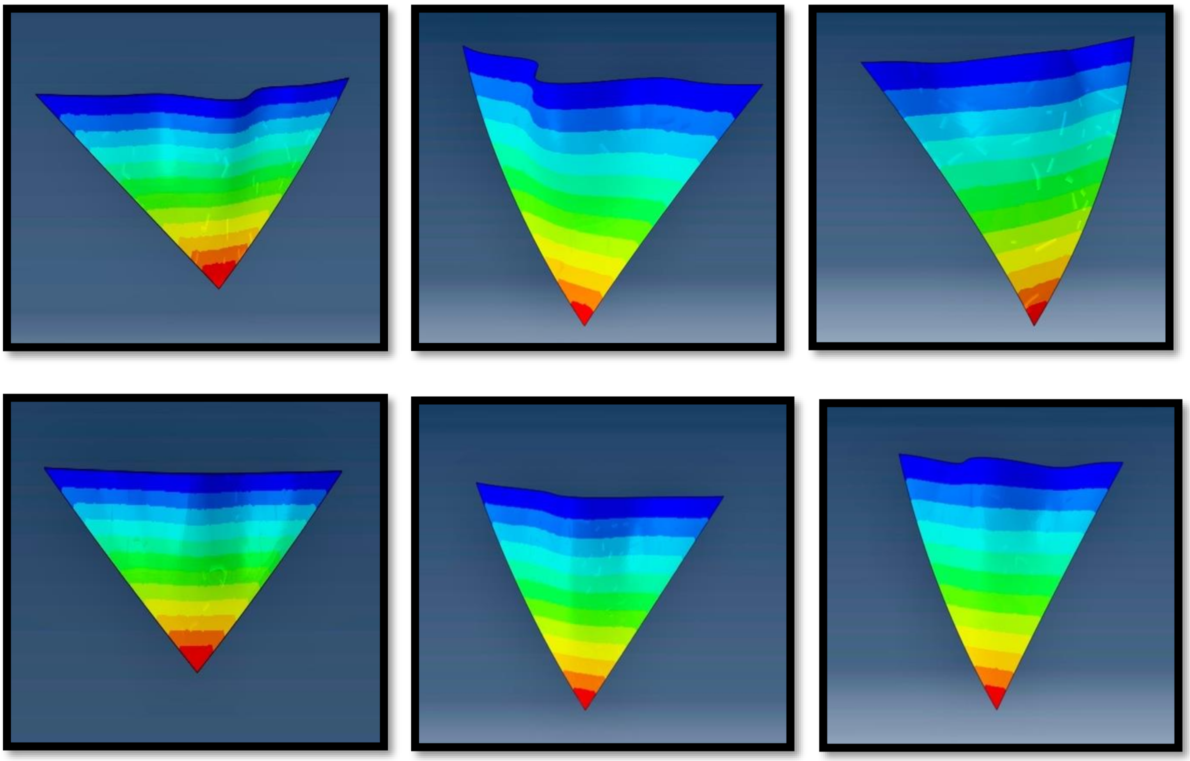

Figure 4.35: Triangular-valley arch dam buckling mode shapes for a = 50m, h=10%, t_1=0.5m t_2=1.0m for parabolic cylinder arch (first three mode shapes with b/a=0.25, 0.50 and 0.75 respectively) and elliptic paraboloid arch (last three mode shapes with b/a=0.25, 0.50 and 0.75 respectively).

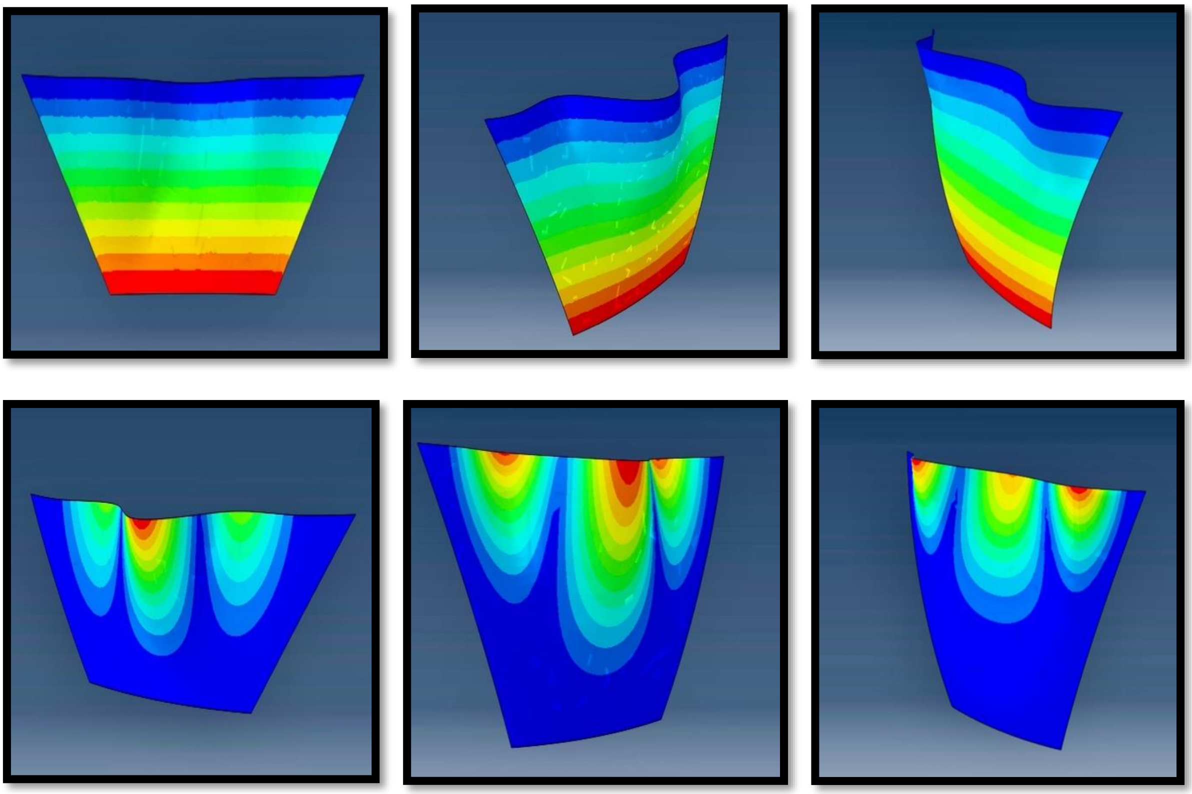

Figure 4.36: Trapezoidal-valley arch dam buckling mode shapes for *a* = 50m, h=10%, t_1=0.5m t_2=1.0m for parabolic cylinder arch (first three mode shapes with b/a=0.25, 0.50 and 0.75 respectively) and elliptic paraboloid arch (last three mode shapes with b/a=0.25, 0.50 and 0.75 respectively).

The tables, 4.27 (a)-(c) and 4.28 (a)-(c) compare the buckling pressures for the triangular and trapezoidal-valley arch dams, with parabolic cylinder and elliptical paraboloid profiles assuming linear thickness expressions, t_1=0.5m & t_2=1.0m and t_1=1.0m & t_2=2.0m for three representative rise ratio values (5%, 10%, 25%).

t1=0.5m and t2=1.0m; h=10%				t1=1.0m and t2=2.0m; h=10%			
Critical Buckling Pressure Pcr (kN/m2)				Critical Buckling Pressure Pcr (kN/m2)			
a=50m				a=50m			
b/a	PC	EP	ξ	b/a	PC	EP	ξ
0,25	17898	17994	1,01	0,25	284201	280750	0,99
0,5	7436	7509	1,01	0,5	61104	61251	1,00
0,75	7287	7102	0,97	0,75	46331	45444	0,98
1	8015	7344	0,92	1	45572	42659	0,94
1,25	8966	7598	0,85	1,25	48607	41870	0,86
1,5	10139	7819	0,77	1,5	52933	41105	0,78
1,75	10763	7833	0,73	1,75	55553	39916	0,72
2	10494	7549	0,72	2	55001	38284	0,70

Table 4.27(a): Triangular-valley arch dam results of parabolic cylinder vs. elliptic paraboloid arch for h=10%.

t1=0.5m and t2=1.0m; h=5%				t1=1.0m and t2=2.0m; h=5%			
Critical Buckling Pressure Pcr (kN/m2)				Critical Buckling Pressure Pcr (kN/m2)			
a=50m				a=50m			
b/a	PC	EP	ξ	b/a	PC	EP	ξ
0,25	19067	17775	0,93	0,25	426147	276989	0,65
0,5	4106	5229	1,27	0,5	54852	53915	0,98
0,75	3148	3645	1,16	0,75	30289	32133	1,06
1	3104	3148	1,01	1	25077	25827	1,03
1,25	3284	2980	0,91	1,25	23452	23290	0,99
1,5	3533	2957	0,84	1,5	23000	22194	0,96
1,75	3721	3008	0,81	1,75	23079	21771	0,94
2	3731	3067	0,82	2	23348	21502	0,92

Table 4.27(b): Triangular-valley arch dam results of parabolic cylinder vs. elliptic paraboloid arch for h=5%.

t1=0.5m and t2=1.0m; h=25%				t1=1.0m and t2=2.0m; h=25%			
Critical Buckling Pressure Pcr (kN/m2)				Critical Buckling Pressure Pcr (kN/m2)			
a=50m				a=50m			
b/a	PC	EP	ξ	b/a	PC	EP	ξ
0,25	33709	32580	1,03	0,25	274898	267695	0,97
0,5	13569	21642	1,59	0,5	90174	121839	1,35
0,75	10231	18761	1,83	0,75	61323	99319	1,62
1	9547	16463	1,72	1	52293	82648	1,58
1,25	9875	14376	1,46	1,25	49760	67485	1,36
1,5	10761	11950	1,11	1,5	50362	55245	1,10
1,75	11915	9296	0,78	1,75	52794	46044	0,87
2	12026	7273	0,60	2	55733	39176	0,70

Table 4.27(c): Triangular-valley arch dam results of parabolic cylinder vs. elliptic paraboloid arch for h=25%.

t1=0.5m and t2=1.0m; h=10%				t1=1.0m and t2=2.0m; h=10%			
Critical Buckling Pressure Pcr (kN/m2)				Critical Buckling Pressure Pcr (kN/m2)			
a=50m				a=50m			
b/a	PC	EP	ξ	b/a	PC	EP	ξ
0,25	8362	8439	1,01	0,25	103648	103228	1,00
0,5	5126	5144	1,00	0,5	31752	31578	0,99
0,75	5710	5476	0,96	0,75	32514	31375	0,96
1	6443	5863	0,91	1	36557	33718	0,92
1,25	7413	6294	0,85	1,25	40266	35052	0,87
1,5	8602	6815	0,79	1,5	41806	35765	0,86
1,75	8393	7003	0,83	1,75	40904	35271	0,86
2	8210	7021	0,86	2	39885	34367	0,86

Table 4.28(a): Triangular-valley arch dam results of parabolic cylinder vs. elliptic paraboloid arch for h=10%.

t1=0.5m and t2=1.0m; h=5%				**t1=1.0m and t2=2.0m; h=5%**			
Critical Buckling Pressure Pcr (kN/m2)				**Critical Buckling Pressure Pcr (kN/m2)**			
a=50m				**a=50m**			
b/a	**PC**	**EP**	**ξ**	**b/a**	**PC**	**EP**	**ξ**
0,25	6935	7621	1,10	0,25	138393	103607	0,75
0,5	2140	3107	1,45	0,5	21393	24529	1,15
0,75	2211	2651	1,20	0,75	16588	19467	1,17
1	2497	2491	1,00	1	16531	17966	1,09
1,25	2733	2478	0,91	1,25	16771	17251	1,03
1,5	2836	2552	0,90	1,5	17063	17012	1,00
1,75	2789	2669	0,96	1,75	16950	17029	1,00
2	2722	2773	1,02	2	16549	17043	1,03

Table 4.28(b): Triangular-valley arch dam results of parabolic cylinder vs. elliptic paraboloid arch for h=5%.

t1=0.5m and t2=1.0m; h=25%				**t1=1.0m and t2=2.0m; h=25%**			
Critical Buckling Pressure Pcr (kN/m2)				**Critical Buckling Pressure Pcr (kN/m2)**			
a=50m				**a=50m**			
b/a	**PC**	**EP**	**ξ**	**b/a**	**PC**	**EP**	**ξ**
0,25	19130	19342	0,99	0,25	136238	132082	0,97
0,5	10492	15153	1,44	0,5	58164	80565	1,39
0,75	8777	13830	1,58	0,75	45788	75589	1,65
1	8571	13081	1,53	1	41955	67800	1,62
1,25	9150	12173	1,33	1,25	42088	57665	1,37
1,5	10252	11079	1,08	1,5	44462	48251	1,09
1,75	10214	8713	0,85	1,75	48293	40749	0,84
2	9634	6842	0,71	2	51871	34899	0,67

Table 4.28(c): Triangular-valley arch dam results of parabolic cylinder vs. elliptic paraboloid arch for h=25%.

Figure 4.37-42 shows the beneficial effect of double curvature for triangular and trapezoidal-valley arch dam with linear varying thickness. Similarly, the parameter ξ increases as the shell becomes thinner at points, t_1 and t_2. Another observation made is that the parameter ξ is almost identical (close to 1.0) for both shells with thickness expressions, t_1=0.5m & t_2=1.0m and t_1=1.0m & t_2=2.0m. This is true for both triangular and trapezoidal-valley arch dam with 10% rise ratio, also the beneficial effect for all three rise ratios peaks at aspect ratio values equal or below 0.75 ($b/a \leq 0.75$).

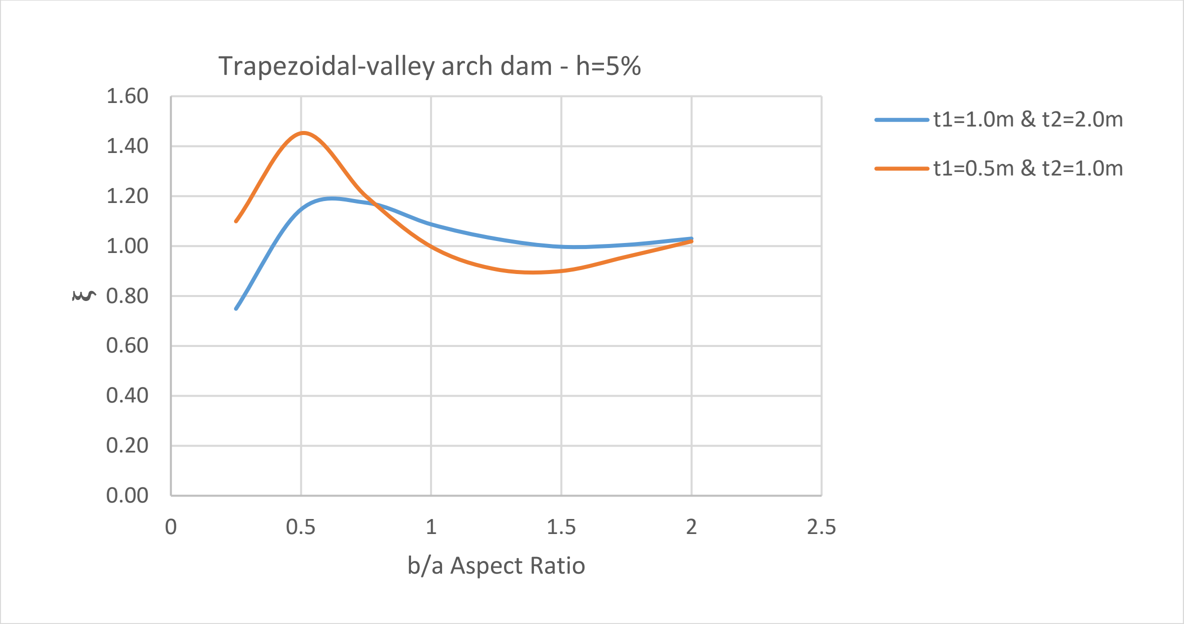

Figure 4.37: Variation of ξ and b/a with 5% rise ratio for various shell thickness expressions (ratio of critical buckling pressure for elliptic paraboloid to critical buckling pressure for parabolic cylinder).

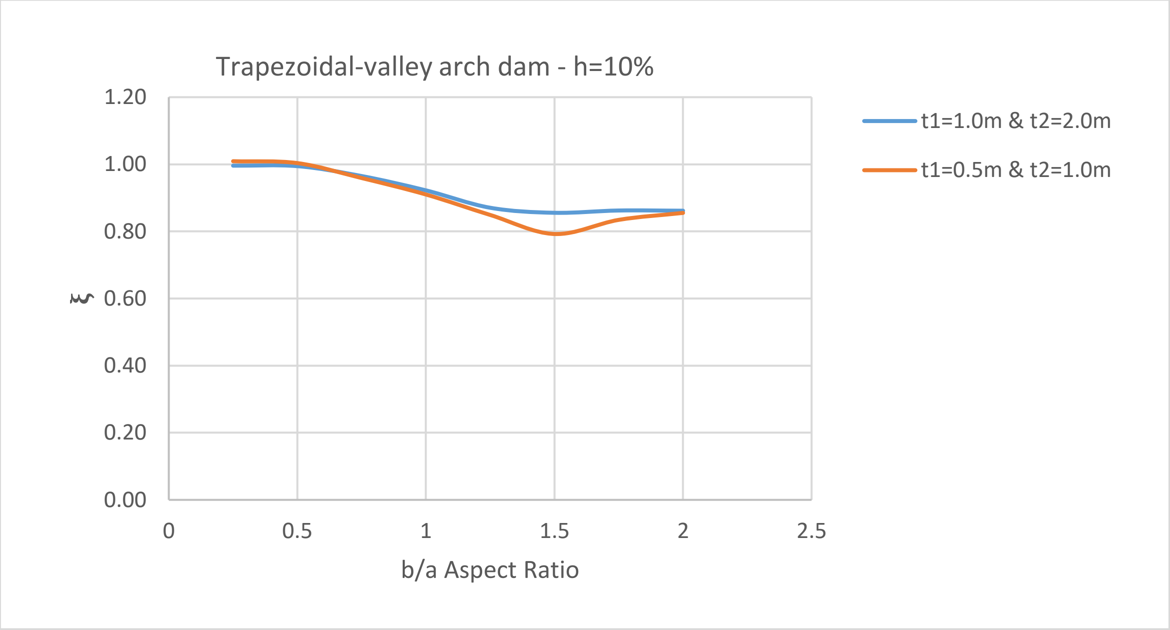

Figure 4.38: Variation of ξ and b/a with 10% rise ratio for various shell thickness expressions (ratio of critical buckling pressure for elliptic paraboloid to critical buckling pressure for parabolic cylinder).

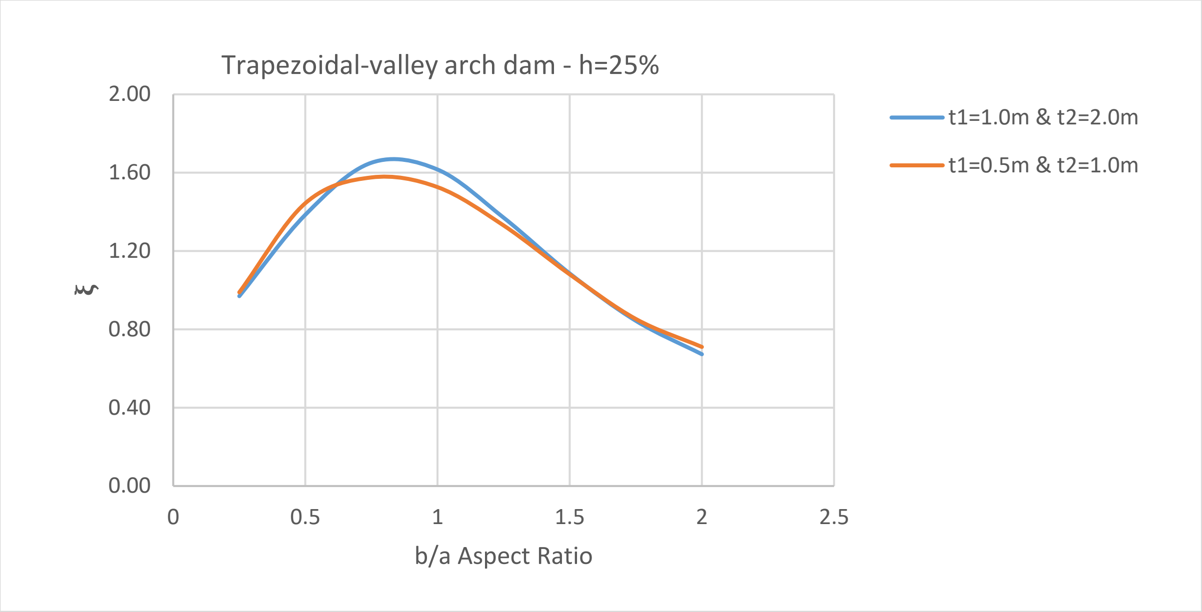

Figure 4.39: Variation of ξ and b/a with 25% rise ratio for various shell thickness expressions (ratio of critical buckling pressure for elliptic paraboloid to critical buckling pressure for parabolic cylinder).

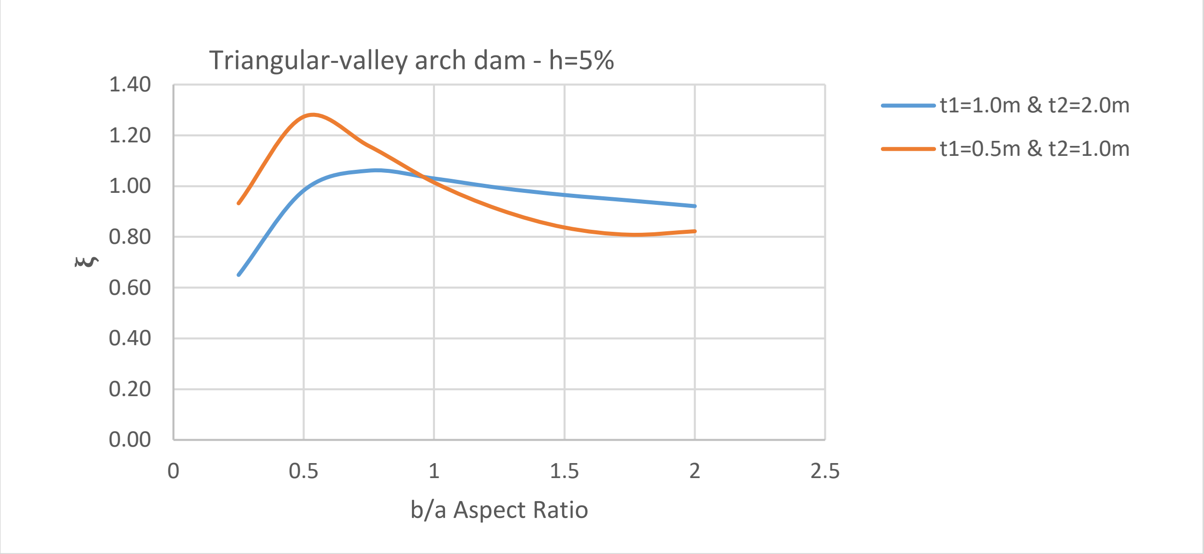

Figure 4.40: Variation of ξ and b/a with 5% rise ratio for various shell thickness expressions (ratio of critical buckling pressure for elliptic paraboloid to critical buckling pressure for parabolic cylinder).

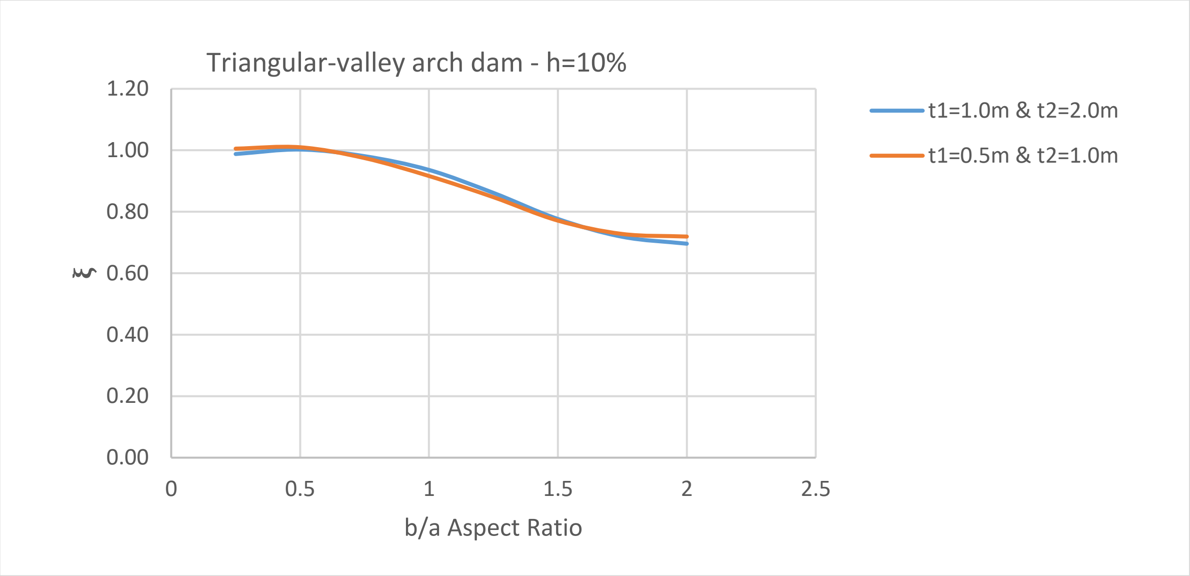

Figure 4.41: Variation of ξ and b/a with 10% rise ratio for various shell thickness expressions (ratio of critical buckling pressure for elliptic paraboloid to critical buckling pressure for parabolic cylinder).

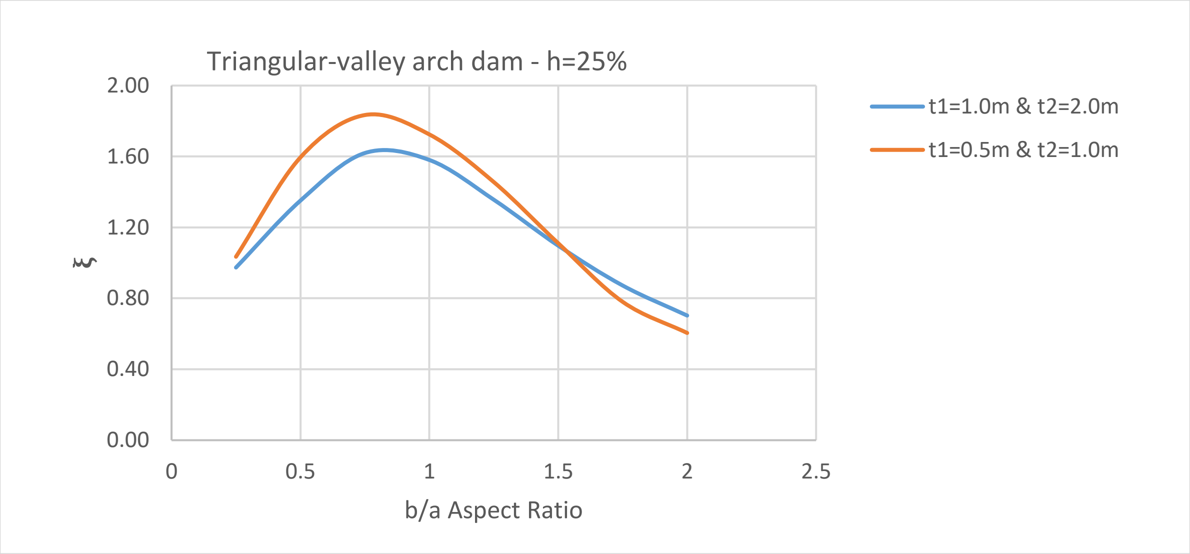

Figure 4.42: Variation of ξ and b/a with 25% rise ratio for various shell thickness expressions (ratio of critical buckling pressure for elliptic paraboloid to critical buckling pressure for parabolic cylinder).

4.2.3 Double Curvature Modelling with Quadratic Varying Thickness

Figures 4.43-4.44 depict typical mode shapes for triangular and trapezoidal parabolic cylinder and elliptic paraboloid arch profiles with quadratic varying thickness.

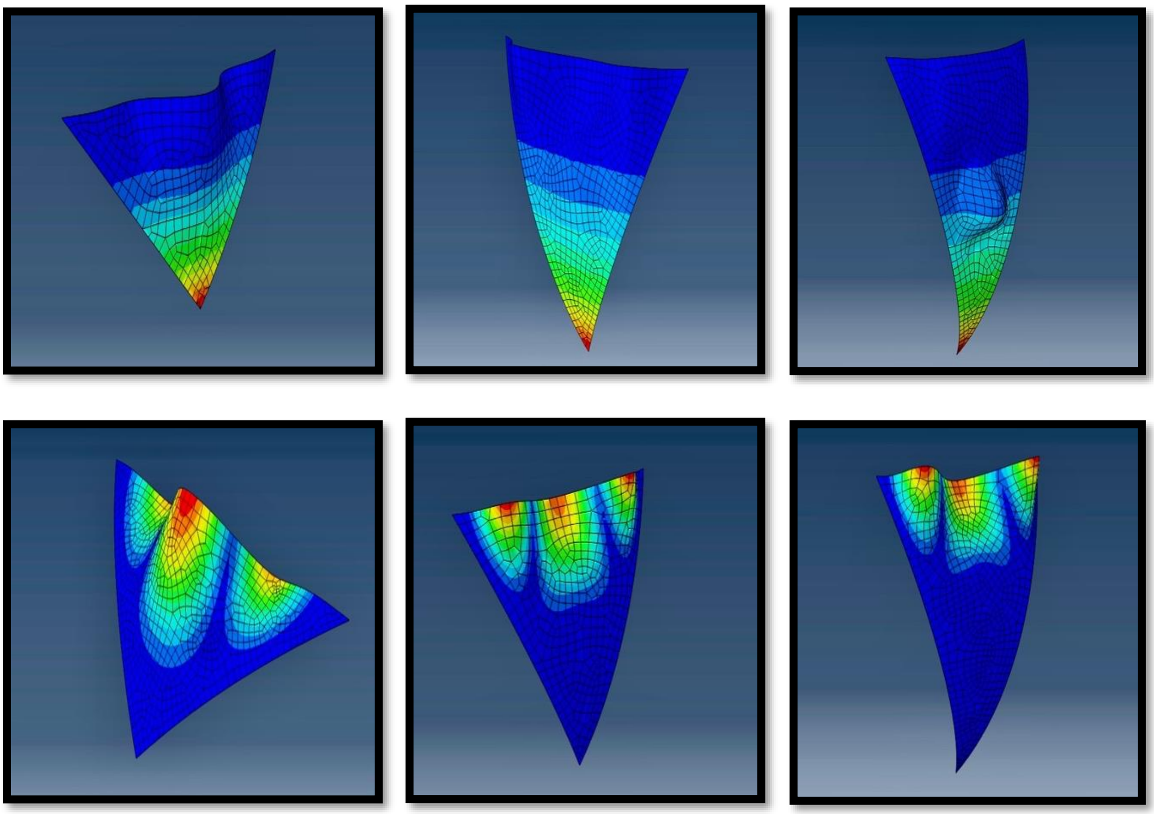

Figure 4.43: Triangular-valley arch dam buckling mode shapes for *a* = 50m, h=10%, t_1=0.5m t_2=1.0m for parabolic cylinder arch (first three mode shapes with b/a=0.50, 1.00 and 1.50 respectively) and elliptic paraboloid arch (last three mode shapes with b/a=0.50, 1.00 and 1.50 respectively).

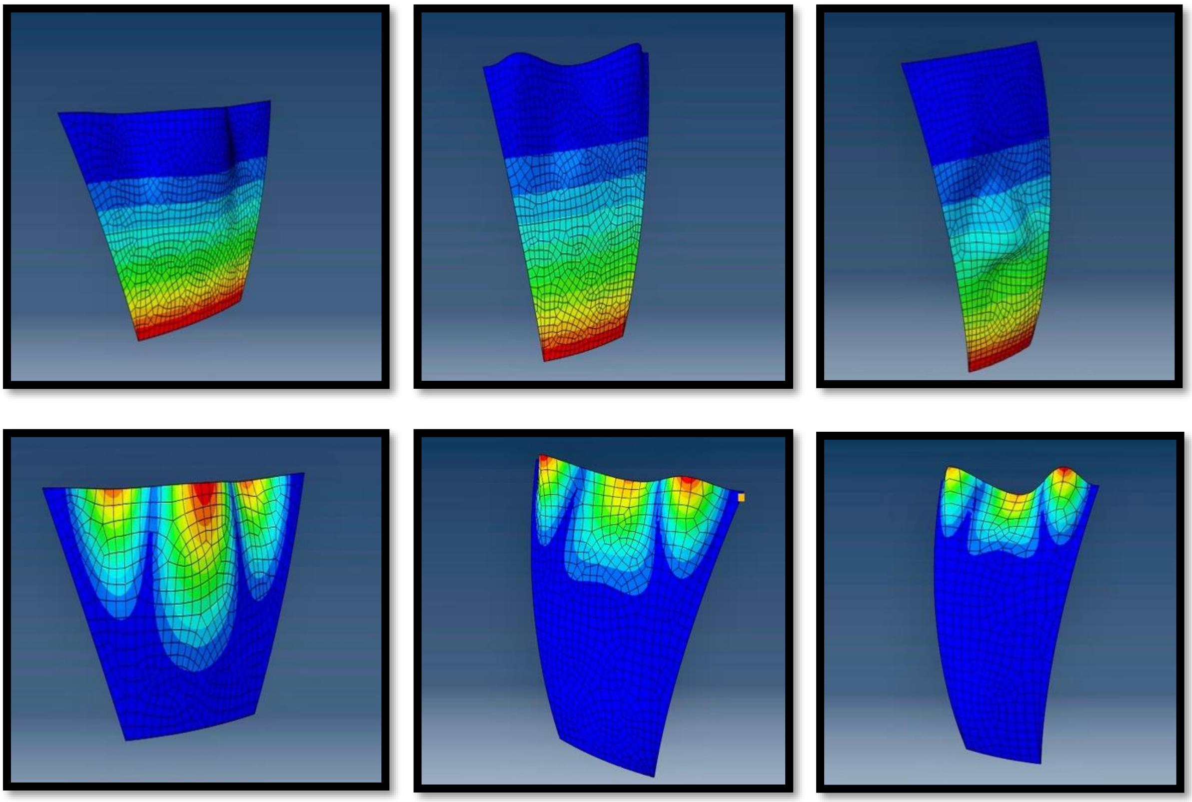

Figure 4.44: Trapezoidal-valley arch dam buckling mode shapes for *a* = 50m, h=10%, t_1=0.5m t_2=1.0m for parabolic cylinder arch (first three mode shapes with b/a=0.50, 1.00 and 1.50 respectively) and elliptic paraboloid arch (last three mode shapes with b/a=0.50, 1.00 and 1.50 respectively).

The tables, 4.29 (a)-(c) and 4.30 (a)-(c) compare the buckling pressures for the triangular and trapezoidal-valley arch dams, with parabolic cylinder and elliptical paraboloid profiles assuming quadratic thickness expressions, t_1=0.5m & t_2=1.0m and t_1=1.0m & t_2=2.0m for three representative rise ratio values (5%, 10%, 25%).

t1=0.5m and t2=1.0m; h=10%				**t1=1.0m and t2=2.0m; h=10%**			
Critical Buckling Pressure Pcr (kN/m2)				**Critical Buckling Pressure Pcr (kN/m2)**			
a=50m				**a=50m**			
b/a	**PC**	**EP**	**ξ**	**b/a**	**PC**	**EP**	**ξ**
0,5	5302	5363	1,01	0,5	39561	39512	1,00
1	6478	5922	0,91	1	34244	31162	0,91
1,5	7296	6649	0,91	1,5	38204	32482	0,85
2	6934	6616	0,95	2	35765	30803	0,86

Table 4.29(a): Triangular-valley arch dam results of parabolic cylinder vs. elliptic paraboloid arch for h=10%.

t1=0.5m and t2=1.0m; h=5%				**t1=1.0m and t2=2.0m; h=5%**			
Critical Buckling Pressure Pcr (kN/m2)				**Critical Buckling Pressure Pcr (kN/m2)**			
a=50m				**a=50m**			
b/a	**PC**	**EP**	**ξ**	**b/a**	**PC**	**EP**	**ξ**
0,5	2642	3472	1,31	0,5	31056	38820	1,25
1	2306	2302	1,00	1	16829	16850	1,00
1,5	2573	2245	0,87	1,5	16054	14127	0,88
2	2432	2292	0,94	2	15890	15136	0,95

Table 4.29(b): Triangular-valley arch dam results of parabolic cylinder vs. elliptic paraboloid arch for h=5%.

t1=0.5m and t2=1.0m; h=25%				**t1=1.0m and t2=2.0m; h=25%**			
Critical Buckling Pressure Pcr (kN/m2)				**Critical Buckling Pressure Pcr (kN/m2)**			
a=50m				**a=50m**			
b/a	**PC**	**EP**	**ξ**	**b/a**	**PC**	**EP**	**ξ**
0,5	16732	9879	0,59	0,5	89420	62017	0,69
1	13820	7713	0,56	1	67235	39369	0,59
1,5	10484	8932	0,85	1,5	45796	39453	0,86
2	6266	8440	1,35	2	31841	40662	1,28

Table 4.29(c): Triangular-valley arch dam results of parabolic cylinder vs. elliptic paraboloid arch for h=25%.

t1=0.5m and t2=1.0m; h=10%				**t1=1.0m and t2=2.0m; h=10%**			
Critical Buckling Pressure Pcr (kN/m2)				**Critical Buckling Pressure Pcr (kN/m2)**			
a=50m				**a=50m**			
b/a	**PC**	**EP**	**ξ**	**b/a**	**PC**	**EP**	**ξ**
0,5	3767	3775	1,00	0,5	22107	21957	0,99
1	5184	4711	0,91	1	27796	25605	0,92
1,5	6118	5779	0,94	1,5	28407	27271	0,96
2	5903	5793	0,98	2	26767	26944	1,01

Table 4.30(a): Trapezoidal-valley arch dam results of parabolic cylinder vs. elliptic paraboloid arch for h=10%.

t1=0.5m and t2=1.0m; h=5%				t1=1.0m and t2=2.0m; h=5%			
Critical Buckling Pressure Pcr (kN/m2)				Critical Buckling Pressure Pcr (kN/m2)			
a=50m				a=50m			
b/a	**PC**	**EP**	**ξ**	**b/a**	**PC**	**EP**	**ξ**
0,5	1485	2174	1,46	0,5	13086	15822	1,21
1	1883	1872	0,99	1	11118	11451	1,03
1,5	1921	2004	1,04	1,5	11240	11802	1,05
2	1816	2123	1,17	2	10325	11735	1,14

Table 4.30(b): Trapezoidal-valley arch dam results of parabolic cylinder vs. elliptic paraboloid arch for h=5%.

t1=0.5m and t2=1.0m; h=25%				t1=1.0m and t2=2.0m; h=25%			
Critical Buckling Pressure Pcr (kN/m2)				Critical Buckling Pressure Pcr (kN/m2)			
a=50m				a=50m			
b/a	**PC**	**EP**	**ξ**	**b/a**	**PC**	**EP**	**ξ**
0,5	11790	7824	0,66	0,5	59809	41564	0,69
1	10962	7045	0,64	1	55791	32445	0,58
1,5	9637	8604	0,89	1,5	40584	35951	0,89
2	5978	7719	1,29	2	28907	38172	1,32

Table 4.30(c): Trapezoidal-valley arch dam results of parabolic cylinder vs. elliptic paraboloid arch for h=25%.

Figure 4.45-50 depicts the beneficial effect of double curvature for triangular and trapezoidal-valley arch dam with quadratic varying thickness. It is clear that the beneficial effect for shells with double curvature and quadratic varying thickness behaves quite opposite towards that of constant and linear varying thickness.

The parameter ξ decreases as the aspect ratio is increased from the starting value of 0.50, until it reaches minimum point at an aspect ratio of b/a = 1.0 (for shells having 10% rise ratio) and then increases again, giving a positive parabolic profile. Another observation made is that the beneficial effect is almost identical for both shells with thickness expressions, t_1=0.5m & t_2=1.0m and t_1=1.0m & t_2=2.0m.

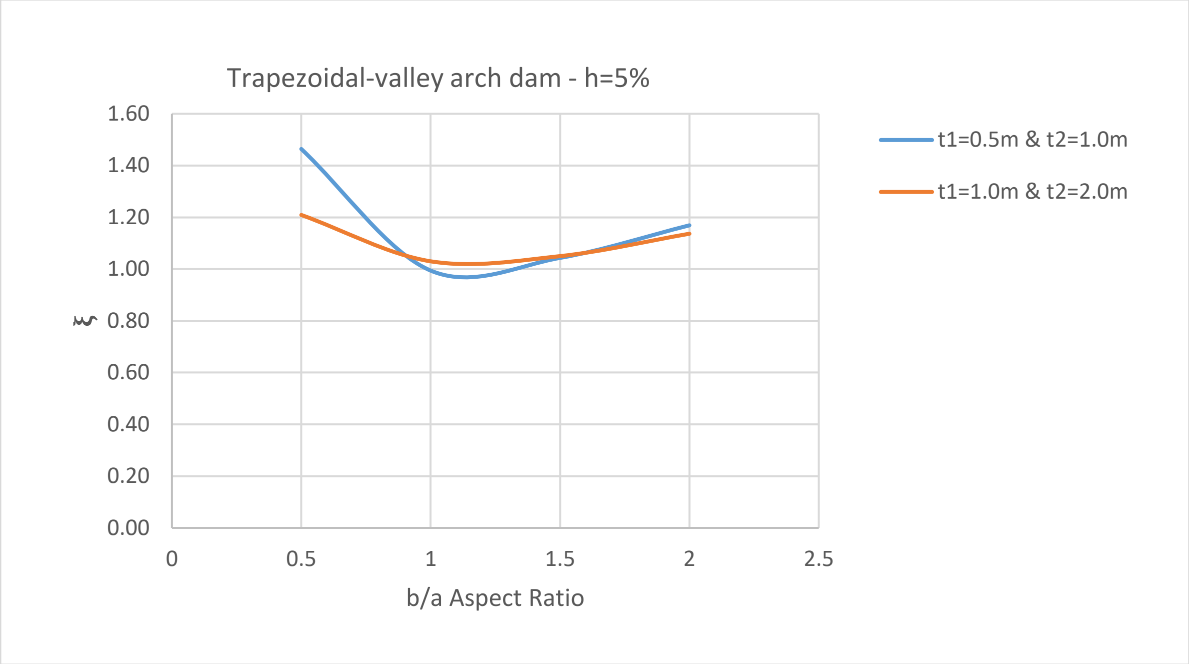

Figure 4.45: Variation of ξ and b/a with 5% rise ratio for various shell thickness expressions (ratio of critical buckling pressure for elliptic paraboloid to critical buckling pressure for parabolic cylinder).

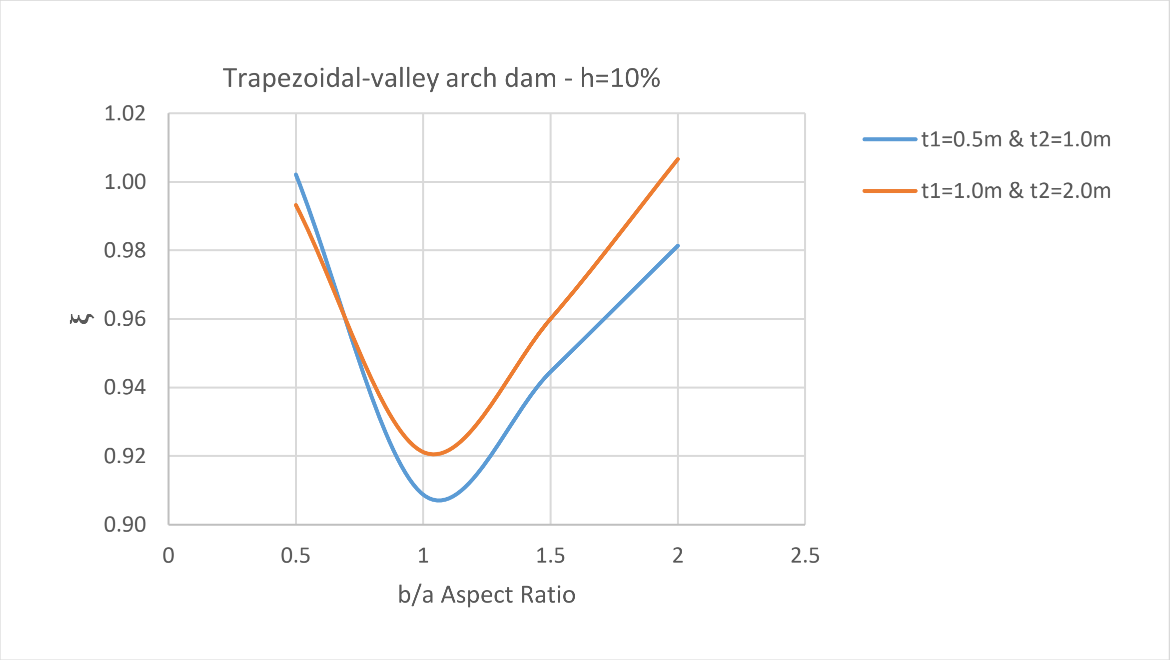

Figure 4.46: Variation of ξ and b/a with 10% rise ratio for various shell thickness expressions (ratio of critical buckling pressure for elliptic paraboloid to critical buckling pressure for parabolic cylinder).

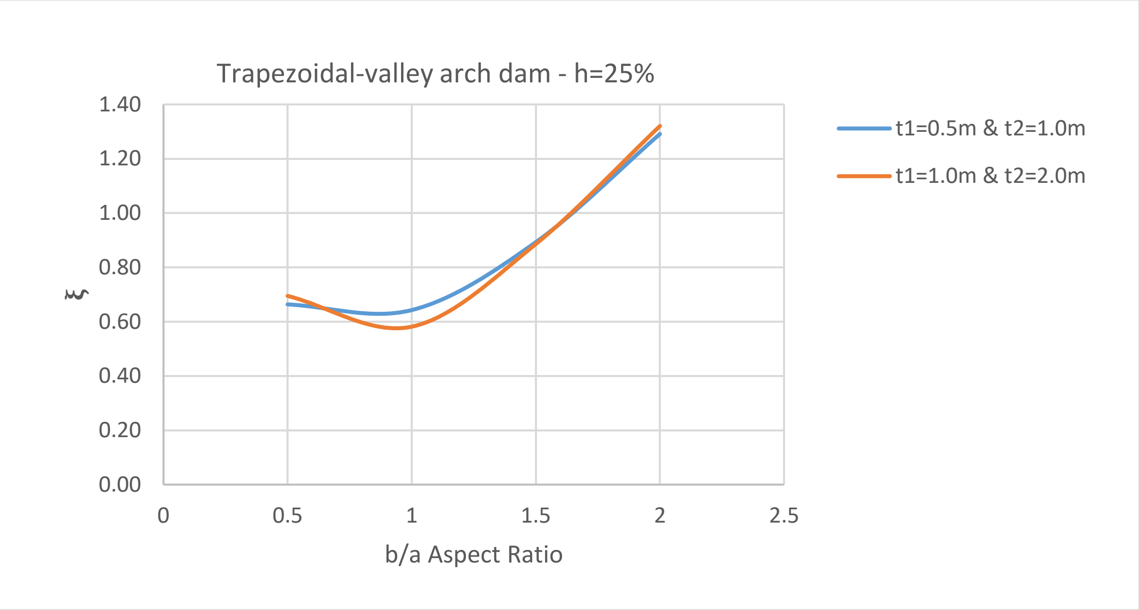

Figure 4.47: Variation of ξ and b/a with 25% rise ratio for various shell thickness expressions (ratio of critical buckling pressure for elliptic paraboloid to critical buckling pressure for parabolic cylinder).

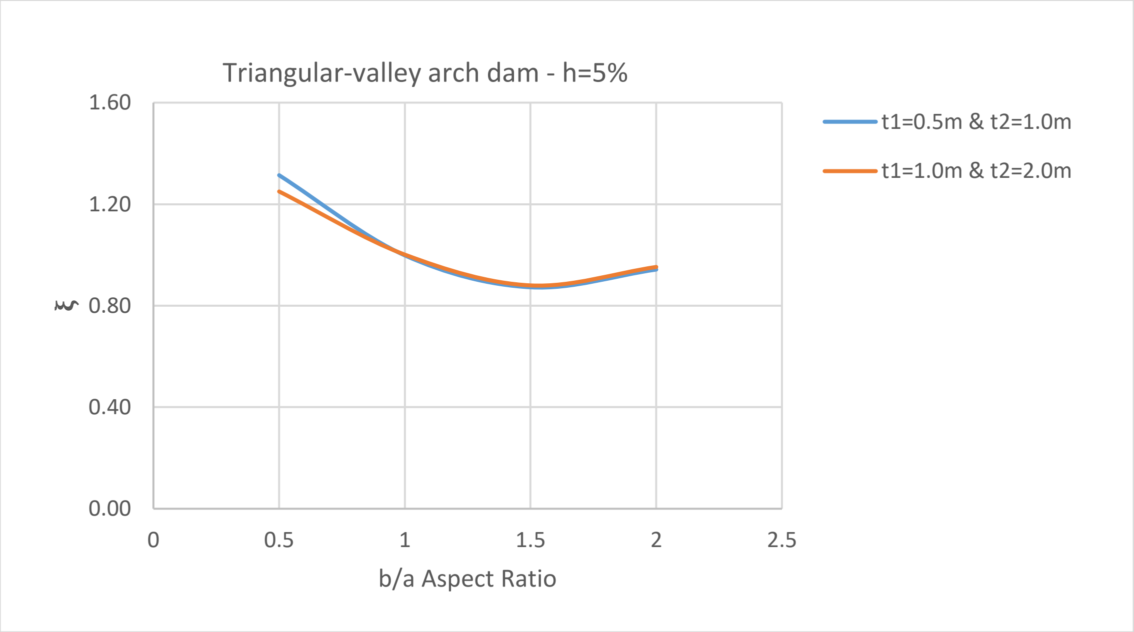

Figure 4.48: Variation of ξ and b/a with 5% rise ratio for various shell thickness expressions (ratio of critical buckling pressure for elliptic paraboloid to critical buckling pressure for parabolic cylinder).

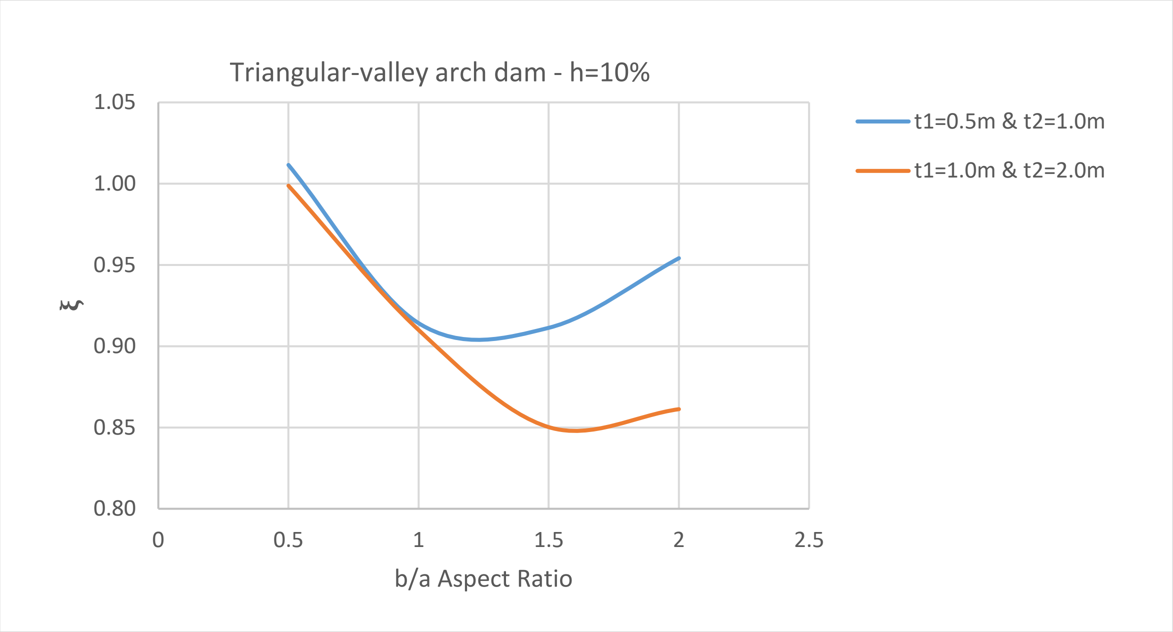

Figure 4.49: Variation of ξ and b/a with 10% rise ratio for various shell thickness expressions (ratio of critical buckling pressure for elliptic paraboloid to critical buckling pressure for parabolic cylinder).

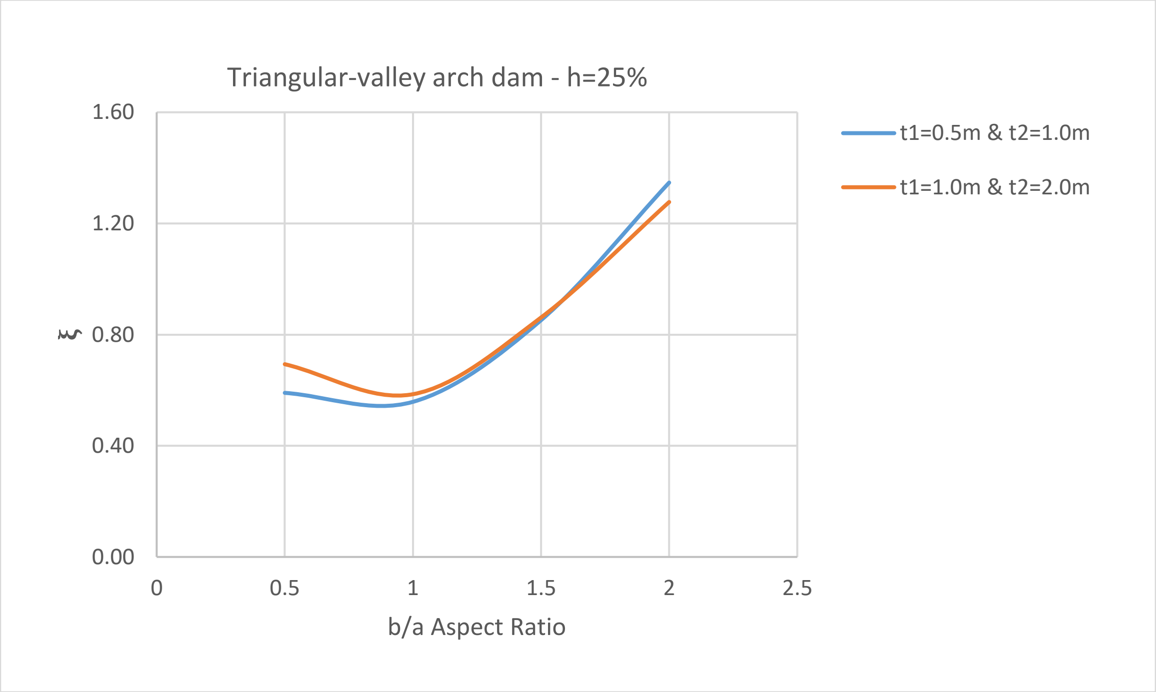

Figure 4.50: Variation of ξ and b/a with 25% rise ratio for various shell thickness expressions (ratio of critical buckling pressure for elliptic paraboloid to critical buckling pressure for parabolic cylinder).

5. Conclusions and Recommendation

5.1 Summary and Conclusions

In this research, the buckling behaviour of concrete arch dams (single and double curvature) having constant, linear, and quadratic thickness variation was explored. The summary of results are presented below in the form of design plots that allow a safe set of design parameters that compare the effect of valley shape and thickness variation on the buckling strength of arch dam with *a* parameter fixed at 50m. Valley shape comparison is made between triangular and trapezoidal-valleys and thickness variation comparison is made between constant thickness of 1m, and linear & quadratic variation having the thickness expression $t_1 = 0.5\text{m}$ & $t_2 = 1.0\text{m}$.

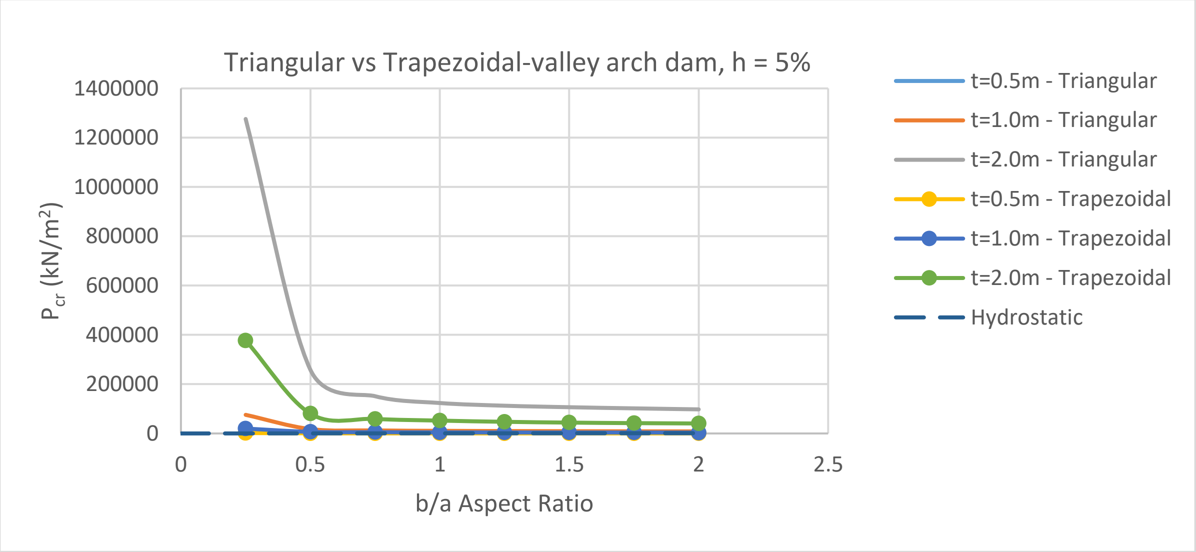

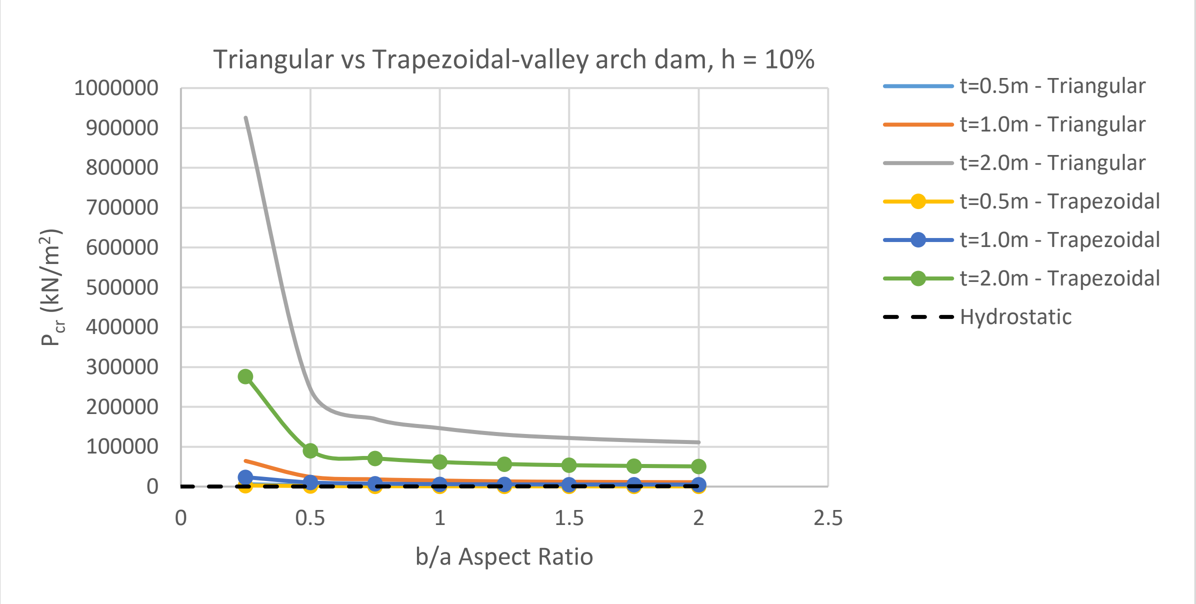

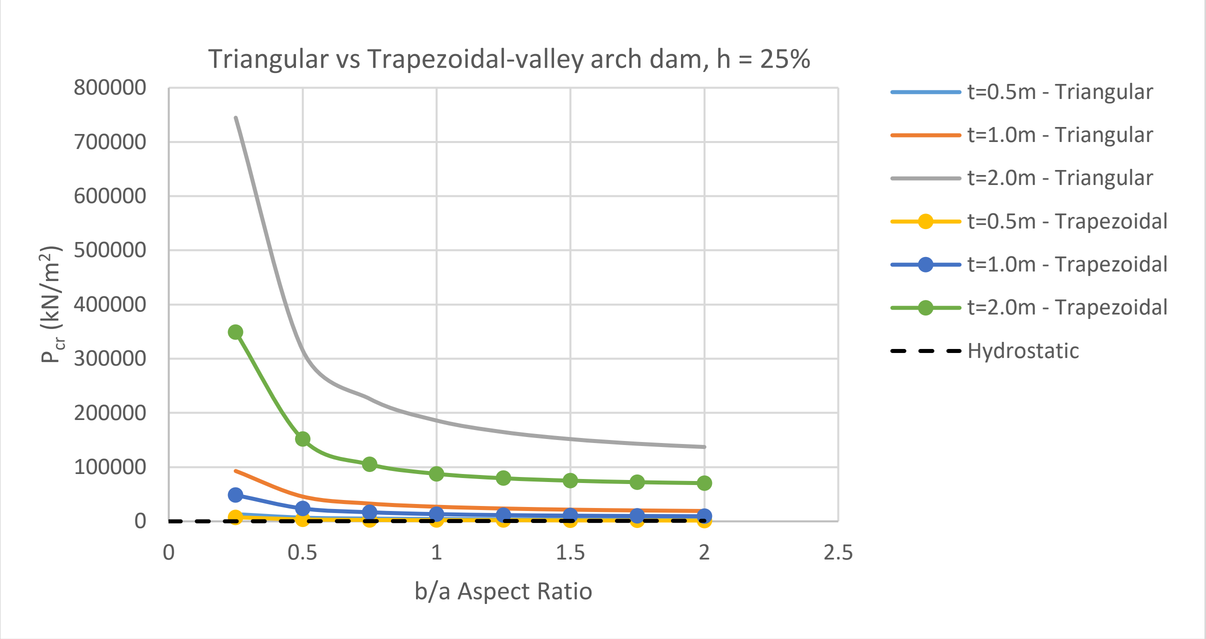

Figure 5.1: Triangular vs. Trapezoidal-valley critical buckling pressure results.

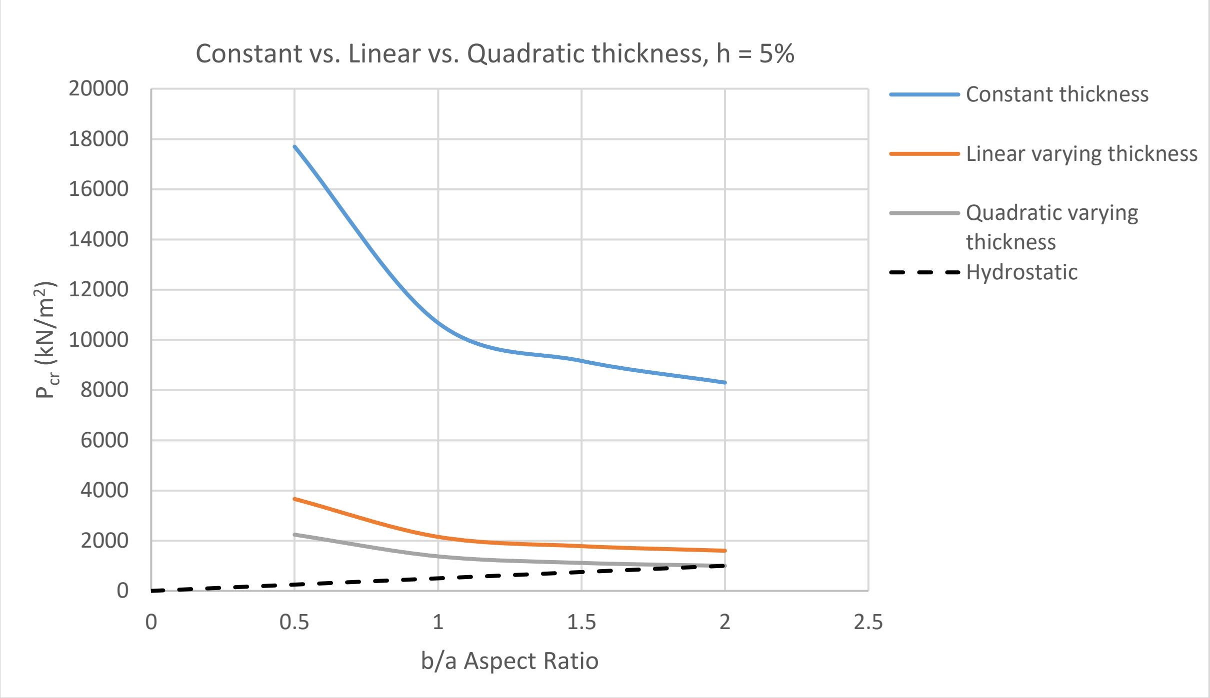

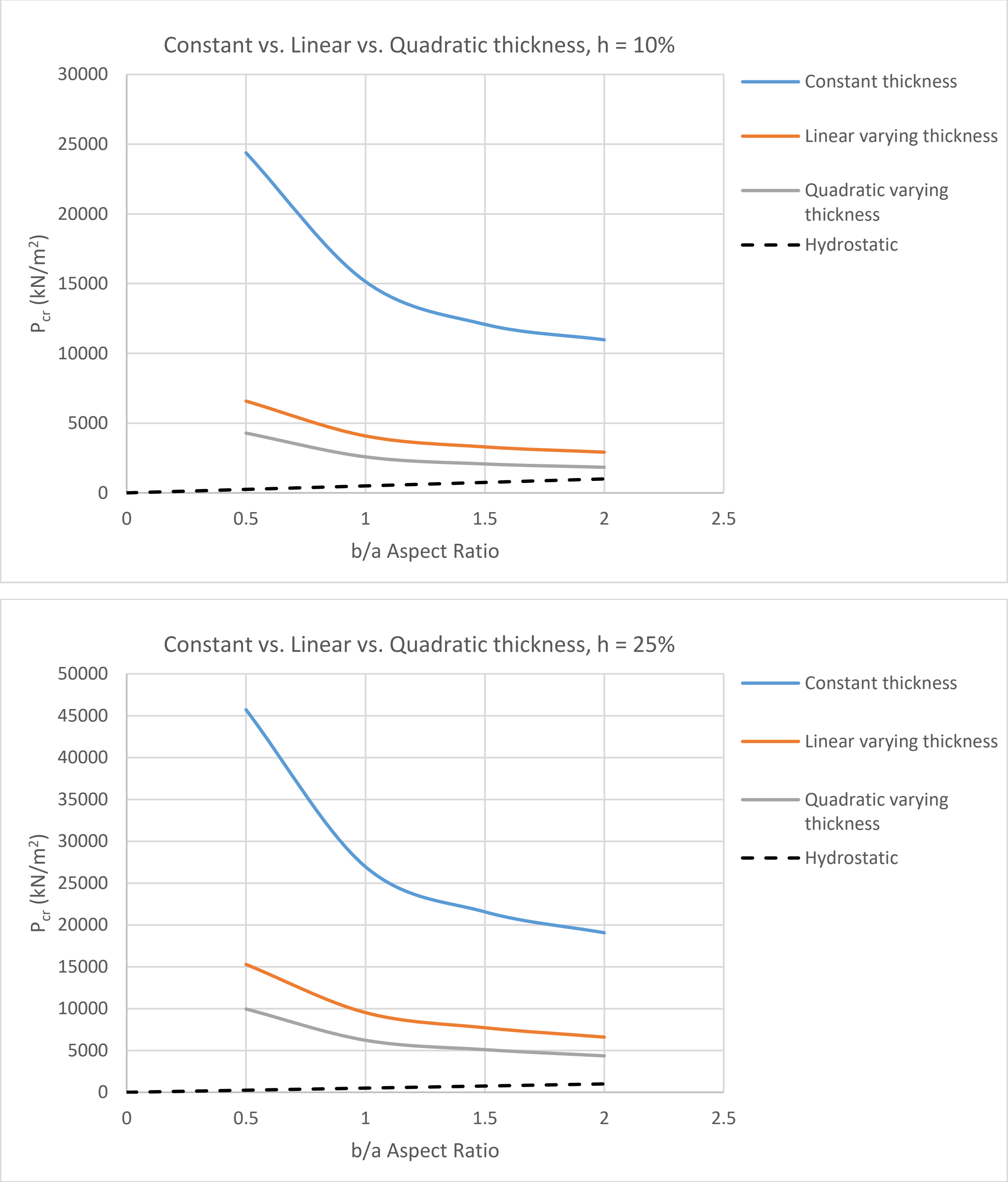

Figure 5.2: Constant vs. Linear vs. Quadratic thickness.

Several noteworthy observations have been made. First, it is seen that the buckling pressures drop drastically with increasing aspect ratio of the arch dam, with the rate of decrease diminishing as b/a increases. The shell rise ratio has a notably large impact on the buckling strength of the arch dam and can thus be utilized to enhance the buckling strength of an arch with specified dimensions a and b without increasing the shell thickness.

Second, the mathematical form of the arch (parabolic/circular) has no appreciable impact on its buckling strength. Thirdly, the geometric aspect of the valley shape does have a significant effect on the buckling strength having showed that a decrease in the dam base width ratio c/a increases the buckling strength significantly. This observation is critical because it plays an economic role in a transformation from rectangular to triangular valley, which has a 50% area decrease while boosting the buckling strength.

Other geometric properties such as shell's variation of thickness t, and aspect ratio b/a have a significant effect too, with the shell having constant thickness performing better than the one having linear and quadratic varying thickness. However, one could argue that linear varying thickness follows the hydrostatic pressure profile with compressive stresses being minimum at the top (therefore the shell being thinner at this point) and maximum at the dam's base (therefore the shell being thicker at this point). Also utilising linear varying thickness saves concrete material by reducing the concrete thickness at the top.

Some of the design parameters discussed especially the geometric aspect of the valley shape, it should be noted that real world valleys usually depict irregular shapes which brings some discrepancy in the results reflected by idealised valley shapes. With this being said, suitable factor of safety to account for the geometric irregularity should be taken into account. Another reasonable attempt could be the use of Simpson rule to approximate the equivalent area to that of an idealized triangular or trapezoidal valley shape.

The results for beneficial effect of double curvature has been presented below for shells having linear and quadratic varying thickness.

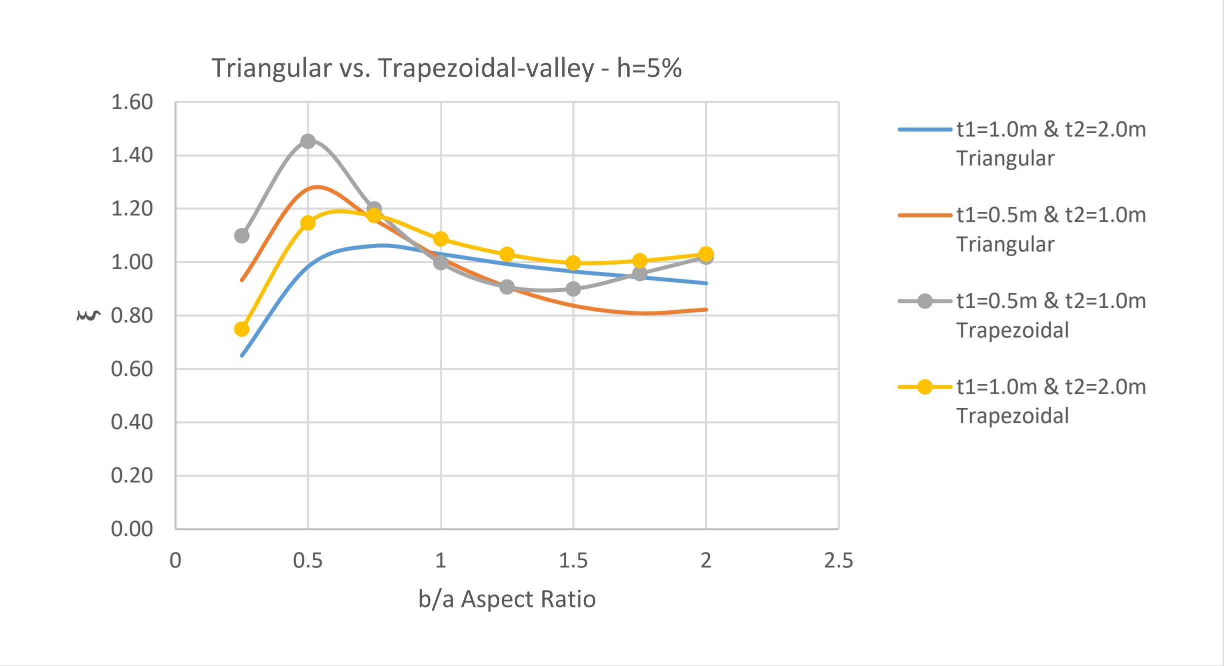
Triangular vs. Trapezoidal-valley - h=5%
ξ
1.60
1.40
1.20
1.00
0.80
0.60
0.40
0.20
0.00
0
0.5
1
1.5
2
2.5
b/a Aspect Ratio
t1=1.0m & t2=2.0m Triangular
t1=0.5m & t2=1.0m Triangular
t1=0.5m & t2=1.0m Trapezoidal
t1=1.0m & t2=2.0m Trapezoidal

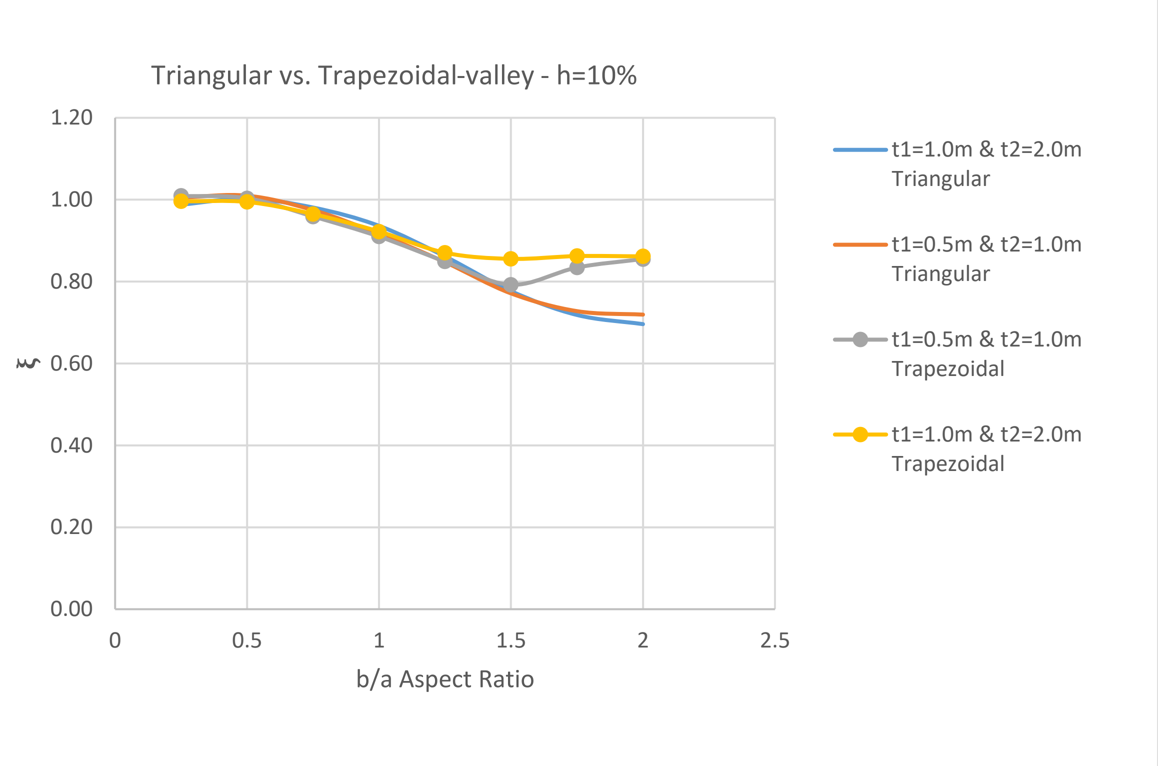
Triangular vs. Trapezoidal-valley - h=10%
ξ
1.20
1.00
0.80
0.60
0.40
0.20
0.00
0
0.5
1
1.5
2
2.5
b/a Aspect Ratio
t1=1.0m & t2=2.0m Triangular
t1=0.5m & t2=1.0m Triangular
t1=0.5m & t2=1.0m Trapezoidal
t1=1.0m & t2=2.0m Trapezoidal

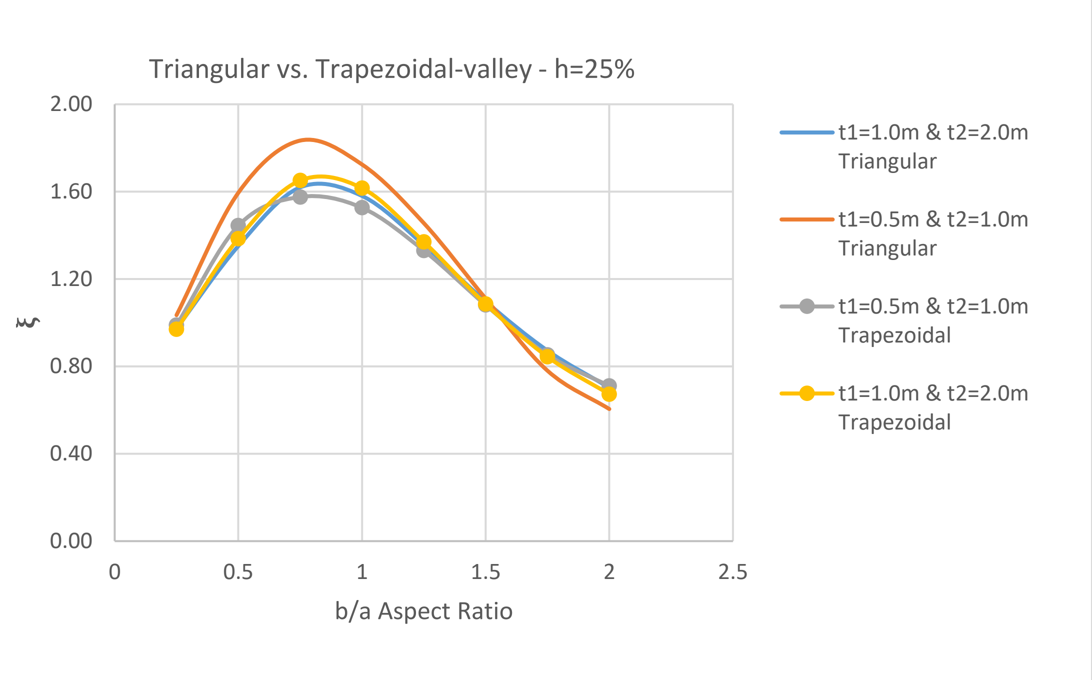

Figure 5.3: Triangular vs. Trapezoidal-valley results for shells with linear varying thickness.

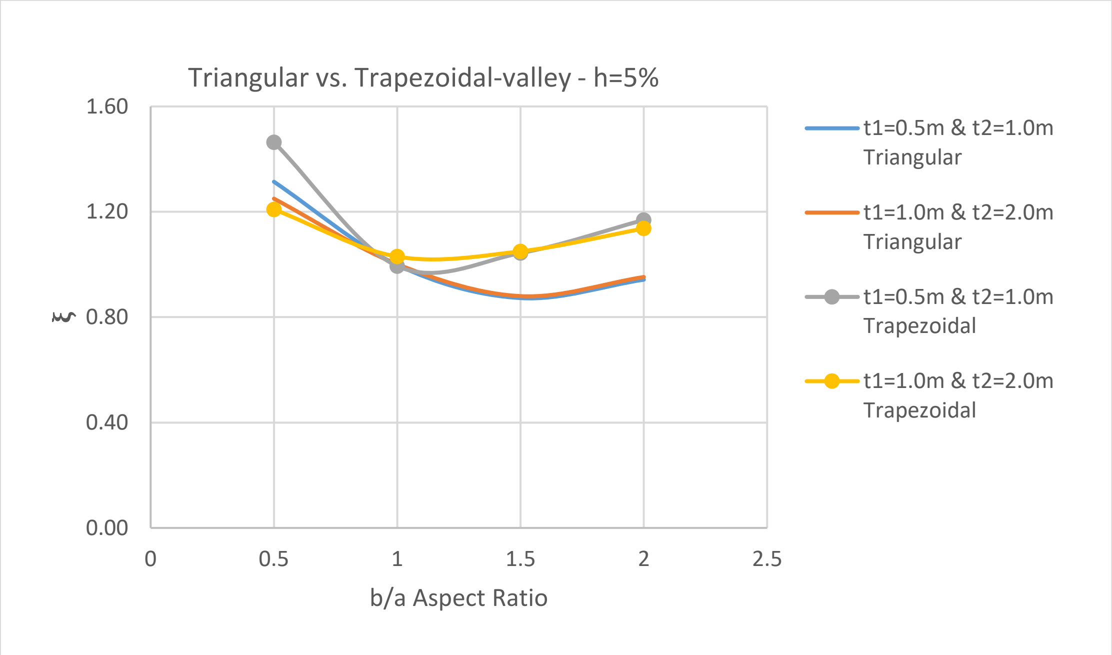

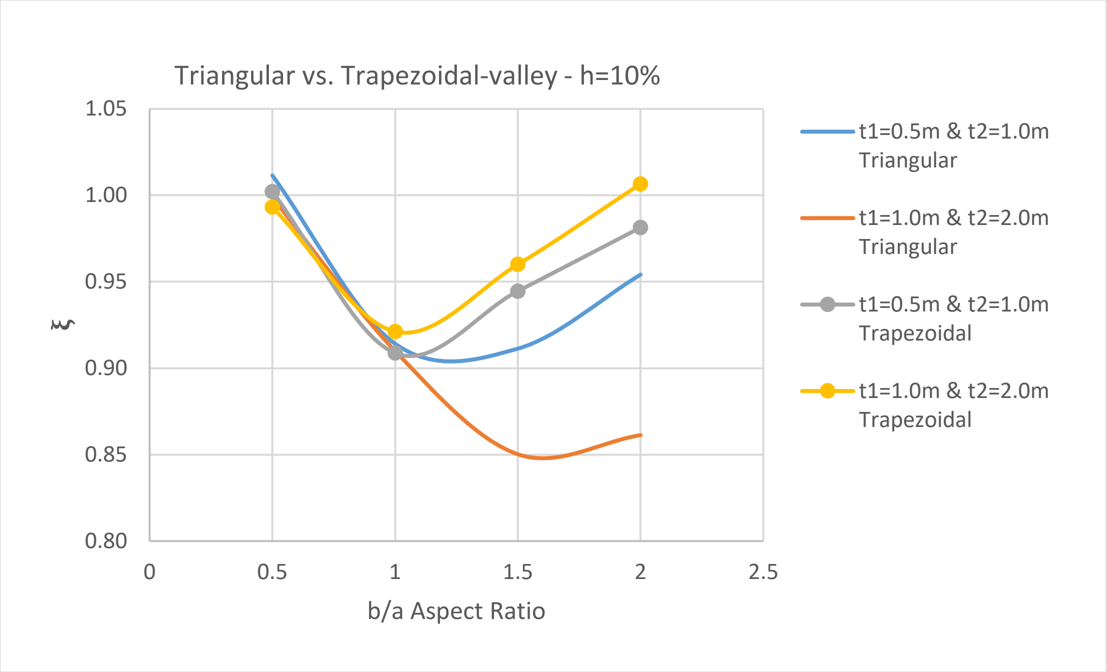

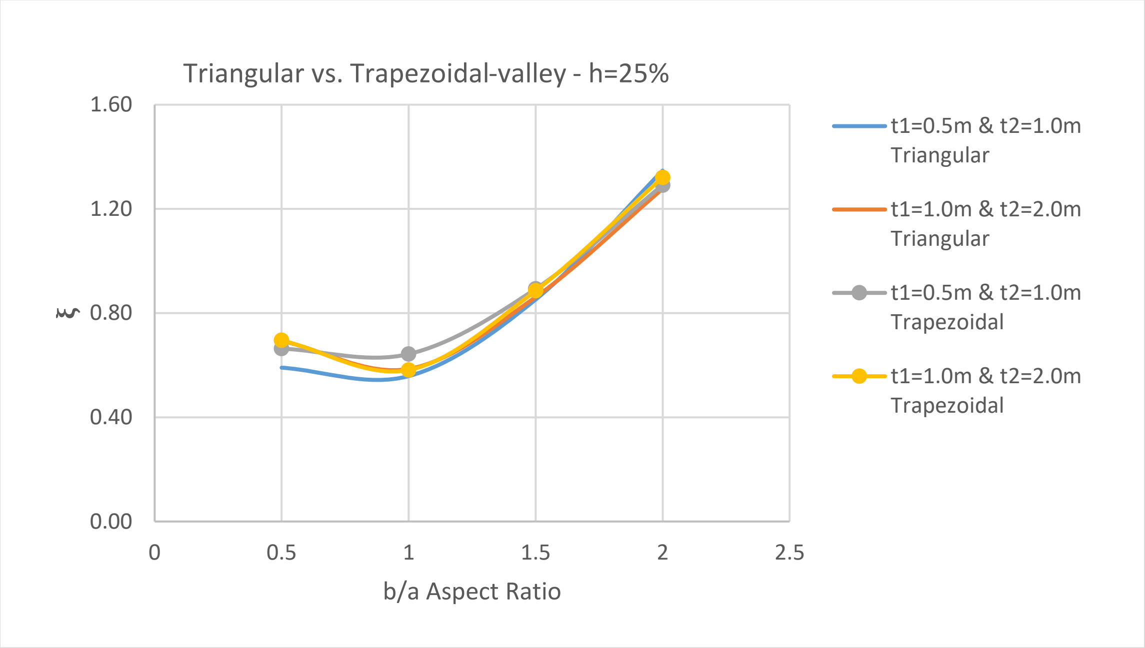

Figure 5.4: Triangular vs. Trapezoidal-valley results for shells with quadratic varying thickness.

For shells with quadratic varying thickness, the beneficial effect is highest at the lower (b/a = 0.25) and higher (b/a = 2.0) aspect ratios, whereas it is highest for shells with linear varying thickness in the aspect ratio range 0.75 ≤ b/a ≤ 1.0.

Another observation made is that the beneficial effect of double curvature is relatively the same for both shells (having quadratic varying thickness) with thickness expressions, t_1=0.5m & t_2=1.0m and t_1=1.0m & t_2=2.0m. The critical buckling pressure for the elliptic paraboloid is typically 1 to 1.5 times higher for shells with linear and quadratic varying thickness than for the comparable parabolic cylinder.

5.2 Recommendations

To increase the safety of thin concrete arch dams under high hydrostatic loads, additional research on the post-buckling behaviour of thin arch dams is necessary. This is because post-buckling analysis will consider the geometric nonlinear effects. Geometric nonlinear analysis can effectively track the initial nonlinear equilibrium path and identify snap-through and, with some caution, possibly bifurcation buckling by taking nonlinear pre-buckling bending deformations into account. Pre-buckling bending effects will be amplified, which will result in some loss of stiffness around the buckling load and eventually causing the shell structure to collapse from loads lower than anticipated.

This also applies to impact structures and energy absorbers. Also, the extent of deformation at which self-contact can occur during buckling is substantial. Additional research is required on arch dams comprised of shells of alternative double- curvature configurations such as hyperbolic paraboloid and nonlinear material behaviour which is another form of failure should be investigated.

Reference

A.B.Sabir & D.G.Ashwell. 1971. A comparison of curved beam finite elements when used in vibration problems. Available: https://www.sciencedirect.com/science/article/abs/pii/0022460X71901064.

Aftabi Sani, A. & Lotfi, V. 2007. Linear dynamic analysis of arch dams utilizing modified efficient fluid hyper-element. *Engineering Structures*. 29(10):2654–2661. DOI: 10.1016/j.engstruct.2007.01.005.

Akbari, J., Ahmadi, M.T. & Moharrami, H. 2011. Advances in concrete arch dams shape optimization. *Applied Mathematical Modelling*. 35(7):3316–3333. DOI: 10.1016/j.apm.2011.01.020.

Baecher, G.B. 2016. Georisk : Assessment and Management of Risk for Engineered Systems and Geohazards Uncertainty in dam safety risk analysis Uncertainty in dam safety risk analysis. *Georisk*. 10(2):92–108. DOI: 10.1080/17499518.2015.1102293.

Chen, S.-H. 2015. Hydraulic Structures. Available: https://link.springer.com/book/10.1007/978-3-662-47331-3.

Choi, J.K. & Lim, J.K. 1993. Simple curved shear beam elements. Available: https://onlinelibrary.wiley.com/doi/epdf/10.1002/cnm.1640090805?saml_referrer.

Conceição, J., Faria, R., Azenha, M. & Miranda, M. 2020. A new method based on equivalent surfaces for simulation of the post-cooling in concrete arch dams during construction. *Engineering Structures*. 209(December 2019):109976. DOI: 10.1016/j.engstruct.2019.109976.

“Concrete dams: control and treatment of cracks. International Commission on Large Dams; 1997.” 1997. *ICOLD. Bulletin no. 107*.

D.G.Ashwell & A.B.Sabir. 1971. Limitations of certain curved finite elemnts when applied to arches. Available: https://www.sciencedirect.com/science/article/abs/pii/0020740371900178.

Dias, V., Jqlio, E.N.B.S., Engineering, C. & Codex, C. 1997. Computation of Membrane Shapes and Analysis of Arch Dams. 64(1):849–855.

Dutta, S. 2020. A sequential metamodel-based method for structural optimization under uncertainty. *Structures*. 26(April):54–65. DOI: 10.1016/j.istruc.2020.04.009.

Fanelli, A., Fanelli, M. & Salvaneschi, P. 1993. A neural network approach to the definition of near optimal arch dam shape. Available: https://scholar.google.com/scholar_lookup?title=A neural network approach to the definition of near optimal arch dam shape&publication_year=1993&author=A. Fanelli&author=M. Fanelli&author=P. Salvaneschi.

Fialho, J.F.L. 1955. Leading Principles for the Design of Arch Dams – A New Method of Tracing and Dimensioning. Available: https://scholar.google.com/scholar?q=J.F.L. Fialho, Leading Principles for the Design of Arch Dams A New Method of Tracing and Dimensioning, LNEC, Lisbon, Portugal, 1955.

Fumagalli, E. 1973. Statical and geomechanical models. Available: https://books.google.co.za/books?hl=en&lr=&id=iqDzCAAAQBAJ&oi=fnd&pg=PA1&ots=lv0YREFRUa&sig=qNUMjcD0amSQnrW9EcyrrhwvIlI&redir_esc=y#v=onepage&q&f=false

.

Gomes, J.P. 2021. Vibration-based damage detection of a concrete arch dam. 235(October 2020). DOI: 10.1016/j.engstruct.2021.112032.

Gomes, J., Pereira, S., Magalhães, F., Lemos, J. & Cunha, A. 2018. Input-Output vs Output-only modal identification of Baixo Sabor concrete arch dam. In: 9th European Workshop on Structural Health Monitoring. 2018: Available: https://scholar.google.com/scholar?q=Gomes J, Pereira S, Magalhães F, Lemos JV, Cunha Á. Input-Output vs Output-only modal identification of Baixo Sabor concrete arch dam. In: 9th European Workshop on Structural Health Monitoring. 2018: Manchester, United.

Guohua, L. & Shuyu, W. 1990. Optimum design of concrete arch dam. Available: https://scholar.google.com/scholar_lookup?title=Optimum design of concrete arch dam&publication_year=1990&author=L. Guohua&author=W. Shuyu.

Hamidian, D. & Seyedpoor, S.M. 2010. Shape optimal design of arch dams using an adaptive neuro-fuzzy inference system and improved particle swarm optimization. *Applied Mathematical Modelling*. 34(6):1574–1585. DOI: 10.1016/j.apm.2009.09.001.

Lange, D. 2002. Early thermal changes. In: Bentur A, editor. Early age cracking in cementitious systems (Report 25). RILEM Publications SARL; 2002. p. 37–8.

Liu, Y.R., Guan, F.H., Yang, Q., Yang, R.Q. & Zhou, W.Y. 2013. International Journal of Rock Mechanics & Mining Sciences Geomechanical model test for stability analysis of high arch dam based on small blocks masonry technique. *International Journal of Rock Mechanics and Mining Sciences*. 61:231–243. DOI: 10.1016/j.ijrmms.2013.03.003.

Lu, Z., Zhao, Y., Yu, Z. & Ding, F. 2011. Cement and Concrete Research Probabilistic evaluation of initiation time in RC bridge beams with load-induced cracks exposed to de-icing salts. *Cement and Concrete Research*. 41(3):365–372. DOI: 10.1016/j.cemconres.2010.12.003.

M.A. Lotfollahi Yaghin and M.A. Hesari. 2008.

Maheri, M. & Bidokhti, N.T. 2001. shape optimization of concrete arch dams using simple genetic algorithm.

Martins, N., Caetano, E., Diord, S., Magalhães, F. & Cunha, Á. 2014. Dynamic monitoring of a stadium suspension roof : Wind and temperature influence on modal parameters and structural response. 59:80–94. DOI: 10.1016/j.engstruct.2013.10.021.

Mazighi, H. & Mihoubi, M.K. 2018. Study of the effect of upstream slope on water pressure in concrete gravity dam. *Procedia Structural Integrity*. 13(January 2018):1438–1441. DOI: 10.1016/j.prostr.2018.12.298.

Meng, Z., Zhou, H., Li, G. & Yang, D. 2016. A decoupled approach for non-probabilistic reliability-based design optimization. *Computers and Structures*. 175:65–73. DOI: 10.1016/j.compstruc.2016.06.008.

Mohr, G.A. 1979. Design of shell shape using finite elements. Available: https://www.sciencedirect.com/science/article/abs/pii/0045794979900385.

Okuma, N., Etou, Y., Kanazawa, K. & Hirata, K. 2008. Dynamic properties of a large arch dam after forty-four years of completion in The 14th World Conference on Earthquake Engineering. Available: https://scholar.google.com/scholar?q=Okuma N, Etou Y, Kanazawa

K, Hirata K. Dynamic properties of a large arch dam after forty-four years of completion in The 14th World Conference on Earthquake Engineering. 2008: Beijing, China.

Papadakis, G. 2008. International Journal of Solids and Structures Buckling of thick cylindrical shells under external pressure : A new analytical expression for the critical load and comparison with elasticity solutions. 45:5308–5321. DOI: 10.1016/j.ijsolstr.2008.05.027.

Pereira, S., Reynders, E., Magalhães, F., Cunha, Á. & Gomes, J.P. 2020. The role of modal parameters uncertainty estimation in automated modal identification , modal tracking and data normalization. *Engineering Structures*. 224(November 2019):111208. DOI: 10.1016/j.engstruct.2020.111208.

Pereira, S., Magalhães, F., Cunha, Á., Moutinho, C. & Pacheco, J. 2021. Modal identification of concrete dams under natural excitation. *Journal of Civil Structural Health Monitoring*. 11(2):465–484. DOI: 10.1007/s13349-020-00462-9.

Pi, Y.L., Bradford, M. & Uy, B. 2005. A spatially curved-beam element with warping and Wagner effects. Available: https://onlinelibrary.wiley.com/doi/10.1002/nme.1337.

Prathap, G. 1985. The curved beam/deep arch/finite ring element revisited. Available: https://onlinelibrary.wiley.com/doi/epdf/10.1002/nme.1620210302?saml_referrer.

Rahim, A.S. 1983. Optimum Shape of An Arch Dam for Static Loads, MEng Thesis, Asian Institute of Technology, Bangkok, 1983.

Rajan, M.K.S. 1968. Shell Theory Approach for Optimization of Arch Dam Shapes, Ph.D Thesis, University of California, Berkeley,1968.

Ricketts, R.E. & Zienkiewicz, O.C. 1975. Shape optimization of concrete dams, Criteria and Assumptions for Numerical Analysis of Dams. (Quadrant Press, Swansea, London, UK). Available: https://scholar.google.com/scholar_lookup?title=Shape optimization of concrete dams&publication_year=1975&author=R.E. Ricketts&author=O.C. Zienkiewicz.

Sabir, A.B. & Lock, A.C. 1973. Large deflexion, geometrically non-linear finite element analysis of circular arches. Available: https://www.sciencedirect.com/science/article/abs/pii/0020740373900441.

Salajegheh, J., Salajegheh, E., Seyedpoor, S.M. & Gholizadeh, S. 2008. Optimum design of arch dams including hydrodynamic effects for earthquake loading using the simultaneous perturbation stochastic approximation method. (B.H.V. Topping, M. Papadrakakis (Eds.), Proceedings of the Ninth International Conference on Computational Structures Technology, Civil-Comp Press, Stirlingshire, UK). Available: https://scholar.google.com/scholar_lookup?title=Optimum design of arch dams including hydrodynamic effects for earthquake loading using the simultaneous perturbation stochastic approximation method&publication_year=2008&author=J. Salajegheh&author=E. Sala.

Serafim, J.L. 1966. New shapes for arch dams. Available: https://scholar.google.com/scholar_lookup?title=New shapes for arch dams&publication_year=1966&author=J.L. Serafim.

Sharma, R.L. 1983. Optimal Configuration of Arch Dams, Ph.D Thesis, Indian Institute of Technology, Kanpur.

Sharpe, R. 1969. The optimum design of arch dams, in: Proceeding of Institution of Civil Engineers (ICE). Available: https://scholar.google.com/scholar?q=R. Sharpe, The optimum design of arch dams, in: Proceeding of Institution of Civil Engineers , 1969, Paper. 7200s, Suppl Vol., pp. 7398.

The Constructor, B.I. 2008. *Types of Arch Dam Construction*. Available: https://theconstructor.org/water-resources/types-of-arch-dam-construction/20087/.

Veletsos, A.S., Austin, W.J., Pereira, C.A.L. & Wung, S.J. 1972. Free In-Plane Vibration of Circular Arches. Available: https://ascelibrary.org/doi/pdf/10.1061/JMCEA3.0001585.

Wang, R. 1991. Preliminary research on the overall safety and standard control of arch dam.

Wang, R. 2016. Key Technologies in the Design and Construction of 300 m Ultra-High Arch Dams. *Engineering*. 2(3):350–359. DOI: 10.1016/J.ENG.2016.03.012.

Wen-gui, C.A.O., Yong-jie, Z. & Ming-hua, Z. 2007. Non-probabilistic fuzzy reliability analysis of pile foundation stability by interval theory. 864–869. DOI: 10.1007/s11771.

Yang, Y.B., Kuo, S.R. & Yau, J.D. 1991. Use of straight-beam approach to study buckling of curved beams.

Yang, Y.B., Lin, S.P. & Chen, C.S. 2007. Rigid body concept for geometric nonlinear analysis of 3D frames , plates and shells based on the updated Lagrangian formulation. 196:1178–1192. DOI: 10.1016/j.cma.2006.07.013.

Yao, T.M. & Choi, K.K. 1989. Shape Optimal Design of an Arch Dam. 9445(September 1989). DOI: 10.1061/(ASCE)0733-9445(1989)115.

Yau, J.D. & Yang, Y.B. 2008. Geometrically nonlinear analysis of planar circular arches based on rigid element concept - A structural approach. *Engineering Structures*. 30(4):955–964. DOI: 10.1016/j.engstruct.2007.06.003.

Ye, J., Zhou, H. & Zhou, X. 2023. Hydrodynamic pressure on lateral side of dam excited by harmonic seismic vibration: A novel formulation. *Soil Dynamics and Earthquake Engineering*. 164(February 2022):107626. DOI: 10.1016/j.soildyn.2022.107626.

Zhao, E. & Wu, C. 2021. Long-term safety assessment of large-scale arch dam based on non-probabilistic reliability analysis. *Structures*. 32(February):298–312. DOI: 10.1016/j.istruc.2021.03.012.

Zhou, W. & Chang, X. 2004. Stability study based on buckling analysis of high arch dam. In: Proceedings of the international symposium on safety science and technology. Part A; Available: https://scholar.google.com/scholar?q=Zhou W, Chang X. Stability study based on buckling analysis of high arch dam. In: Proceedings of the international symposium on safety science and technology. Part A; 2004. 47782.

Zingoni, A., Mudenda, K., French, V. & Mokhothu, B. 2013. Buckling strength of thin-shell concrete arch dams. *Thin-Walled Structures*. 64:94–102. DOI: 10.1016/j.tws.2012.12.001.

6. Appendix A:

6.1 Appendix A1

Linear varying thickness equation derivation for single curvature arch dam.

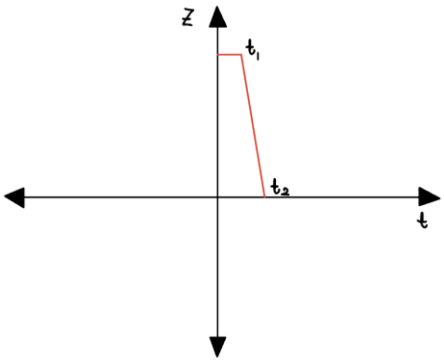

The generic linear equation, $y = mx + c$, is transformed into the z-y plane (where y represents the thickness, t) coordinate system.

∴ The newly adopted equation: $z = mt + c$.

Arch dam having the width, a=50m and aspect ratio, $b/a = 0.25$ with the thickness expression, t_1 = 0.50m & t_2=1.0m. The dam height, b = 12.5m at thickness, t_1 = 0.50m and b = 0m at the thickness, t_2 = 1.0m.

∴ The newly adopted coordinates, (0.5 ; 12.5) & (1 ; 0).

∴ Using above coordinates, the gradient, m, = -25

∴ $z = -25t + c$

∴ Using the point (1 ; 0) to solve for the z-intercept, c, we get: $c = 25$

∴ $z = -25t + 25$

∴ Solving for the thickness, t, we get:

t = -0.04Z + 1.0 for the 50m wide arch dam (with single curvature) having aspect ratio, b/a =0.2

The rest of the equations with their respective aspect ratio depths follow the same procedure.

6.2 Appendix A2

Linear varying thickness equation derivation for double curvature arch dam.

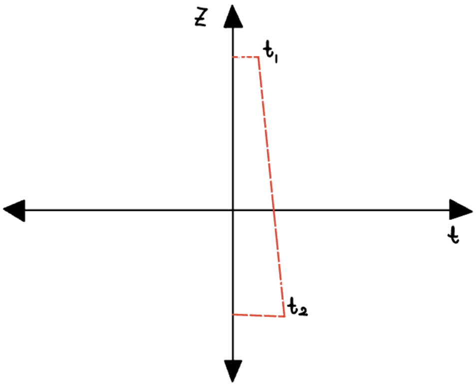

The generic linear equation, $y = mx + c$, is transformed into the z-y plane (where y represents the thickness, t) coordinate system.

∴ The newly adopted equation: $z = mt + c$.

Arch dam having the width, a=50m and aspect ratio, b/a = 0.25 with the thickness expression, t_1 = 0.50m & t_2=1.0m.

N.B: Since the *shell revolution* technique was adopted in creating the geometric part for double curvature analysis, the dam's height dimension is taken between the coordinates, 6.25 & -6.25, for a 12.5m (i.e. 6.25 – (-6.25) = 12.5m) high dam.

∴The dam height, b = 6.25m at thickness, t_1 = 0.50m and b = -6.25m at the thickness, t_2 = 1.0m.

∴ The newly adopted coordinates, (0.5 ; 6.25) & (1 ; -6.25).

∴ Using above coordinates, the gradient, m, = -25

∴ $z = -25t + c$

∴ Using the point (1 ; -6.25) to solve for the z-intercept, c, we get: c = 18.75

∴ $z = -25t + 18.75$

$\therefore$ Solving for the thickness, *t*, we get:

***t* = -0.04Z + 0.75** for the 50m wide arch dam (with double curvature) having aspect ratio, b/a =0.25

The rest of the equations with their respective aspect ratio depths follow the same procedure.

7. Appendix B

7.1 Appendix B1

Quadratic varying thickness equation derivation for single curvature arch dam.

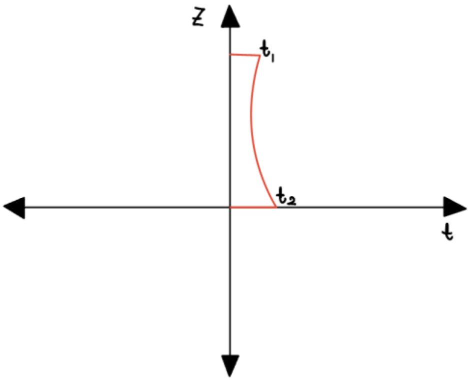

The generic quadratic equation, $x = d(y - k)^2 + h$, is transformed into the z-y plane (where y represents the thickness, t) coordinate system.

∴ The newly adopted equation: $t = d(z - k)^2 + h$……....(1)

Arch dam having the width, a=50m and aspect ratio, b/a = 0.50 with the thickness expression, t_1 = 0.50m & t_2=1.0m. The dam height, b = 25m at thickness, t_1 = 0.50m and b = 0m at the thickness, t_2 = 1.0m.

∴ The newly adopted coordinates, (0.5 ; 25) & (1 ; 0).

Substituting the coordinate (1 ; 0) into equation (1), we get:

$1 = d(0 - k)^2 + h$

∴ $h = 1 - k^2d$………..(2)

Substituting the coordinate (0.5 ; 25) into equation (1), we get:

$0.5 = d(25 - k)^2 + h$……….(3)

∴ Substituting equation (2) into equation (3):

$0.5 = d(25 - k)^2 + 1 - k^2d$

Solving for k, we get:

$k = 12.5 + 0.01d^{-1}$…………(4)

Substituting equation (4) into (2):

$\boldsymbol{h = 1 - (12.5 + 0.01d^{-1})^2 d}$**…………..(5)**

Substituting equation (4) and (5) into equation (1):

$t = d(z - 12.5 - 0.01d^{-1})^2 + 1 - (12.5 + 0.01d^{-1})^2 d$……………….(6)

Using either of the known coordinates (1 ; 0) or (0.5 ; 25) to solve for d in equation (6):

$d = 0.0008$

Substituting d into equation (4) and (5):

$k = 25$ & $h = 0.5$

∴ Equation (1) can be written as:

$\boldsymbol{t = 0.0008(z - 25)^2 + 0.5}$ **for a 50m wide arch dam (with single curvature) with 0.50 aspect ratio**

The rest of the equations with their respective aspect ratio depths follow the same procedure.

7.2 Appendix B2

Quadratic varying thickness equation derivation for double curvature arch dam.

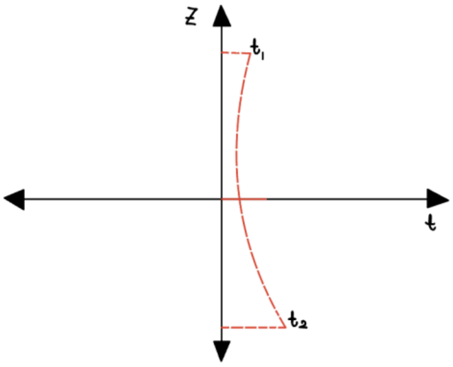

The generic quadratic equation, $x = d(y - k)^2 + h$, is transformed into the z-y plane (where y represents the thickness, t) coordinate system.

∴ The newly adopted equation: $t = d(z - k)^2 + h$……....(1)

N.B: Since the *shell revolution* technique was adopted in creating the geometric part for double curvature analysis, the dam's height dimension is taken between the coordinates, 12.5 & -12.5, for a 25m (i.e. 12.5 – (-12.5) = 25m) high dam.

Therefore, arch dam having the width, a=50m and aspect ratio, $b/a = 0.50$ with the thickness expression, t_1 = 0.50m & t_2=1.0m. The dam height, b = 12.5m at thickness, t_1 = 0.50m and b = -12.5m at the thickness, t_2 = 1.0m.

∴ The newly adopted coordinates, (0.5 ; 12.5) & (1 ; -12.5).

Following the similar steps as in appendix B1,

$t = 0.0008(z - 12.5)^2 + 0.5$ **for a 50m wide arch dam (with double curvature) with 0.50 aspect ratio**

The rest of the equations with their respective aspect ratio depths follow the same procedure.